Development Of New Multifunctional Catalysts For The Hydrodeoxygenation Of Biomass-Derived Oxygenated Molecules

Ana Rita Ferreira Nunes

Thesis to obtain the Master of Science Degree in

Chemical Engineering

Supervisors:
Professor Doctor Ângela Maria Pereira Martins Nunes
Doctor Auguste Rodrigues Fernandes

Examination Committee

Chairperson: Professor José Nuno Aguiar Canongia Lopes
Supervisor: Doctor Auguste Rodrigues Fernandes
Members of the Committee: João Paulo Gil Lourenço

October 2021

Declaration

I declare that this document is an original work of my own authorship and that it fulfills all the requirements of the Code of Conduct and Good Practices of the Universidade de Lisboa.

Acknowledgements

This work could not be done without the valuable help of the exceptional people I have come across over the last few months.

Firstly, I would like to express my deepest gratitude and admiration for my supervisors, Dr. Auguste Fernandes and Prof. Dr. Ângela Martins Nunes, for always being available to listen to my doubts and concerns, for the lessons they have taught me and for the time dispensed.

I would also like to thank Prof. Dr. Filipa Ribeiro, not only for putting me in contact with my supervisors, but also for the availability that has always been shown towards me and for all the help that has been provided.

To all the people in the 9th floor, especially in the CATHPRO lab I express my sincerest thank you for always making me feel welcome.

A special thank you must be said to ISEL, who received me in the warmest way possible. I would like to highlight Prof. Nelson Nunes, who has always shown to be available to listen to my doubts and ready to help solve problems. Thank you.

I would also like to extend my gratitude to Dr. Maria da Conceição Oliveira, who has shown nothing but availability and good will to help in the best way possible.

To my friends, I would like to express my most sincere gratitude, they have been with me through thick and thin. A special thank you to the friends that Técnico gave me, who made these 5 years a lot easier. The sense of belonging I got from them is priceless. I would like to highlight here my good friend and car partner, Daniel, for making the most difficult problems look easy, whether these were work related or not.

Last, but definitely not least, I would like to thank my family, in particular my mom, Otília, my aunt, Olga and my uncle, Luís, for being my safety net and for always believing in me, even when I don’t.

Abstract

New bifunctional catalysts comprising heteropoly acids have been developed for the hydrodeoxygenation (HDO) of guaiacol, a biomass model compound. Three catalysts groups were studied based on the supports: Pt-Al_2O_3, Ni28-Al_2O_3 and NiO25-Al_2O_3 (industrial catalyst). The heteropoly acid was introduced in two ways: by incipient wetness impregnation of 12-tungstophosphoric acid ($H_3PW_{12}O_{40}$, HPW) and by a physical mixture of $Cs_{2.5}H_{0.5}PW_{12}O_{40}$ ($Cs_{2.5}$ salt), a cesium heteropoly salt. Each support by itself, impregnated with HPW and physically mixed with $Cs_{2.5}$ salt forms a group. Nine catalysts were tested. The $Cs_{2.5}$ salt was synthetized by the dropwise addition of a cesium precursor to an aqueous HPW solution. The content of the heteropoly acid or the salt was constant (20 wt. %) for all catalysts and the reaction was carried out at 300 ºC, atmospheric pressure and with a H_2/guaiacol molar ratio of 50. The catalysts characterization was performed by powder X-Ray diffraction, UV-Vis DRS, IR Spectroscopy, H_2-TPR and TGA analysis. The presence of HPW could not be confirmed by all techniques although $Cs_{2.5}$ salt presence was proved. The catalytic results showed that the conversion follow the group order NiO25-Al_2O_3 > Ni28-Al_2O_3 >> Pt-Al_2O_3 and that the impregnated HPW on Ni catalysts showed the best selectivity to deoxygenated products. These catalysts, however, showed a significant conversion decrease with reaction time on stream, probably due to the deposit of carbonaceous species, in particular guaiacol, that adsorbs strongly onto the alumina support. HPW/Ni-Al_2O_3 showed to be the most promising catalysts studied in the HDO of guaiacol.

Keywords: biomass valorization, hydrodeoxygenation, heteropoly acid, heteropoly acid salt, bifunctional catalysts, guaiacol

Resumo

Desenvolveram-se novos catalisadores com heteropoliácidos incorporados para o estudo da hidrodesoxigenação do guaiacol, molécula modelo da biomassa. Os catalisadores foram divididos em três grupos, baseados no suporte: Pt-Al_2O_3, Ni28-Al_2O_3 e NiO25-Al_2O_3 (catalisador industrial). A introdução dos heteropoliácidos executou-se duas maneiras: por impregnação a seco do ácido 12-fosfotúngstico ($H_3PW_{12}O_{40}$, HPW) e por mistura mecânica com $Cs_{2.5}H_{0.5}PW_{12}O_{40}$ (sal de $Cs_{2.5}$), um sal de heteropoliácido de césio. Este sal foi sintetizado através da adição gota-a-gota de um precursor de Cs a uma solução aquosa de HPW. Cada suporte por sozinho, impregnado com HPW e mecanicamente misturado com o sal formam um grupo, obtendo-se nove catalisadores. O teor de heteropoliácido ou sal foi constante (20 % (m/m)) em todos os catalisadores e a reação decorreu a 300 ºC, pressão atmosférica, com um rácio molar H_2/guaiacol de 50. A caracterização foi feita por difração de Raio-X (método do pó), UV-Vis DRS, Espetroscopia IV, TPR de H_2 e Termogravimetria. Não foi possível confirmar a presença do HPW em todas as técnicas, ao contrário do sal de $Cs_{2.5}$. Através dos resultados catalíticos, os valores de conversão seguem a ordem de suportes NiO25-Al_2O_3 > Ni28-Al_2O_3 >> Pt-Al_2O_3 e os catalisadores de Ni impregnados com HPW obtiveram os melhores valores de seletividade em produtos desoxigenados. Porém, estes catalisadores levaram a um maior decréscimo de conversão com o tempo de reação, devido provavelmente à deposição de materiais carbonáceos e guaiacol, que adsorve fortemente no suporte de alumina. Os catalisadores de HPW/Ni-Al_2O_3 mostraram-se os mais promissores para a hidrodesoxigenação do guaiacol.

Palavras-Chave valorização de biomassa, hidrodesoxigenação, heteropoliácidos, sais de heteropoliácidos, catalisadores bifuncionais, guaiacol

Index

List Of Figures

List Of Tables

Glossary

ANI	Anisole
a_{Pt}	Area Occupied by a Platinum Atom on a Polycrystalline Surface
COD	Crystallography Open Database
$Cs_{2.5}$ salt	$Cs_{2.5}H_{0.5}PW_{12}O_{40}$
DIBK	Diisobutyl Ketone
DRS	Diffuse Reflectance Spectroscopy
DDO	Direct Deoxygenation
D_M	Metal Dispersion
d_{mp}	Mean Particle Size
$F(R)$	Kubelka Munk Function
FCC	Fluid Catalytic Cracking
FID	Flame Ionization Detector
GC	Gas Chromatography
GDP	Gross Domestic Product
GHG	Green House Gas
GUA	Guaiacol
HDO	Hydrodeoxygenation
HDN	Hydrodenitrogenation
HDS	Hydrodesulfurization
HDT	Hydrotreatment
HPA	Heteropoly Acid
HPMo	$H_3PMo_{12}O_{40}$, Phosphomolybdic Acid
HPW	$H_3PW_{12}O_{40}$, Phosphotungstic Acid
HYD	Hydrogenation
IS	Internal Standard
IR	Infra-Red
IWI	Incipient Wetness Impregnation
K	Absorption Refletance
LC	Liquid Chromatography
MIBK	Methyl Isobutyl Ketone
MM_{Pt}	Molar Weight of Platinum
MP	Methylpentane
MS	Mass Spectroscopy
NiO25-Al_2O_3	Nickel Oxide Industrial Catalyst
Ni28-Al_2O_3	25% Nickel on PURAL calcined at 600 ºC catalyst
Ph	Phenol
RF	Response Factor
R	Diffuse Reflectance

RT	Retention Time
SDG	Sustainable Development Goals
S	Scattering Reflectance
S_P	Selectivity to Product *P*
STEM-EDX	Scanning Transmission Electron Microscopy- Energy Dispersive X-ray Spectroscopy
TGA	Thermogravimetric Analysis
TGA-DSC	TGA- Differential Scanning Calorimetry
TPD	Temperature Programmed Desorption
TPR	Temperature Programmed Reduction
TT	Thermal Treatment
UX	Unknown Number x
$V_{H_2\ consumed}$	Volume of H_2 consumed
V_{molar}	Molar volume of a perfect gas
v_{Pt}	Volume Occupied by an Atom of Platinum in the Bulk of the Metal
$x_{guaiacol}$	Conversion of Guaiacol
x_{Pt}	Weight Fraction of Platinum
XRD	X-Ray Diffraction
Y_P	Yield to Product *P*

Introduction

Many environmental issues have been raised over the years as a result of the use of fossil fuels. These account for around 80 % of the primary energy use [1] and about 90 % of the CO_2 emissions have their source on the burning of fossil fuels.[2] Although there is a need to reduce the CO_2 emissions, due to their negative environmental impact, it is unlikely that it will be done through a reduction in energy production, mainly because the energy demand is growing.[2] From this point of view, the energy sector must approach its production in an effective way, so that the prejudicial greenhouse gas emissions can be controlled.

To address this issue carbon neutral energy sources are becoming more and more popular, with biomass being one example. It is carbon neutral (the biomass consumes the CO_2 that is released when its burned, creating a cycle), renewable and available.[3] To achieve a workable starting material, biomass must go through pyrolysis to produce bio-oil.[4] However this bio-oil's composition is far from the desired for fuel. This is mainly caused by the presence of oxygenated molecules, which make the acidity and viscosity higher than the desirable and the heating value (heat that is released during combustion) lower, amongst other problems.[5,6] Thus, an upgrade is needed and it is usually done by hydrodeoxygenation or HDO. This process conventionally accompanies hydrodesulfurization (HDS) in hydrotreating (HDT) processes. HDO is however more important than HDS for bio-oil feedstocks once the sulfur content is much lower than the oxygen content.[1] The conventional HDT process usually uses harsh conditions, particularly very high pressures and the catalysts are only active in their sulfided form. This constitutes a problem in bio-oil upgrading because, as stated before, the sulfur content of bio-oil is very low, so an external sulfur source must be added to maintain the catalyst active, however, this will contaminate the bio-oil stream.[1]

Thus, to make the HDO process more feasible, new catalysts that are active at lower pressures and without the presence of sulfur are the focus of the HDO research. HDO catalysts are usually bifunctional catalysts, with a metallic component, for the dissociation of H_2 and an acidic function, for the activation of the C-O bond. Examples of catalysts are metals with hydrogenation capacity, such as Pt or Ni added to acidic supports, such as γ-Al_2O_3 or HZSM-5.[7,8] The acid function can be provided by heteropoly acids and their salts, whether as a support or impregnated onto other supports. These are very versatile materials that possess Brønsted acids sites and whose properties can drastically change depending on their composition.[9,10]

In this work, two forms of 12-tungstophosphoric acid, an heteropoly acid were used: i) the acid itself, $H_3PW_{12}O_{40}$ (HPW) and ii) the cesium salt of this acid, $Cs_{2.5}H_{0.5}PW_{12}O_{40}$ ($Cs_{2.5}$ salt). The former is soluble in water, so an impregnation method was possible to be used. The latter in insoluble so it was physically mixed with the supports. The main goal of this work was to study the effect of the addition of the heteropoly acids in catalysts that are already applied for HDO. The supports chosen were Pt-Al_2O_3 and two forms of Ni-Al_2O_3, one totally synthetized in our lab, Ni28-Al_2O_3 and the other is an industrial catalyst that will be called NiO25-Al_2O_3. Having said that, nine catalysts were obtained: the three supports by themselves, three HPW impregnated on the supports chosen and three physically mixed

$Cs_{2.5}$ with the supports. In all catalysts, the heteropoly acid or salt content was 20 wt. % After synthetized, the catalysts were characterized by Powder X-Ray Diffraction, UV-Vis Diffuse Reflectance Spectroscopy and Infrared Spectroscopy, H_2 Temperature Programmed Reduction and Thermogravimetric analysis. The catalysts were then tested for the HDO of guaiacol, an oxygenated molecule with two $C_{aromatic}$-O groups. The reaction conditions were atmospheric pressure, 300 ºC and a molar ratio of H_2 to guaiacol of 50.

1. State Of The Art

1.1 Context

Until the second half of the 20th century, little or no attention was paid to the impact of human exploration of the earth and its undoubtfully useful resources. It was only when the world's population started growing faster and faster that the pressure on the resources used became significant and was felt in resources such as water, arable land, raw materials and others.[11] Not only did the planet experience a growth in the global population[12], but also in its habitants' Gross Domestic Product [13](GDP), which caused a growth in the quality of life of families, as can be observed in Figure 1.

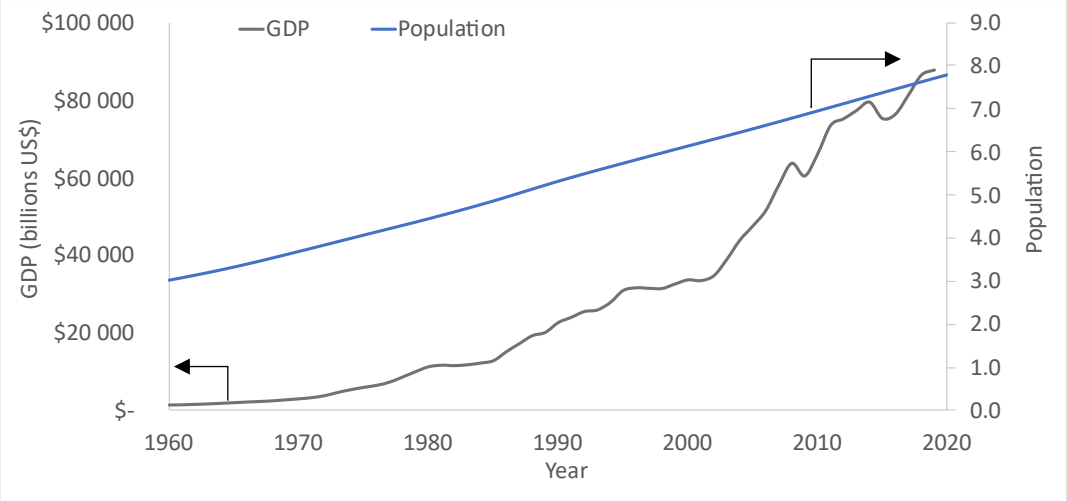

Figure 1: Population, in billions of people, and GDP since 1960.[2],[3]

As a consequence, the energy demand also increased, being its main source fossil fuels, which account for approximately 80% of the primary energy consumption[1]. This happens as a result of a known correlation between economic development and easier access to energy. [14]

Another serious problem faced in the current days, also due to human activity, is global warming. Global warming is mainly caused by an increase of the concentration of greenhouse gas (GHG) in the atmosphere, which absorb the infrared radiation, causing the temperature on the surface of the earth to rise. This originates a cause and effect chain[11]: with increasing temperature, humanity faces both a climate and sea level change, which ultimately causes life adjustments and, in the worst case scenario, mortality. It is estimated that 65 % of these emissions are generated from energy usage.[14] Carbon dioxide (CO_2), amongst others, is a greenhouse gas, with emissions between 30 and 35 Gt.[14] Around 90 % of the CO_2 emissions that origin from human activity derive from the burning of fossil fuels[2]. In Figure 2 it is possible to observed that in fact, the majority of GHG comes from energy consumption.

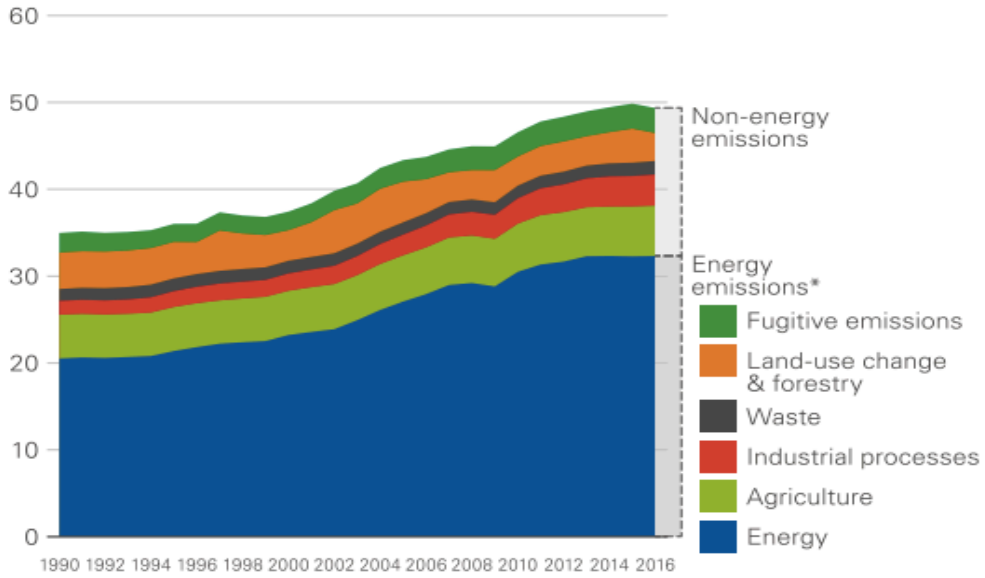

Figure 2: Global greenhouse gas emissions, in Gt of CO_2 equivalent, from reference 15.

To avoid an unsustainable use of energy as well as a large amount of GHG emissions, which raise significant environmental issues, measures must be taken. The Sustainable Development Goals[15] (SDG) is a very good example of what is being done, with one of the agendas for action being the 2015 Paris Agreement on climate change.[16] Although there is a need to reduce the negative human impact on the planet, it is likely that the energy demand will continue to grow[14]. Nonetheless, it is expected a change in the way energy is produced, meaning a shift from fossil fuels to renewable sources such as bioenergy, geothermal and solar energy and hydro and wind power[1]. This is of course accompanied by challenges both technological and economic but it is important to highlight that these new renewable energies will create new business opportunities which will probably create as many as 6.5 millions jobs.[1]

1.2 Biomass: current scenario and challenges

From these new energy sources, biomass is the only that is available worldwide and also renewable, abundant and carbon-neutral[3]. The carbon neutrality of the biomass derives from the way it grows. For example, plants consume CO_2 through photosynthesis, this CO_2 captured from the atmosphere by the biomass is then released when it is burned and is ready to be recaptured by another plant. In this way, a CO_2 cycle is created. In spite of that, the neutrality of this process will depend on the type of biomass feedstock and the technology of the process.[17] The biomass feedstock can be non-food crops and its residues, forest and wood processing residues, algae, sorted municipal waste and wet waste.[18] In the past, research used to focus also on edible crops as biomass feedstock. However, this was pointed out as the cause of the food crisis around 2007[19]: with the rise of oil prices, the production cost of cereal increased due to an increase of energy costs. At the same time, the demand of biofuels increased because its price was then competitive with the oil prices practiced. As the biofuel was being produced using the cereal maize (in the United States) as the feedstock, this was another reason for the rise of the price of cereal and ultimately raised the discussion on whether it was feasible

or not to produce biofuel from food crops, also called 1st generation biofuels[20]. As soon as the connection between the food crises and the production of biofuel was made, the research became mainly focused on the non-food crops. One of the feedstocks that gathers a reasonable amount of interest is non-edible lignocellulosic biomass or lignocellulosic materials, that usually refers to both woody and nonwoody plants.[21] Lignocellulose is mainly composed by cellulose, hemicellulose and lignin, which can be observed in Figure 3. Depending on the source of lignocellulosic material, different ratios of these three components can be found. Cellulose is a glucose polymer[22] and accounts for 30 to 50 %[3] of lignocellulose composition, hemicellulose is composed by shorter polymers of various sugars[22] and accounts for 20 to 35 %[3] of lignocellulose and lastly lignin is a propyl-phenol polymer[22] that corresponds to between 10 and 25 %[3] of the lignocellulose composition

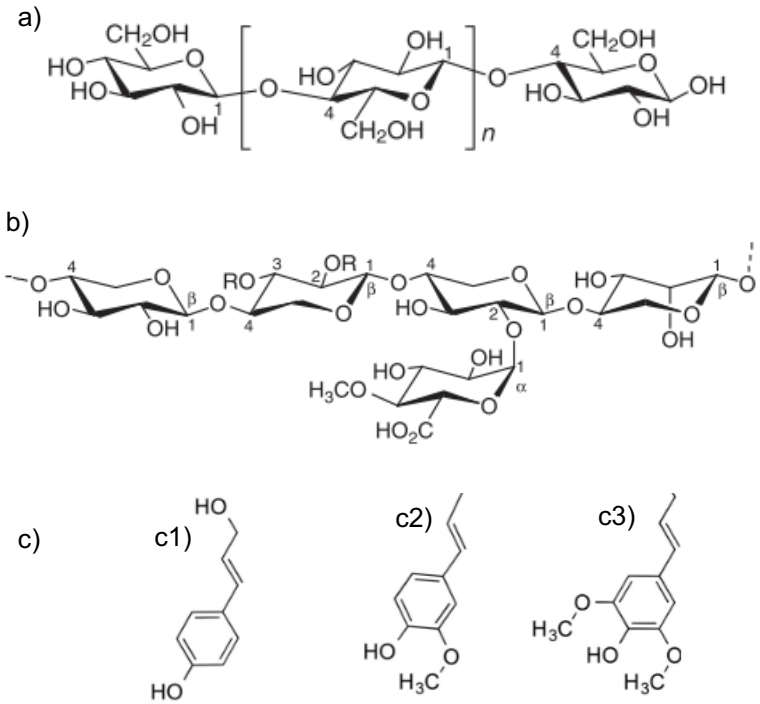

Figure 3: Main structures found in lignocellulosic materials.[15] a) Representation of the structure of cellulose; b) Xylan, one of the major structures of hemicellulose; c) Lignin precursors: c1) p-coumaryl alcohol; c2) coniferyl alcohol; c3) sinapyl alcohol.

Lignin is a very important component of plants, as it is responsible for the rigidity of the cell walls and for keeping the cells together[21], as well as holding around 40% of the lignocellulosic biomass energy.[23] Lignin is usually described by its precursors or monolignols, pictured in Figure 3, which give rise to the building blocks of lignin, *p*-hydroxiphenyl (H), guaiacyl (G) and syringyl (S) phenylpropanoid units. Lignin is a complex macromolecule, with molecular weights between 20 and 70 thousand, assembled by these building blocks, which are linked randomly[21], through β-O-4 aryl ether bonds.[24] Thus, it is very unlikely to find two exactly equal lignin macromolecules, which is why it is considered an amorphous natural polymer. It is also aromatic, hydrophobic and a thermoplastic, meaning that it becomes softer with increasing temperature.[21] Lignin is also the most resistant to degradation constituent of lignocellulosic biomass[4], due to its β-O-4 bonds, that account for between 50 to 65 % of

all bonds present.[24] The bond dissociation energy will also depend on the group attached to the α carbon.[25] In addition, lignin has other bonds that will have to go through cleavage to get the monomers, such as 4-O-5 linkage, 5-5 linkage, β-1 linkage, among others, present in Figure 4.

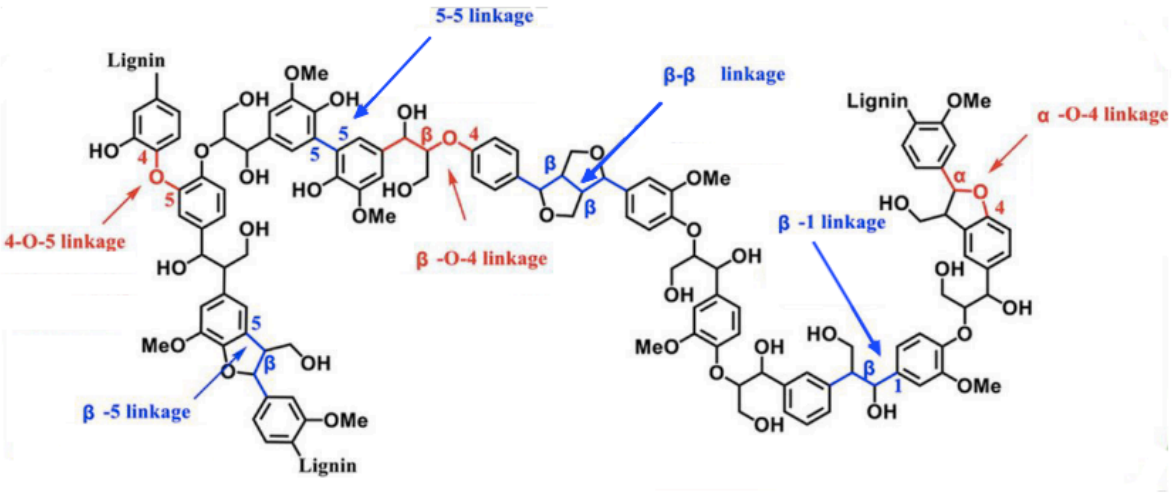

Figure 4: Representation of lignin bonds. Adapted from ref. 23.

Lignin is a material with high potential once it is, from all the biomass constituents, the one with most chemical similarities with petroleum.[26] To take advantage of this potential, the chemical bonds need to be broken to achieve a workable starting material for the production of fuels, called bio-oil. There are several ways to process biomass[5]:

1. Through Gasification, to produce syngas;
2. Through Pyrolysis or Liquefaction, to produce bio-oils;
3. Through Hydrolysis, to produce sugar monomer units.

For the production of bio-oils, due to the high yield and economic efficiency the usually preferred process is pyrolysis.[4] Pyrolysis is the thermal cracking of compounds in the absence of air.[19,22] Depending on the operating conditions, there are different type of pyrolysis, from slow to fast pyrolysis. On the one hand, in conventional or slow pyrolysis, the heating rate is slow, the temperature is lower (when compared with fast pyrolysis) and there is a significant coke yield, which is then used as a solid fuel.[5] On the other hand, fast pyrolysis has a high heating rate and heat transfer rate, a higher temperature (well controlled around 500 ºC) and rapid cooling of the products, which are condensed to produce a liquid bio-oil. This yields around 80 % weight (dry feed) of bio-oil.[28]

This bio-oil, however, cannot be directly used as fuel, needing further upgrading. One of the reasons is the immiscibility of the bio-oil with the streams of liquid hydrocarbons in the refinery.[26] Thus, an integration of processes is not achievable at this point but it would be beneficial due to not only the economy of scale practiced but also the know-how that comes from operating a conventional refinery[6]. The main reason for the impossibility of blending bio-oil with liquid hydrocarbon streams is its oxygen

content, which is significantly high.[22,26] Other characteristic problems of bio-oil are the high water content; its acidity, which can damage both vessels and pipes; its low thermal stability; aging, that consists of on-going undesirable secondary reactions, mainly polymerization, which then causes an increase of its viscosity; high density; lower higher heating value.[5,6,26]

Table 1: Properties of bio-oil and crude oil.

	Bio-oil[29]	**Crude oil**
Properties		
Higher Heating Value (MJ/kg)	16 - 19	42 – 47[30]
Density (kg/L)	1.05 – 1.25	0.8 – 1.0[31]
Water (wt %)	15 - 30	0.1[29]
Elemental Composition		
C (wt%)	55 - 65	83 – 87[32]
O (wt%)	28 – 40	0.05 – 1.5[32]
H (wt%)	5 – 7	10 – 14[32]
S (wt%)	< 0.05	0.05 – 6[32]

Although biofuels from biomass are promising, it is important to understand that this technology will not probably be the main solution nor the substitute for the fossil fuels once there is a degree of risk being taken while fighting climate change with a feedstock which is climate dependent.[33]

1.3 Hydrodeoxygenation

Bio-oil upgrade can be achieved by different processes such as hydrodeoxygenation, known as HDO, zeolite upgrading or steam reforming.[5,34] HDO consists in removing the oxygen from the bio-oil mixture by feeding H_2, at the appropriate reaction conditions and in the presence of a suitable catalyst[35] and fits in the hydrotreatment (HDT) category. Zeolite upgrading consists in converting bio-oil in transportation fuels, by removing the oxygen as CO_2[6], with acidic zeolites as catalysts, at atmospheric pressure, without the presence H_2, which leads to economic advantages when compared to HDO. The temperatures are comprised between 350 and 500 ºC, making the reaction conditions resemble Fluid Catalytic Cracking (or FCC) ones.[22] However, this upgrading route has low hydrocarbon yield but high coke yield, as well as a high amount of phenolic compounds in the products.[5,22] Steam reforming produces synthesis gas (CO + H_2 or syngas) or H_2.[5]

The HDO is the most common method of bio-oil upgrading.[36] Hydrodeoxygenation was first introduced by Furimsky in 1983[37], with the emergent problem of liquid synthetic fuels and their high oxygen content, as previously mentioned. Until this review, all information came as a bonus and attached to the hydrodesulfurization (HDS) and hydrodenitrogenation (HDN) problematic. Furimsky furthermore suggested the use of model compounds (very relevant for the study of HDO), mainly because of their resistance towards upgrade. These model compounds make it possible to untangle

slightly the complexity of bio-oil by selecting the most unstable molecules and studying the transformation they go through instead of dealing with a complex mixture of molecules and their respective transformations.[34] The compounds suggested were furanic rings, phenols and arylethers. Of these, phenolic compounds are a possible model compound of lignin.[35] Examples of phenolic compounds are phenol, guaiacol and anisole, which can be seen in Figure 5.

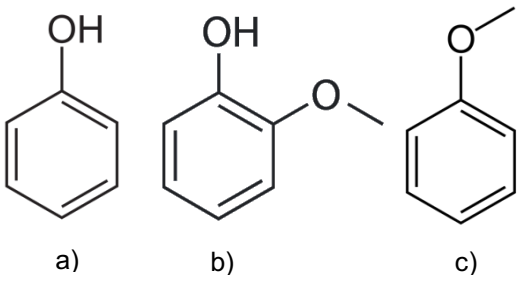

Figure 5: Example of model compounds. a) Phenol; b) Guaiacol; c) Anisole

The removal of oxygen from phenol itself is very difficult due to the nature of the $C_{aromatic}$-OH bond, with a bond dissociation energy of 468 kJ·mol^{-1}, as a consequence of the delocalization effect of the lone pair electron orbital of the oxygen.[38] When compared with other functional groups present in phenolic compounds, it is the one with the highest bond dissociation energy, as it can be observed in Figure 6. Aside of the $C_{aromatic}$-OH, guaiacol has yet another oxygen containing group, a methoxy group, $C_{aromatic}$-OCH_3, also pictured in Figure 6.

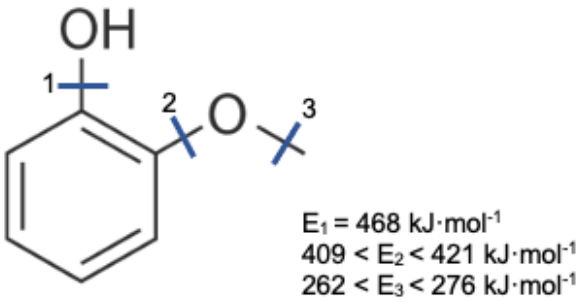

Figure 6: Bond dissociation energies of the different functional groups of guaiacol, from ref. 38.

There are two main HDO routes, as shown in Figure 7: the first one, the aromatic ring is kept untouched and there is a selective hydrogenolysis of the $C_{aromatic}$-O bond, or Direct Deoxygenation route (DDO).[39] The second route involves first the hydrogenation (HYD) of the aromatic ring and only then, the cleavage of the C-O bond, which has a lower bond dissociation energy, 385 kJ·mol^{-1}, when compared with $C_{aromatic}$-O.[23,40,41] The reaction pathway is dictated by the catalyst chosen.[42]

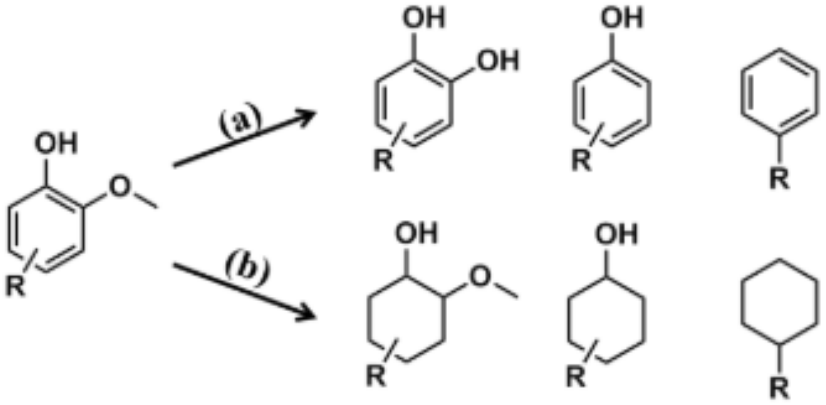

Figure 7: Two main HDO routes, from ref. 24: a) Selective hydrogenolysis (DDO); b) hydrogenation followed by deoxygenation (HYD).

In both routes, the removal of oxygen is done by a number of different reactions, such as hydrolysis, hydrogenation, hydrogenolysis, dehydration, demethoxylation, demethylation, transalkylation, deoxygenation and they can even go through tautomerization routes.[3,23,34]

Concerning operating conditions, temperatures range between 100[43] and 400 ºC.[44] According to Elliot[45], under hydrotreatment conditions, phenolic ethers start to react at 325 ºC and phenols at 350 ºC. The temperature is an important parameter, once when it is not high enough not only the C-O bond is incapable of cleavage due to being thermodynamically unfavorable but also the methyl transfer is not possible. However when the temperature becomes too high, some structural changes can occur in the catalyst, while aromatic condensation might start above 400 ºC.[23]

Hydrogen feeding can be integrated in the process as a gas or as hydrogen donor solvent.[23,46] Pressures are comprised between atmospheric pressure and 300 bar, in the case of gaseous H_2[44]. These high pressures present one of the main disadvantages of this route for upgrade,[5] once it leads not only to high operating costs but also because of safety reasons.[4,47] It is however important to have a good control of H_2 pressures. When the reaction occurs in the liquid phase, higher pressures increase the solubility of H_2 in the bio-oil, increasing its contact with the catalyst, which ultimately leads to an increase in the reaction rate and a decrease in coke formation.[48] When the reaction is carried out in gas phase, higher H_2 pressures will give preference to hydrogenation followed by deoxygenation path, increasing the hydrogen consumption as well as the selectivity to saturated products.[49] Moreover, hydrogenation of the aromatic rings would decrease the octane number in case of gasoline blends.[5] Another factor to be taken into consideration is the reaction solvent. If it is not well chosen, it can interact with the active sites, which is not desirable. The most common solvents are long chain alkanes, alcohols, water and acid solutions.[23]

1.3.1 Catalysts for HDO

As aforementioned, the hydrodeoxygenation reaction is carried in the presence of a catalyst. For HDO optimization, the catalysts must be carefully designed according to the nature of the reaction.

Firstly, and because the reaction is taking place in the presence of H_2, a metal function is needed for hydrogenation purposes. Besides hydrogenation, these sites are also responsible for decarbonylation and decarboxylation (C-C bond cleavage).[36,47]

The metals that are usually applied to HDO are transition metals and the reaction pathway will depend highly on the metal chosen. For example, noble metals will favor hydrogenation due to the weak metal-oxygen bond while more oxophilic metals will favor C-O cleavage.[50] Some authors[50,51] defend that a good compromise would be a bimetallic catalyst that has both hydrogenation and oxophilic function. Fang *et al.*[52] reported the synergetic effects of Ni and Fe for the HDO of guaiacol, at 3 MPa of H_2 and 300ºC, due to the formation of a Ni-Fe alloy. Supported noble metals have shown to be efficient HDO catalysts and are active at lower pressures of H_2 and lower temperatures. [23,36] Thus, possible HDO metals could be Pt[53,54], Ru[55], Re[38], Fe[38,56] and Ni.[8,56,57] Noble metals present a good hydrogenation activity, which increases the H/C ratio of bio-oils, however, their high cost and difficult recovery are the main drawbacks for their industrial application.[34]

A good complement for the metal function is an acidic support. The activation of the C-O bond of the reactant takes place on the acid sites[50] which catalyze dehydration, hydration, isomerization and hydrolysis reactions. The acid sites involved are both Brønsted and Lewis acids[47], and when both are present, a synergetic effect is created and promotes both alkylation and hydrodeoxygenation.[58] When studying support acidity there are a few aspects to be take into consideration. First of all, the acidity of the support must be well controlled once increasing it will also increase the coke formation, leading to the catalyst deactivation.[4] Secondly, the distance between acid and metal sites has an optimum value that does not correspond with “the closer the better”.[59] Lastly, the acidity of the support influences the reaction mechanism which consequently influences the product distribution.[60] The acidic supports can be metal oxides, e.g. Al_2O_3[59,7,61], ZrO_2[38,62] or TiO_2[54,58] as well as zeolites such as HBEA[38], HY[38] or HZSM-5.[8]

When noble metals are impregnated onto an appropriate acidic support, the selectivity to totally deoxygenated products increases. With a bifunctional acidic and noble metal supported catalyst, the acid function catalyzes transalkylation while the metal function promotes demethylation and HDO.[63] The Pt-Al_2O_3 catalyst is widely studied however, alumina supports give rise to issues that will be discussed in the Chapter 1.3.1.2 (Alumina Supports). Fisk *et al.*[54] studied the HDO of a model bio-oil comprising methanol, guaiacol vanillin, water, amongst others, with a 1 wt. % Pt in TiO_2, ZrO_2, CeO_2 and γ-Al_2O_3, being the Pt-Al_2O_3 the most active for oxygen removal. This group managed to achieve a reduction in oxygen content from 41.4 to 2.8 wt. % with the latter catalyst, at 350 ºC and around 7 bar. The presence of water in the model bio-oil was actually advantageous and without its presence, the final oxygen content was only 8.0 wt. %. The C–O cleavage in guaiacol and vanillin was done through hydrogenolysis reactions, producing aromatic compounds that are then hydrogenated. The products are also rich in alkyl-substituted benzenes and cyclohexanes, which is thought to be a consequence of the acidic reaction medium. Runnebaum *et al.*[7] studied once again HDO with Pt- Al_2O_3 with guaiacol as the model compound, yielding mainly phenol, catechol and 3-methylcatechol, all oxygenated compounds. This research group identified hydrogenolysis and hydrogenation as reactions catalyzed by the metal function and transalkylation catalyzed by the alumina support. When studying the effect of temperature

and pressure, it was shown that with increasing temperature transalkylation was favored and with increasing H_2 partial pressures the selectivity to deoxygenated products was higher.

Metallic nickel catalysts are also possible catalysts for HDO. This metal is not as expensive as platinum and it has shown promising results. Yang *et al.*[64] reported reaction conversions up to 99 % on Ni supported on Al_2O_3, CeO_2, SBA-15 and other supports. This group also reported that the support's acidity in combination with the metallic function are important factors once it contributes to the hydrogenolysis and further hydrogenation of anisole. They also found that an increase on reaction temperature from 290 to 310 ºC (3 bar), in Ni/Al_2O_3 catalysts, shifts the product distribution from cyclohexane to benzene and even *n*-hexane. However, an increase on space velocity (from 20.4 h^{-1} to 81.6 h^{-1}) leads to considerably lower conversions, accompanied by a decrease in selectivity of hydrogenated products to oxygenated and deoxygenated aromatics. In agreement, Song *et al.*[8] reported a synergetic effect between Ni and Brønsted acid sites in a Ni/HZSM-5 for HDO of oxygenated aromatics, at 200 ºC and 30 bar of H_2. This group reported that the main HDO route depends on the model compounds chosen, with hydrogenation followed by deoxygenation being the main pathway for phenol, where the main reaction product was cyclohexanone whereas for the case of guaiacol is the direct deoxygenation (75 % vs. 25 % for the hydrogenation – deoxygenation pathway), with phenol being the main product, with 5.9 % yield.

There is also a possibility that the acidic function of the catalysts can be granted by heteropoly acids.[58,65] They can be the support itself or added to another support, depending on their compensating cation. The heteropoly acids providing acid function will be approached later on. All in all, HDO is often carried in the presence of a bifunctional metal and acid catalyst[54,66–68] and some design parameters are shown in Figure 8.

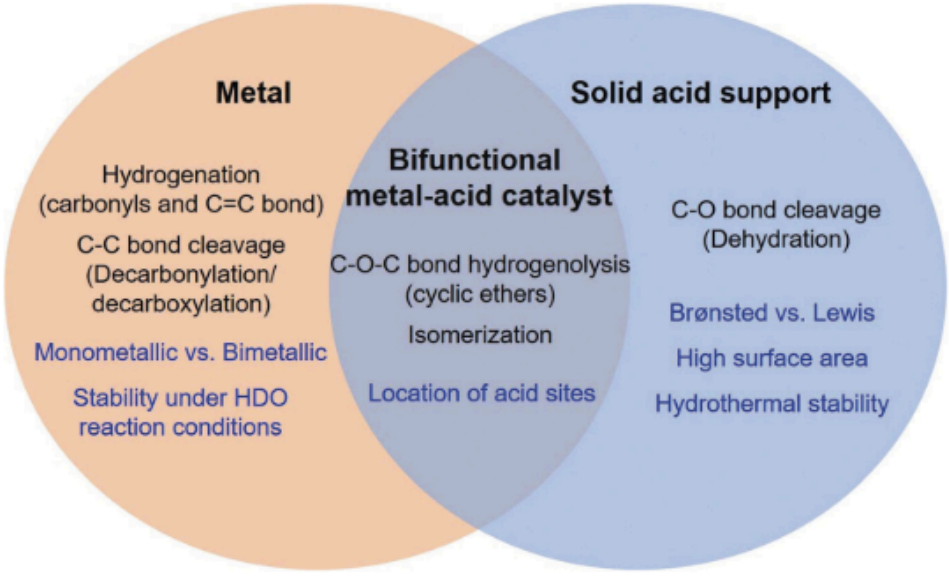

Figure 8: HDO Catalyst design variables, ref. 47.

1.3.1.1 Conventional Hydrotreating Catalysts

As HDO falls in the HDT category, and good results can be obtained with the conventional operating conditions.[23,39] The conventional $CoMo/Al_2O_3$ and $NiMo/Al_2O_3$ are active in their sulfided form. In conventional crudes, this sulfided form can be kept due to high H_2 and H_2S pressures. The H_2S stands for HDS as H_2O stands for HDO, meaning that the sulfur that is removed in HDS is in the form of hydrogen sulfide. However it can be seen in Table 1 that the sulfur content of bio-oils is much lower when compared with conventional crude oil and catalytic activity is dependent on H_2S partial pressure.[5] Thus, an external source of S must be fed to the system to maintain the activity of the catalyst.[5,69,70] This addition of a sulfur source however most likely results in SO_x emissions[4] which are toxic not only for the environment, but also for human health[71] and also contaminate the bio-oil stream.

Performing HDS and HDO simultaneously might be difficult considering the similarities between HDS and HDO sites which represents a mutual inhibition, indicating a competitive adsorption on the same active sites.[40] Moreover, H_2S decreases not only the initial activity for HDO when sulfided $CoMo/Al_2O_3$ catalyst is applied[72] but also the reactivity of phenol.[61] Oxygenated compounds end up poisoning the sulfided sites if adsorbed on the sulfide phase.[73] Nevertheless, it suppresses the hydrogenation/hydrogenolysis reactions, which could be beneficial since it would enable the control of H_2 consumption.[35,72] Furthermore the direct deoxygenation route is preferred in the presence of H_2S.[39,72] Another factor to take in consideration is the water formation in the HDO reaction. Its presence can change the catalyst structure and the geometry of the vacancies if there is not enough amount of S-donating species, which is what happens when dealing with a bio-oil feed. Also the Al_2O_3 support is not thermally stable in the presence of large quantities of water, forming a hydrated boehmite phase which leads to a decrease in surface area.[74,75] In the case of sulfided $NiMo/Al_2O_3$, water presents as the main deactivation agent, not only because of its effect on the alumina support but also because its presence causes the oxidation of Ni.[75] In the sulfided $CoMo/Al_2O_3$ catalyst, the deactivation caused by water happens on the Co-promoted sites, however this happens in a low extent and the effect can be reverted. Thus, Co acts not only as a promoter but also as a stabilizer of the active phase.[76] In Table 2 some examples are presented.

Table 2: Experimental data for conventional HDT catalysts used in HDO.

Entry	Catalyst	H_2 pressure (bar) / Temperature (ºC)	Model Compound	Conversion (%)	Main products
1[77]	CoMo / NiMo*	70 / 280	Guaiacol	57 / 65*	Catechol
2[78]	CoMo	50 / 250-350	Anisole	100 at 300 min	Phenol, *o*-cresol, benzene
3[79]	CoMo / NiMo	34.5 / 250	Guaiacol	54.1 – 77.1/ 37.0 - 91.2	Catechol, phenol
4[80]	CoMo	28.5 / 300	Phenol	30	Methyl substituted benzene, cyclohexene, cyclohexane

***The conversions are separated with / to show the results for each catalysts respectively. Catalysts are also separated by /.**

The conversions on entry 3 depend on the sulfidation method.

1.3.1.2 Alumina Supports

Alumina is widely used as support in acid catalysis. The most used are η-Al_2O_3 and γ-Al_2O_3[81], being the latter considered the most relevant.[82] The γ-Al_2O_3 can be obtained through the calcination, under air, of boehmite, AlOOH.[83] The final characteristics of the γ-Al_2O_3, mainly specific surface area and particle shape and size, depend on the amount of water of the starting boehmite. Moreover, the calcination temperature will define the types of Al_2O_3 that can be obtained. For instance, a pseudo-boehmite, which is a boehmite with a larger amount of water molecules when compared with crystalline boehmite, will yield a poorly crystallised γ-Al_2O_3 with a large surface area, in the temperature range of approximately 300 - 900 ºC.[81]

Alumina presents an acid-base nature, which is dictated by the surface hydroxyl groups. The nature of these types of supports changes with temperature: with increasing temperatures the condensation of neighbour hydroxyls (dihydroxylation) occurs, forming Al-O-Al bonds and water molecules. The catalytic active sites only start to form ate around 300 - 400 ºC. As temperature continues to increase, the number of oxygen vacancies on the surface increases, forming Lewis acid sites. As these increase, the strength of neighbour Brønsted acids also increases. Although it might seem that there are is a large number of Brønsted acid sites in alumina, this type of acidity is actually low, when compared with, for example, zeolites.[81]

The main form of deactivation in this type of support is the deposition of coke, which binds strongly to the alumina.[23,47,75] This happens in a more severe way when dealing with aromatic and phenolic compounds since these are known to be coke precursors.[48] Furthermore, in the presence of water and temperatures between 140 and 380 ºC, the γ-Al_2O_3 tends to return to its boehmite form.[48,75]

1.3.2 Heteropoly acids

1.3.2.1 Introduction

Heteropoly acids (HPA) or polyoxometalates present outstanding properties which makes them good candidates to be catalysts[9,84], in both homogeneous and heterogeneous systems:

1. They can have acidic or redox properties, if chosen adequately;
2. Their structure can be better defined at a more molecular level than other conventional oxide catalysts;
3. They bring unique reaction fields: not only bulk-type I (where the reaction takes place at the surface and in the inner bulk of the catalyst[9,85]) and type II catalysis (the reaction only takes place at the surface of the catalyst) but also shape selectivity;
4. In the case of homogeneous catalysis, the softness of the polyoxometalates increases both activity and selectivity, through intermediate stabilization.

1.3.2.2 Structure

Heteropoly anions can adopt different structures, being the most typical Keggin and Dawson structures. The Keggin structure can be written as $XM_{12}O_{40}^{(8-n)}$, with X being the central or heteroatom, M the addenda or poly-atom and n the charge of the central atom.[84] If we take a 12-tungstophosphoric anion, a well-known Keggin type anion[86], as an example, then the formula will be $PW_{12}O_{40}^{3-}$, presented

in Figure 9. The structure of the of the Keggin unit consists of a central tetrahedron[86], which is formed by the heteroatom and 4 oxygens (ex. PO_4), surrounded by 12 octahedra of the poly-atom and oxygens (ex. WO_6), as it can be seen in Figure 9.

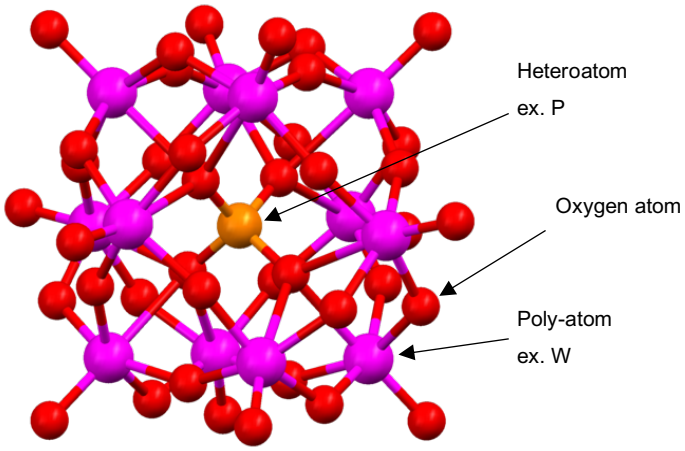

Figure 9: Keggin Unit. The orange ball represents the heteroatom, the red ball represents the oxygens and the pink ball represents the poly-atoms.

Regarding the compensating cation, the heteropoly compounds can be classified in two groups, proposed by Niiyama *et al*[87], presented in Table 3.[9,87]

Table 3: Classification of heteropoly compounds (group A or B) as a function of the nature of the compensating cation.

	Group A	**Group B**
Cation size	Small	Large
Solubility in water and polar solvents	High	Low (hydrophobic[88])
Surface area ($m^2 \cdot g^{-1}$)	1-10	50-200
Amount of water of crystallization	High	Low
Examples	H^+, Na^+, Mg^+	Cs^+, K^+, NH_4^+

The HPA ionic structure is discrete and mobile[89], meaning the cation can move freely throughout the structure.[86] When the compensating cations are H^+ and because of this ion mobility[90], the heteropoly acids are almost pure Brønsted acids.[10]

The hierarchical structure of heteropoly compounds is essential to understand its catalytic properties.[91]

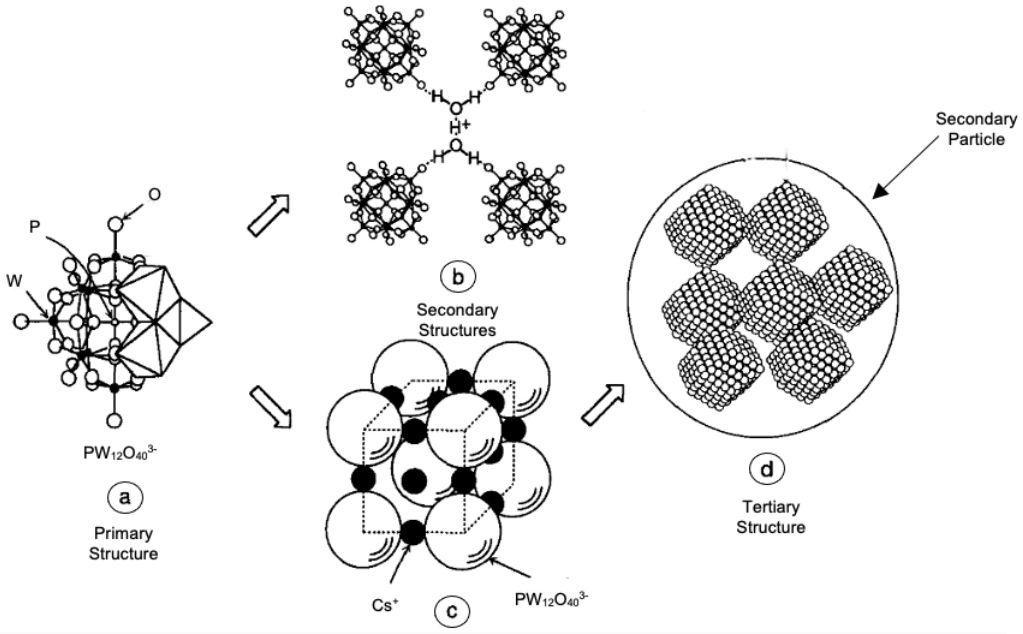

Figure 10: Hierarchical Structure of heteropoly compounds. a) Primary structure; b) Secondary Structure with $H_2O_5^+$ as compensating cation; c) Secondary structure with Cs^+ as compensating cation; d) Tertiary structure. Adapted from ref. 91

The primary structure is the structure of the heteropoly anion itself. The secondary structure is the 3D arrangement of the heteropoly anion (primary structure) and its compensating cations. The secondary structure is very variable and flexible, as it can be seen in Figure 10, b) and c). One anion with the respective compensating cation forms a primary particle. The tertiary structure is the arrangement of primary particles (an arrangement of secondary structures), forming the secondary particles. The tertiary structure is responsible for the particle size, surface area and pore structure.[9] The pores of heteropoly acids and the respective salts are intercrystalline. This means that there are no open pores in the crystalline structure and that the existing pores are formed by spaces between the primary particles, as it can be seen Figure 12 a).[9,92]

Depending not only on the compensating cation nature but also on the amount present, there may be micro pores and meso pores.[93] The acid amount on surface (surface protons) is also greatly dependent on the amount and type of the compensating cation present, as it can be seen in Figure 11.[94]

Table 4: Porosity and surface area of various heteropoly salts. From ref. 93, unless stated otherwise.

Heteropoly salt	Pore Type	Pore size diameter (nm)	Surface Area ($m^2 \cdot g^{-1}$)
H	Non-porous		5
Cs_1	Non-porous		2
Cs_2	Non-porous		1
$Cs_{2.1}$	Ultramicropores	<0.59[91]	
$Cs_{2.2}$[94]	Micropores	0.62-0.75[91]	

$Cs_{2.5}$	Micro and Mesopores	0.5-1 (micro) , 4-5 (meso)[9]	135
Cs_3	Micro and Mesopores	~ 6 (meso)	147

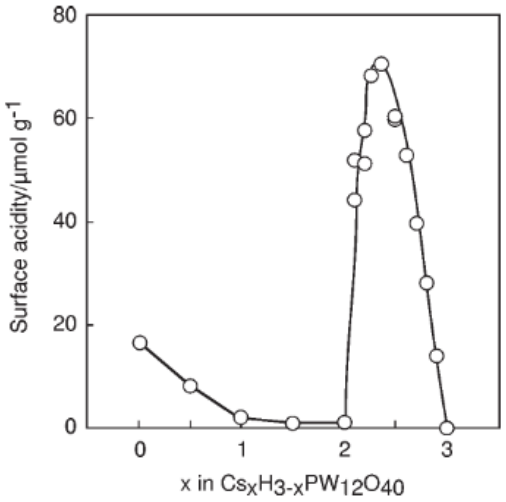

Figure 11: Surface acidity in function of Cs amount. From ref. 92

The heteropoly salts, such as $Cs_{2.5}5H_{0.5}PW_{12}O_{40}$ can be synthesized through a titration method, where a Cs precursor is added dropwise to a solution of the desired heteropoly acid. An important factor during the synthesis is the thermal treatment (TT) or calcination. When preparing the heteropoly salt, the acid form, $H_3PW_{12}O_{40}$, tends to adsorb on the surface of the precipitated $Cs_3PW_{12}O_{40}$, which makes an uneven distribution of the cations. Upon TT, an homogenization of the cations is observed[9,93], as it can be seen in Figure 12 b). However, the Keggin structure is only retained until around 400 ºC.[43]

1.3.2.3 HPA and catalysis

Due to their potential and as aforementioned heteropoly acids and salts have been widely used as acid catalysts. When the compensating cations are only H^+, there might be a need to support the heteropoly acid, not only because it is soluble in water and other polar solvents, but also to increase its low surface area, as it can be seen in Table 4. The loading levels should not be too low, otherwise the interaction between the HPA and the support is too strong and the bulk properties of the bulk heteropoly acid are lost. High loading levels do not report any problems. Generally acid or neutral supports work well with the heteropoly acids. [90,95] Solids that have some basicity, such as Al_2O_3 (Al_2O_3 is amphoteric by nature[81]) tend however to decompose the structure of the HPA, due to strong adsorption on the support with a consequent loss of acidity.

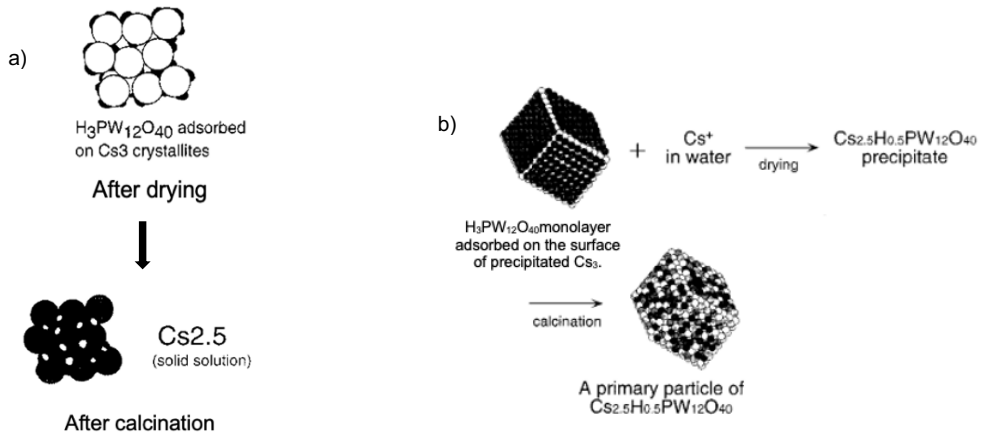

Figure 12: a) Example of pore formation of $Cs_{2.5}H_{0.5}PW_{12}O_{40}$. Adapted from ref. 85. b) Formation of $Cs_{2.5}H_{0.5}PW_{12}O_{40}$ and effect of thermal treatment (calcination). From ref. 91.

The $Cs_{2.5}H_{0.5}PW_{12}O_{40}$ ($Cs_{2.5}$ salt) is particularly active as an acid catalyst, mainly due to the strength and number of acid sites, the high surface area, the presence of mesopores which facilitates the diffusion of reactants and products.[93] This salt has almost the same acid strength as the acid form, $H_3PW_{12}O_{40}$, as observed by ammonia and pyridine TPD experiments. Since the salt's surface area is very large, more than a half of the protons are located near or even on the surface, making them accessible.[9] Moreover, this salt is also water tolerant, mainly due to the fact that is moderately hydrophobic.[88] The $Cs_{2.5}$ salt is active, for example, for the alkylation of isobutane with *n*-butenes to produce an alkylate blend. Commercially applied homogeneous catalysts include HF or H_2SO_4, which are not environmentally friendly, are toxic and corrosive, as opposed to heteropoly acids, which can be considered green catalysts[88]. Okuhara *et al.*[96] tested $Cs_{2.5}$ salt which proved to be active for the alkylation reaction and Mobil patented a supported $H_3PW_{12}O_{40}$ for this reaction[91,97] as well as Guisnet *et al.*[98] and Liu *et al.*[99] who reported Cs salts for alkane isomerization, from *n*-butane to *n*-heptane, reactions where strong acid sites are needed.

1.3.3 HPA in HDO processes

Because they are green (considering safety and quantity of waste issues) and versatile catalysts[88], heteropoly acids and their salts can be used as the HDO catalysts of the future. These acid compounds along with a metal function, given by one of the known metals active for this type of reactions, would be ideal catalysts for HDO reactions. This could be achieved by impregnation of a heteropoly acid solution and a metal promoter solution on a support[58], metal promoter impregnation on $Cs_{2.5}$ salt[68] or even physical mixture of the HPA or $Cs_{2.5}$ salt with a supported metal.[43]

Anderson *et al.*[58] studied de HDO of anisole and 4-propylguaiacol in the presence of $H_3PMo_{12}O_{40}$ (HPA) supported on TiO_2, HPA/TiO_2. Besides the HDO reactions, the authors found alkylation also to be an important reaction once it increases not only the energy density of the products but also the "atom economy" (which is the second of the 12 Principles of Green Chemistry and states that by-products - or waste - should be minimized, with the ideal case being all the atoms that form the reactants also form the desired product).[100] This happens because the methyl group present in the methoxy group, that was once lost in the form of methane migrates to another molecule. Under the same conditions, 300 ºC, 1.01 bar of H_2, and time on stream (TOS) of 7 h, they obtained for anisole 72 % of selectivity into deoxygenated products with a total conversion of 82 % and for the 4-

propylguaiacol a selectivity of 4 % in deoxygenated products and 92 % conversion. In the case of anisole, minimum ring hydrogenation was observed, with cyclohexene being 0.16 C mol % of the product. Of the oxygenated products, 70 % were phenolic compounds. The decrease in anisole conversion was caused by a decrease in the HDO conversion since the alkylation activity remained constant. After 16 h on stream, the catalyst lost 5 % of its activity. In the case of 4-propylguaiacol, the selectivity to fully deoxygenated products was only 4 %, however, the catalysts promoted the deoxygenation of the methoxy group, which, as it can be seen in Figure 6, has a lower bond dissociation energy when compared with the phenolic group. When the mass-averaged contact time was increased from 0.26 h to 0.77 h it was noticed an increase in the selectivity of fully deoxygenation to 61 %, concluding that the activation of $C_{aromatic}$-OH needs higher contact times. The increase on the selectivity of fully deoxygenated products came with the cost of a decrease on the selectivity of alkylated products, thus changing the products distribution. Moreover, this research group concluded that the presence of the oxygen in the aromatic ring influences the alkylation rate: at high HDO conversions there were less alkylated products while, at lower HDO conversions, the selectivity was higher for multi-alkylated products. Concerning the reaction mechanism, it starts with a catalyst surface reduction caused by H_2, which produces an oxophilic Lewis acid vacancy (step 1 in Figure 13) and then the reactant molecule adsorbs on the newly formed Lewis site (step 2 of Figure 13).

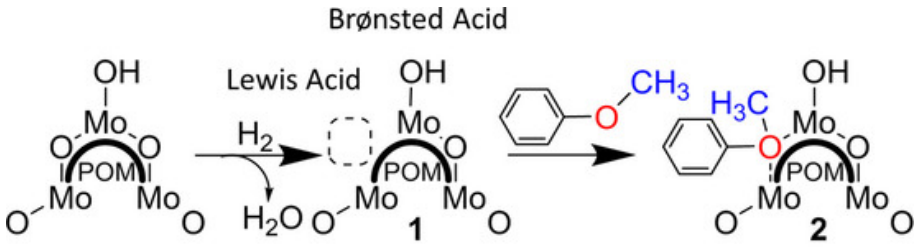

Figure 13: Representation of surface reduction, step 1, and reactant adsorption, step 2.

From here on, there are two possible pathways. The first one will be called A and occurs through the hydrogenolysis of anisole to produce methane. The rest of the molecule can desorb, producing phenol, or it can further react, producing benzene and water. The pathway B does not produce methane, instead the methyl group is transferred to the adjacent Brønsted acid site. This forms a reactive methoxy species, which will lead to inter or intra alkylation. The adsorbed molecule can now desorb or it can further react, producing a deoxygenated product. Both A and B pathways, for the HDO of anisole, can be seen in Figure 14.

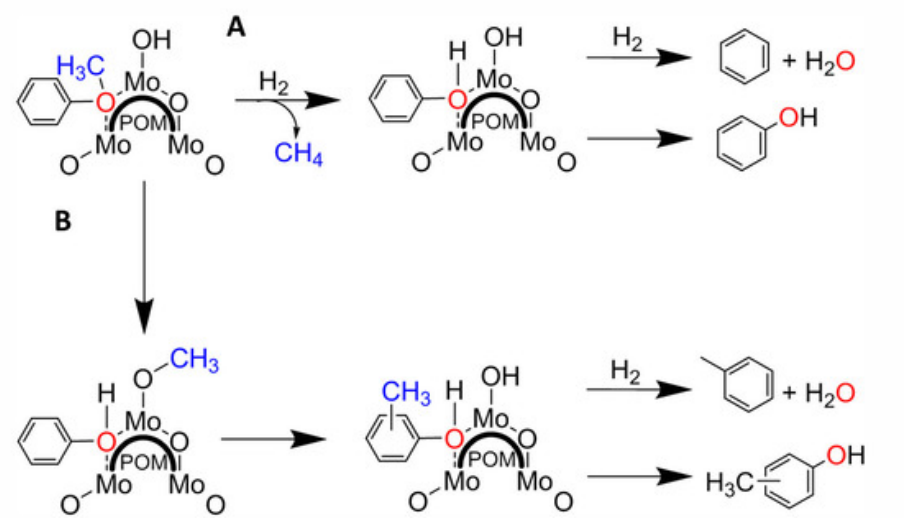

Figure 14: Reaction pathways A and B.

Both Itagaki *et al.*[68] and Prof. Kozhevnikov's research group[43,101,102] have studied HDO with metal supported on $Cs_{2.5}$ salt. Itagaki *et al.*[68] reported Pt/$Cs_{2.5}$ as the best catalyst from the metals studied: Pt, Pd, Rh and Ru, under the conditions of operation, 5 atm of H_2 and 120 ºC, which can be considered mild conditions, for aromatic and phenolic compounds. The support was chosen, not only for the remarkable Brønsted acidity, but also for the ability of the polyanions to stabilize the carbocation-type intermediate. Pt supported on $Cs_{2.5}$ salt showed a better catalytic performance when compared with Pt/C and Pt-Al_2O_3, which did not yield a totally deoxygenated product. With Pt/$Cs_{2.5}$, this group managed to obtain cyclohexane, with a 92% yield from phenol and 68% yield from guaiacol. With guaiacol, however, there was the formation of cyclohexyl methyl ether, however with only 2 % yield.

Kozhevnikov's group studied the HDO of ketones[101,102], esters and ethers[43] at very mild conditions, from 40 to 100 ºC and 1 bar of H_2. For the HDO of ketones, and because dehydration of secondary alcohols on heteropoly acids is fast, the catalysts showed good activity.

Alotaibi *et al.*[102] reported the hydrodeoxygenation of biomass derived ketones, methyl isobutyl ketone (MIBK) and diisobutyl ketone (DIBK), in the presence of the a metal and different supports, such as $Cs_{2.5}$ salt, SiO_2, activated carbon and HZSM-5 at 1 bar of H_2 and temperatures of 100 ºC for the $Cs_{2.5}$ salt support and ranging from 100 to 400 ºC for the other supports. The active carbon showed better performance than the SiO_2 and with increasing temperature it was observed that the conversion decreased, however the selectivity for totally deoxygenated products increased, for both Pt and Pd supported on active carbon. For the HZSM-5, the increase of temperature led not only to an increase of conversion but also to an increase of selectivity to the fully deoxygenated product, methylpentane (MP), as it can be seen in Table 5.

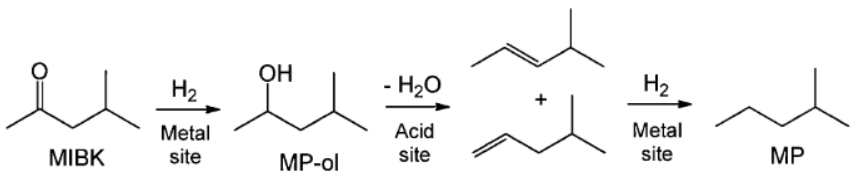

Figure 15: HDO of MIBK over bifunctional metal-acid catalyst.

Table 5: HDO of methyl isobutyl ketone over metal-acid catalysts. From reference 97. 0.20g of catalyst, H2 flow 20 mL·min-1, 4h on stream.

Catalyst	T (ºC)	Conversion (%)	Selectivity to MP-ol (%)	Selectivity to MP (%)
0.5%Pt/SiO_2	100	64	86	14
10%Pt/C	100	95	93	6
10%Pt/C	300	52	9	87
0.5%Pd/SiO_2	100	3	100	0
10%Pd/C	100	95	93	6
10%Pd/C	300	94	5	94
0.5%Pt/HZSM-5	100	94	34	65
0.5%Pt/HZSM-5	200	100	0	83
0.5%Pt/$Cs_{2.5}$	100	99	0	100
0.5%Pt/$Cs_{2.5}$	200	95	0	88
0.5%Ru/$Cs_{2.5}$	100	5	0	100
5%Ru/$Cs_{2.5}$	100	99	0	100

With the $Cs_{2.5}$ salt support, it can be seen, in the case of Pt, that an increase of temperature leads to a decrease both in conversion (slight) and in the selectivity of MP. The other products were *n*-hexane, 3-methylpentane and 2,3-dimethylbutane, all deoxygenated as well. The acid strength of $Cs_{2.5}$ is higher when compared with HZSM-5 and so, the group concluded that a strong acidity is essential for the HDO of MIKB. In the case of Ru, the authors studied the effect on the metal loading, which was found to be beneficial once the conversion increased from 5 to 99 %. The selectivity, however, did not change, being the deoxygenated MP the only reaction product. The group also studied the effect on Pt loading and concluded that an increase of Pt weight in the catalyst leads to higher conversions with a selectivity to MP almost constant, being the Pt supported on $Cs_{2.5}$ a very effective ketone HDO catalyst.

Alharbi *et al.*[43], again from the research group of Prof. Kozhevnikov, studied the HDO of anisole, amongst others, in the presence of a metal supported on $Cs_{2.5}$ salt. The metals tested were Pt, Ni, Ru and Cu. The reaction occurred also under mild conditions, with 1 bar H_2 and temperatures from 60 to 100 ºC. The catalysts were prepared by impregnation of a suitable metal precursor onto the acidic support and also a physical mixture of the metal supported on activated carbon or silica, with the $Cs_{2.5}$ salt after a calcination at 150 ºC and 10^{-3} kPa, for 1.5 h. This group also tested separately acid and metal catalysts for HDO of anisole. With the acid catalyst alone, the conversion of anisole was only 19 % and the main product yielded was phenol. With metal catalyst only, tested with Pt/C, the conversion of anisole was 100 % with selectivity to cyclohexane of 83 % and toluene of 12 %, both fully deoxygenated products. Thus, the metal function plays the main role in the HDO. It is important to highlight that methanol was also produced in these reactions, with 80 – 99 % selectivity based on anisole conversion, which is not shown. The physical mixture of Pt/C/$Cs_{2.5}$ salt with a total Pt loading of 0.35 % gave an almost 100 % yield to cyclohexane (between 98 and100% for reaction temperatures between

80 and 100 ºC), with 20 h on stream. This catalyst was even active for temperatures as low as 60 ºC, with a 90 % yield to cyclohexane (100 % conversion and 90 % selectivity). The same results were obtained for Pt/SiO_2 /$Cs_{2.5}$ with a total Pt loading of 0.5 %. Regarding impregnation, the metal precursor influences the activity, which can be observed in the case of the 0.5 % $Pt/Cs_{2.5}$. The group explained these findings by the dispersion of the metal on the support: the smaller the dispersion, the larger the Pt particles and, consequently, the more resistance to deactivation. it is. As it can be seen, the addition of a metal function increases the selectivity to deoxygenated products. The other metal-supported catalysts tested, 5 % Ru, 10 % Cu and 10 % Ni on $Cs_{2.5}$ salt were not as active as the Pt one. The conversion for the Ru catalysts (64 %) was the highest, with a 86 % selectivity to cyclohexane and the Cu was the lowest (7 %), with a 63 % selectivity to cyclohexane. Therefore, the order of the activity of metal supported onto $Cs_{2.5}$ is Pt ≫ Ru > Ni > Cu. The performance of the catalysts relies highly on their preparation process. In the case of anisole, the physical mixtures of Pt/C or Pt/SiO_2 with $Cs_{2.5}$ showed higher activity and this is thought to be because of the higher distance between proton and metal sites. A higher distance between the two types of active sites would mean that the formation of coke is inhibited and therefore less coke is produced. The group showed yet the mechanism for the production of cyclohexane, which in most cases is the primary product, which involves the hydrogenation of the aromatic ring in the Pt sites first, followed by demethoxylation on the acid sites, forming cyclohexene, which is then hydrogenated to cyclohexane in the Pt sites.

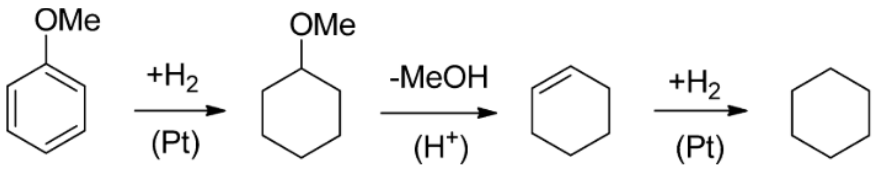

Figure 16: Reaction mechanism for the HDO of anisole for the formation of cyclohexane.

Poole *et al.*[101] went further and studied the effect of the presence of gold on the HDO of ketones with $Pt/Cs_{2.5}$ and 1 bar of H_2 and 40 to 80 ºC. They demonstrated that with the addition of Au there is the creation of a Pt-Au alloy (demonstrated by STEM-EDX and X-Ray Diffraction (XRD)), which decreases the rate of catalyst deactivation and increases the rate of the first catalytic step, which is the hydrogenation of the ketone to a secondary alcohol, on the metal sites. The Pt-Au ratios range from 0.5 to 7.7. The catalyst preparation was done by co-impregnation and sequential impregnation of the metals on the support with an adequate metal precursor and with mechanical mixtures of the metal-supported carbon and $Cs_{2.5}$ salt. The metal loadings ranged from 0.28 to 5.8 % of Pt and 0.35 to 4.3 % Au. In agreement with Alharbi *et al.,* the preparation of the catalyst plays a primary role on the catalyst's performance. Co-impregnation showed to be the best method and the mechanical mixture the worse, with a decrease in the conversion of the ketone. This effect is thought to be caused by the alloying in the case of co-impregnation and the lack of proximity between metal and proton site in the case of the physical mixture. The authors believe that the addition of Au as a promoter increased the hydrogenation of C=O bond and gave preference over C=C hydrogenation. Without the presence of Au, the reaction rate is highly dependent on the dispersion and on the loading of Pt. When the Pt loading increases, the

particle size increases and the consumption of H_2, measured by O_2-H_2 titration, also decreases. When the Au promoter is added, regardless of the Pt particle size, there is an increase in the turnover rate. The deactivation of the catalyst was caused by coke formation through the oligomerization of alkane intermediates and increased with increasing support acidity.

1.4 Thesis Objectives

Given the issues raised by the high oxygen content of bio-oil and the high HPA catalytic potential, the main objective of this work is to prepare, characterize and test the catalytic performance on HDO catalysts comprising heteropoly acids.

For that matter, and based on the HDO catalysts reviewed before, three bifunctional metal supported alumina catalysts were chosen as supports: 1 wt. % Pt on γ-Al_2O_3, an industrial NiO on Al_2O_3 and a Ni on a boehmite calcined at 600 ºC to produce γ- Al_2O_3. The introduction of the heteropoly acid was done in two different ways to study how it would influence the final catalytic performance. The first way was by incipient wetness impregnation of the HPA onto the supports while the second was through a physical mixture of the supports with a synthetized cesium salt. Nine different catalysts were obtained, including the raw supports, the impregnated and physically mixed catalysts.

The characterization through X-Ray Diffraction and UV-Visible Diffuse Reflectance Spectroscopy (Uv-Vis DRS) was done to better understand the active phases of the catalysts, meaning the metallic and acid phases and functions. Temperature Programmed Reduction (TPR) was done to study the reducibility of the nickel catalysts, H_2/O_2 Titration to study the metallic dispersion of platinum, Thermogravimetric Analysis(TGA) to study the water content of the heteropoly acid and also the spent catalysts. It would be also interesting to study the textural properties of the supports and mainly the cesium salt, that has the potential to be used as a support by itself instead of physically mixed only. Furthermore, a lot of information could also be obtained from Infrared Spectra, such as the confirmation of the Keggin structure and also would give information about the coke that might have deposited on the surface of the catalyst, by comparing the spectra of spent and fresh catalysts.

The catalytic tests were carried out at 300 ºC and under atmospheric pressure, with guaiacol, and allowed the study of possible HDO products, giving insight on the favored mechanism and products with different types of catalysts using low pressures. This catalytic study allowed the different catalysts to be compared and to evaluate in more details the role of the heteropoly acids in the guaiacol HDO reaction.

2. Experimental Methodology

In this chapter, the methodologies used for catalyst synthesis, characterization and performance will be presented. It is divided in three subchapters: catalysts preparation, catalysts characterization and catalytic tests.

2.1 Catalysts preparation

Nine catalysts were prepared. Three of them are the supports themselves, three are the HPW impregnated on the three supports and the last three are physical mixtures of cesium salt and the supports. The supports are a commercial 1 wt. % Pt-Al_2O_3, an industrial 25 % NiO on alumina (NiO25-Al_2O_3), which is then reduced to form Ni on alumina and Ni28-Al_2O_3, which is 25 wt. % nickel on PURAL SB calcined at 600 ºC. PURAL SB is a pseudo-boehmite that when heated at temperatures between 450 and 700 ºC[103] under air flow, becomes γ-Al_2O_3.[81,103]

2.1.1 Materials

The tungsten heteropoly acid, $H_3PW_{12}O_{40}\cdot x\ H_2O$ (HPW) was purchased from ThermoFischer (Kandel) GmbH, Cesium Acetate (95%) from Fluka, Platinum on Alumina (1 wt.% of Pt) from Sigma-Aldrich, PURAL SB (Al_2O_3, 70.3 %) from Condea, Nickel (II) nitrate hexahydrate (99 %) from Merck and NiO25-Al_2O_3.

2.1.2 Cesium salt

The $Cs_{2.5}$ salt was prepared according to Okuhara *et al.*[93], by adding the appropriate amount of cesium precursor solution (0.04 mol·dm^{-3}) dropwise to an aqueous solution of HPW (0.01 mol·dm^{-3}) with continuous and vigorous stirring (J.P. SELECTA AGITAMATIC-N), at room temperature. In this case, 20 mL of cesium acetate was added to 50 mL of HPW solution. As the cesium acetate is added, the Cs salt starts to precipitate, forming a milky looking solution. This solution was left aging overnight and then washed several times by centrifugation (Centurion Scientific – C2 Series, 4 washings 6000 rpm, with times ranging from 15 to 20 min each). The yield of this process was calculated considering that all HPW was transformed into $Cs_{2.5}$ salt and it was 69 wt. %. The powder obtained was calcined in air in a muffle (Nabertherm) at 350 ºC for 2 h, with a heating rate of 5 ºC·min^{-1}, for an even distribution of the cations.

2.1.3 Preparation of the supports

The platinum on alumina support (1 wt.% Pt) was purchased from Sigma-Aldrich. The industrial NiO on alumina was not synthesized, however it needed to be reduced to obtain Ni in its metallic form. The third support, Ni28-Al_2O_3 was the only one prepared in our laboratory. The following paragraph details the steps for the preparation of the latter support.

Firstly, the PURAL SB was calcined in air in a muffle (Nabertherm). The heating rate was 5 ºC·min^{-1} until 600 ºC, followed by a plateau of 5 h. A solution of nickel precursor, in this case nickel nitrate (6 mol·dm^{-3}), was prepared and then impregnated onto the support, by incipient wetness

impregnation (IWI), which consists of impregnating only the necessary amount of solution to completely fill the volume of the pores of the support.[104] The volume of solution impregnated was 3.5 mL to 3.05 g of calcined PURAL SB. With the volume of solution impregnated, the amount of Ni added to the support was calculated and it was 28 %. The resulting slurry was left to dry overnight at 120 ºC. The powder obtained was treated, in a reductive atmosphere, to reduce Ni and to decompose the nitrate, which occurs ate around 400 ºC.[105] When decomposing metal salts for catalyst preparation, it is a common procedure to carry out a calcination in air and after, to reduce the metal oxide in a reductive atmosphere. However, Bartholomew *et al.*[105] reported that a more complete Ni reduction is obtained if the decomposition of nitrate is done in a hydrogen atmosphere rather than an air one. The same thermal treatment was applied to both Ni28-Al_2O_3 and to the NiO25-Al_2O_3. The heating rate was 5 ºC·min^{-1} with a flow of 60 mL·min^{-1} of N_2 until it reached the final temperature of 450 ºC, followed by a plateau of 30 min at this temperature. Then, a H_2 flow (20 mL·min^{-1}) was added to complete a total flow rate of 80 mL·min^{-1} (N_2 and H_2), during 4 additional hours.

2.1.4 HPW Impregnated On The Supports

An aqueous solution of 0.01 mol·dm^{-3} of HPW was prepared and then used for impregnation onto the supports, by incipient wetness impregnation. Moreover, for characterization purposed, HPW was also impregnated onto PURAL calcined at 600 ºC. Because the solution of HPW was diluted and the volumes impregnated were small, the density of solution was assumed to be 1 g·mL^{-1} (the same as the solvent, water). Based on the volume impregnated, the amount of HPW and W were calculated and can be observed in Table 6.

Table 6: HPW and W content onto the three supports and PURAL SB calcined at 600 ºC.

Support	**Pt-Al_2O_3**	**NiO25-Al_2O_3**	**Ni28-Al_2O_3**	**PURAL c. 600 ºC**
m support (g)	0.4718	1.3565	1.0460	1.16
m HPW impregnated (g)	0.4392	1.224	0.8826	1.1206
HPW (wt. %)	18	16	18	20
W (wt. %)	1	1	1	1

The obtained materials were left to dry overnight at 120 ºC. The final powders were treated in an inert atmosphere. The same thermal treatment was applied to all the HPW supported catalysts. The heating rate was 5 ºC·min^{-1} with a flow of 60 mL·min^{-1} of N_2 until it reached the final temperature of 350 ºC. When this temperature was reached, there was a 2 h plateau.

2.1.5 Physical mixture of supports - $Cs_{2.5}$

After thermal treatment of the three supports and also of the Cs salt, physical mixtures between each support and $Cs_{2.5}$ were made, comprising 20 wt. % of the salt. The powders were ground until an homogeneous mixture was obtained.

2.1.6 Aggregates size

In order for aggregate size not to be a differentiator factor between catalysts in the course of the reaction, to avoid diffusional problems, after all the catalysts were prepared, pellets were made from the resulting powders. The applied pressure was 1 ton and after these were gently crushed and sieved to 63-125 μm aggregate size.

2.2 Catalyst characterization

2.2.1 Powder X-Ray Diffraction

Powder XRD allows the study of crystalline structures through inter-reticular plan distance.[104] It can be used for crystal size measurement or phase identification, for example.[106] The phase identification is carried out by analyzing simultaneously the position (2θ angles) of the diffractograms peaks and their intensity. With the obtained diffractogram and Crystallography Open Database (COD) database, a free database, it is possible to identify most of the present phases. The diffractograms were recorded on a Bruker D8 Advanced X-Ray Diffractometer, with Cu Kα radiation (1.5406 Å) and equipped with a 1D LYNXEYE XE detector. The measurement conditions were the following: 40 kV–40 mA, a step size of 0.05 º (2 Theta), a step time of 1s; a Ni filter was also used to remove Cu Kβ contribution.

2.2.2 H_2 Temperature Programmed Reduction

H_2 Temperature Programmed Reduction (or TPR) is used to evaluate the reducibility profile of supported metal oxides.[107] The profiles were recorded on a micrometrics AutoChem II by using the following experimental conditions: a) 50 mg of sample, b) gas flow of 30 $cm^3 \cdot min^{-1}$(5% H_2 diluted in Ar), c) heating rate of 10 ºC·min^{-1} until 900 ºC.

2.2.3 H_2/O_2 Titration

H_2/O_2 titration was used to determine the metal dispersion of the Pt- Al_2O_3 support. This method consists in the injection of O_2 pulses, followed by H_2 pulses, on a reduced sample at 35 ºC. This method has a higher sensitivity due to a threefold increase in the O_2 reaction stoichiometry over the direct H_2 chemisorption, as it can be seen in Equations (1) to (3), for the case of Pt metal. The equipment used was a micrometrics AutoChem II, the volume of the loop that injects both H_2 and O_2 was 0.07 cm^3 and the mass of the sample was about 200 mg. The metal dispersion was calculated from Equation (4), where MM_{Pt} is the atomic mass of Pt, $V_{H2consumed}$ is the total volume of H_2 that is consumed by the sample, V_{molar} is the molar volume, x Pt is the Pt content in the sample and Stoich. H_2:Pt is stoichiometric amount of H_2 in relation to Pt.

$$\mathrm{Pt} + \frac{1}{2}\mathrm{H_2} \rightarrow \mathrm{PtH} \quad (1)$$

$$2\ \mathrm{PtH} + \frac{3}{2}O_2 \rightarrow 2\ \mathrm{PtO} + \mathrm{H_2O} \quad (2)$$

$$\mathrm{PtO} + \frac{3}{2}H_2 \rightarrow \mathrm{PtH} + \mathrm{H_2O} \quad (3)$$

$$D_M = \frac{MM_{Pt} \times \frac{V_{H_2\,consumed}}{sample\ mass} / V_{molar}}{\frac{x\ Pt}{Stoich.\ H_2:Pt}} \quad (4)$$

From the metal dispersion, it is possible to calculate the mean particle size of the metal, through Equation (5)[108], where d_{mp} is the mean particle size, D_M the metal dispersion, v_{Pt} the volume occupied by an atom of Pt in the bulk of the metal and a_{Pt} the area occupied by a Pt atom on a polycrystalline surface, assuming a spherical particle. The values used for all Equations 1 to 5 are present in Appendix A.

$$d_{mp} = \frac{6}{D_M} \times \frac{v_{Pt}}{a_{Pt}} \quad (5)$$

2.2.4 Thermogravimetric Analysis

The thermogravimetric studies allow to determine and quantify transformations on the catalyst that occur at different temperatures, namely the loss of water of crystallization and coke deposited on the catalyst. Two cycles of temperature were applied to the sample, with the first being the cycle of the analysis itself while the second cycle was used to remove the Archimede effect on the apparent mass loss and the effect of the heat flow. The analysis was carried out on a Setaram SETSYS Evolution 16. For the analysis of the heteropoly anion the mass of the sample was 20 mg, and temperatures ranged from 25 to 250 ºC. For the analysis of the spent catalysts, the mass of the samples was 15 mg and temperatures ranged from 25 to 800 ºC. Temperature profiles for the two types of analysis done are presented in Appendix B.

2.2.5 UV-Visible Diffuse Reflectance Spectroscopy

Ultraviolet-Visible Diffuse Reflectance Spectroscopy (UV-Vis DRS) was used to study the catalysts absorption spectroscopic properties, especially the presence of the Keggin structure during synthesis. Equation (6) is the Kubelka Munk function, describing an infinitely thick layer (where both light absorption and light scattering occur), and is analog to the absorbance transformation of transmission spectroscopy, with K, S and R being respectively, the absorption, scattering and diffuse reflectance.[109]

$$\mathrm{F(R)} = \frac{K}{S} = \frac{(1-R)^2}{2R} \quad (6)$$

The apparatus used was a Varian Cary 5000 with wavelengths ranging from 200 to 800 nm, with a Praying Mantis (integration sphere) accessory for DRS measurements.

2.2.6 Infrared Spectroscopy

This technique was used to study the presence of the heteropoly acids on the supports. It allows the observation of the vibrational fingerprint of molecules with permanent dipoles through absorption of infrared radiation.[110] The apparatus used was a Nicolet 6700 FTIR from ThermoScientific, with wavenumbers between 4000 and 400 cm^{-1} and a 4cm^{-1} resolution (64 scans). The technique used was KBr in transmission mode, which was then converted in absorbance. Samples were diluted (1 wt.%) in KBr and then pressed at 8 tons to get a final pellet for transmission measurements.

2.2.7 N_2 sorption measurements

Nitrogen adsorption was used to measure the isotherms and obtain the BET (Brunauer, Emmett and Teller) surface area and also the total pores volume. The measurements were carried out on a Micromeritics ASAP 2010 analyzer. Prior to N_2 sorption, samples were outgassed under vacuum at 90 ºC for 1h and then at 300 ºC for at least 4h.

2.3 Catalytic tests

2.3.1 Materials

The materials used for the catalytic tests were guaiacol (≥ 98.0 %) from Sigma-Aldrich, *n*-heptane (≥ 99.5 %) from Merck and ethylbenzene from Sigma-Aldrich (> 99 %).

2.3.2 HDO Reaction

The reaction was carried out on a pyrex fixed bed tubular reactor (internal diameter of 1 cm). The feed consisted of a liquid solution of 5 % of guaiacol (% v/v) with n-heptane as a solvent, with a total flow rate of 3 $mL \cdot h^{-1}$, corresponding to 0.15 $mL \cdot h^{-1}$ of guaiacol. The liquid solution was fed to the reactor through a pump (776 Dosimat, Methrom). Both the H_2 and the liquid feed entered the reactor from the top. The H_2 to guaiacol molar ratio was 50, with a H_2 flow rate of 2 $L \cdot h^{-1}$, controlled by a mass flow controller (Model 400, Hastings Instruments). At the bottom, a glass collector vase was assembled to collect the reactor effluent at 10, 20, 40, 60, 80, 100 and 120 min of time on stream. At 120 min (2 h), the reaction was stopped. At the beginning of the reaction, ice was added to the collector vase in order to condensate the majority of the gaseous effluent (although the feed was in liquid phase, at the temperature of the reaction it would turn to gaseous phase). However, probably some products that did not condensate were flushed away and lost. For all the catalytic tests, the temperature was set at 300 ºC on a ThermoLab oven and controlled with a thermocouple at atmospheric pressure. The reactor was packed with 100 mg of catalyst with an aggregate particle size of 63-125 μm. Prior to the beginning of

the reaction, the catalyst was pre-treated with H_2 at the reaction temperature, for 1 h. The reaction set up can be seen in Appendix C.

2.3.2.1 Control reaction

After all catalysts were tested, a control reaction was carried out with only *n*-heptane (the solvent without guaiacol) to verify if there was any *n*-heptane transformation. The reaction conditions were the same that were applied for the HDO reactions, with the exception of the flow rates. There was no guaiacol flow and the flow rate of *n*-heptane was 3.0 $mL \cdot h^{-1}$. This was performed with the catalyst that showed the highest conversion, $NiO25\text{-}Al_2O_3/Cs_{2.5}$.

The chromatograms obtained can be seen in Appendix D. As it was mentioned, the retention time of benzene (around 4.6 min, Appendix E) overlaps with the peaks of the possible products that resulted from *n*-heptane transformation. The criterion for considering benzene a product was based on the number of peaks of the chromatogram of each sample analyzed. If there was only one peak between the initial time and the *n*-heptane retention time (around 5.4 min), then it was considered benzene. If there were multiple peaks, like the ones seen in Figure 68 (Appendix D) then it would not be considered benzene.

2.3.3 Products analysis

Product Analysis was done by Gas Chromatography (GC) of the condensed reactor effluent on a Perkin Elmer AutoSystem Gas Chromatograph, with N_2 as the carrier, with a Flame Ionization Detector (FID) with an air and H_2 flame and a DB-5MS column from Agilent (30 m length × 0.250 mm internal diameter × 0.25 μm film thickness). The temperature profile of the GC column is presented in Figure 17.The temperature of the detector was 275 ºC.

§

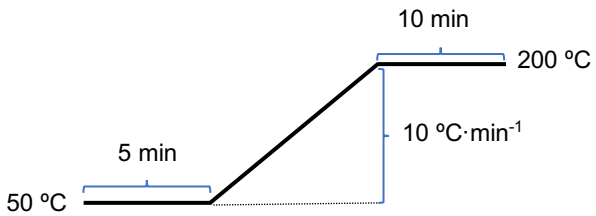

Figure 17: GC column conditions during analysis.

The peak areas were measured with the software CSW 32 (Datapex) and ethylbenzene was used as an Internal Standard (IS) by adding 3 wt.% to the liquid samples collected from the reaction. Prior to the reaction, the IS method was applied to collect the response factors (RF) of both reagent (guaiacol) and main expected products (anisole, benzene, cyclohexanone, phenol) to achieve reliable values of peak areas and consequently conversion and selectivity results. In Equation (7), the ratio of areas is proportional to the ratio of mass concentrations, with the slope being the RF.

$$\frac{Area_i}{Area_{IS}} = RF \times \frac{Concentration_i}{Concentration_{IS}} \quad (7)$$

As an example, the methodology for the determination of the RF of guaiacol is presented. The determination of RT and RF of products is present in Appendix E but the procedure was the same. For the case of guaiacol, a solution of 3 wt. % of IS (constant) was prepared, with the solvent being *n*-heptane. Guaiacol was then gradually added to this solution to achieve higher reagent concentrations. The samples were injected in the chromatograph and the mass ratio of guaiacol and IS as a function of areas ratio of the same components was plotted, being the RF of guaiacol determined to be 1.06 as it can be observed Figure 18.

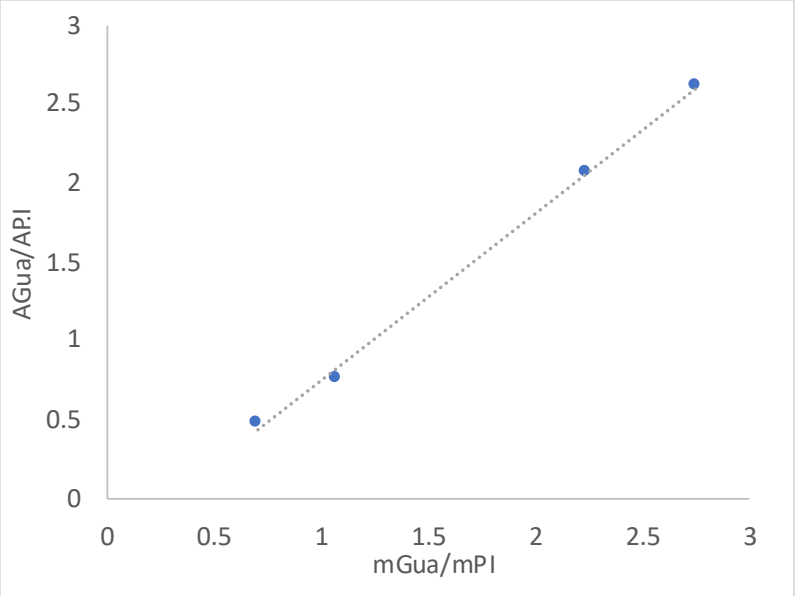

Figure 18: Calibration curve of guaiacol (GUA). y = 1.06x - 0.31; R^2=0.998

With the RF determined, the area of each component could be correctly calculated. However, there were compounds present in the chromatograms that were unidentified. These were called UX, where U stands for unknown, and X is a number for differentiation purposes. For these compounds, the RF used was 1. Having the corrected peak areas, the conversion ($x_{guaiacol}$) was calculated as in Equation (8), yield (Y_P) from Equation (9) and selectivity (S_P) from Equation (10).

$$x_{guaiacol} = 1 - \frac{Area_{guaiacol}}{\sum Area_i} \quad (8)$$

$$Y_P = \frac{Area_P}{\sum Area_i} \quad (9)$$

$$S_P = \frac{Y_P}{x_{guaiacol}} \quad (10)$$

3. Results and Discussion

In this chapter, the results obtained will be shown, analyzed and discussed. Their presentation will be organized in four groups: heteropoly acids, platinum alumina catalysts (Pt-Al_2O_3), nickel on PURAL SB calcined at 600 ºC (Ni28-Al_2O_3) and industrial nickel oxide catalysts (NiO25-Al_2O_3).

3.1 Catalysts characterization

3.1.1 Heteropoly acids

3.1.1.1 Structural Analysis

X-Ray Diffraction was done for samples HPW and $Cs_{2.5}$ salt ($Cs_{2.5}H_{0.5}PW_{12}O_{40}$). Concerning $Cs_{2.5}$ salt, two batches were produced and XRD results confirmed that the structure was the same, confirming the reproducibility of the synthesis method. The diffractograms were then compared with a thermal treated $Cs_{2.5}$ salt to observe if the structure remained unchanged after the treatment (Appendix F), which was confirmed. Both HPW and thermal treated $Cs_{2.5}$ diffractograms can be seen in Figure 19 and Figure 20.

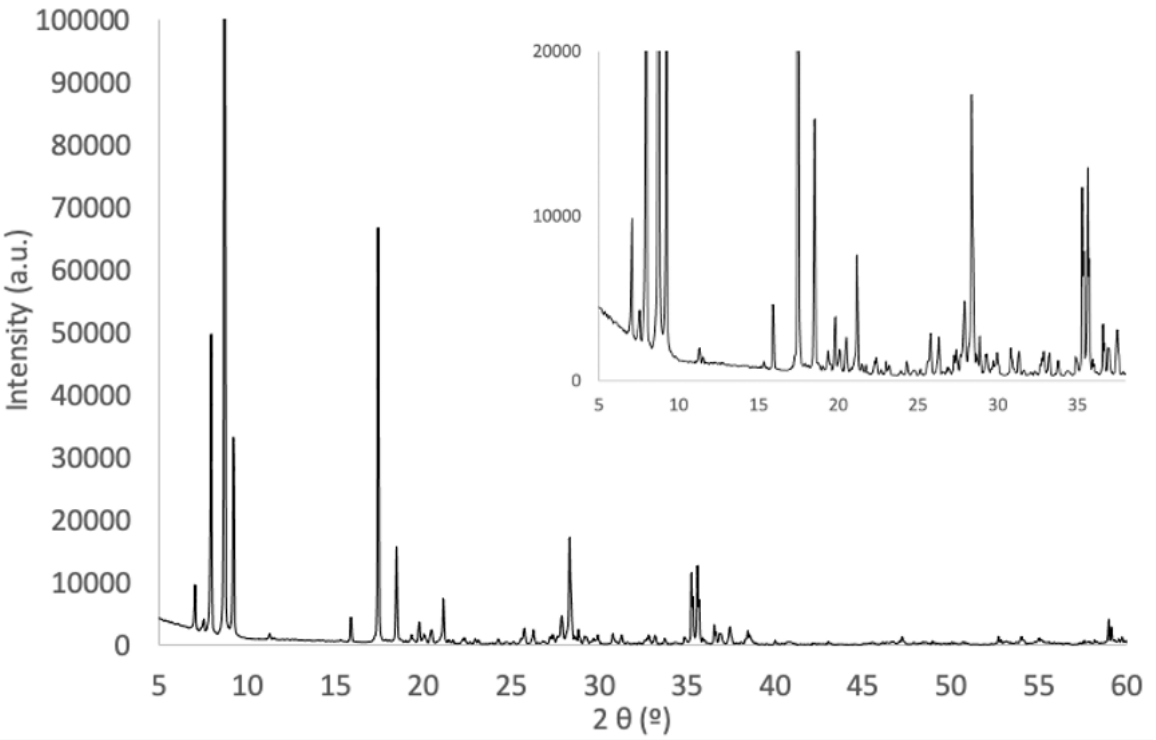

Figure 19: X-Ray Diffractogram of HPW. On the upper right side is a zoom between 5 and 38º.

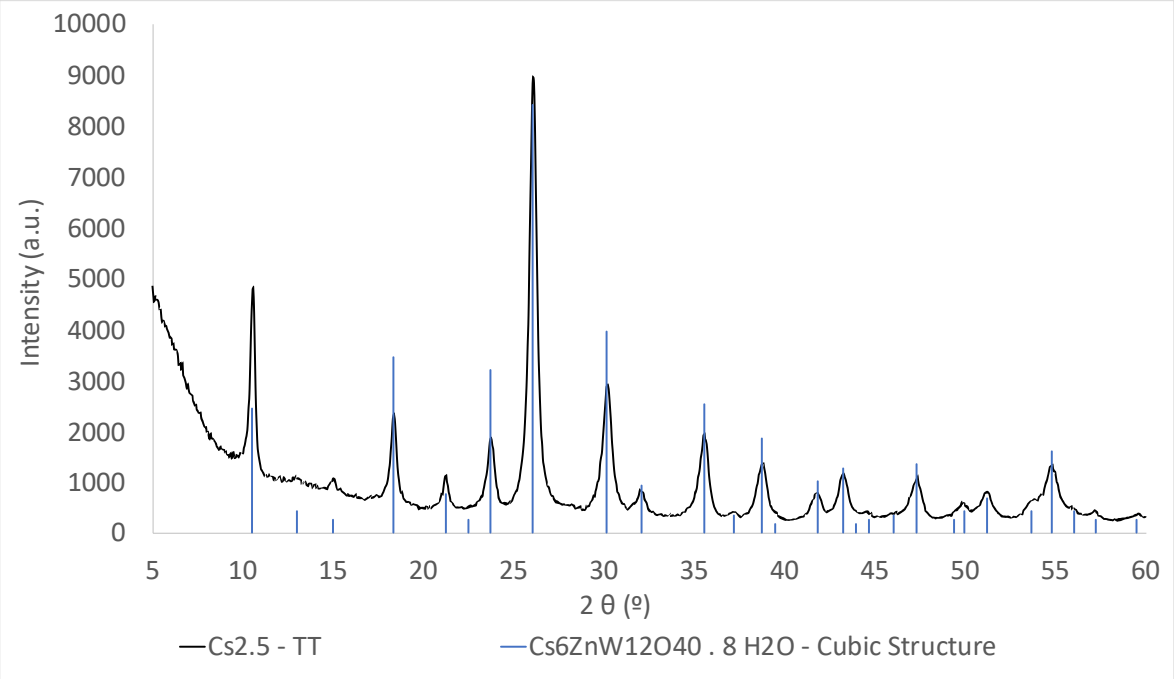

Figure 20.: X-Ray Diffractogram of Cs2.5 salt compared with $Cs_6ZnW_{12}O_{40}\cdot 8H_2O$ (PDF 43-0001)

Concerning HPW sample (Figure 19), no reasonable match with Crystallography Open Database was found as the diffractogram obtained is not in agreement with some studies.[92,111] The peaks reported in literature for HPW presenting a cubic structure appear at 10.3 º, 25.3 º and 35.6 º, with the one at 25.3 º being the most intense[111]. This mismatch could be explained by the amount of crystallization water present. Crystalline structure of heteropoly acids can change depending on the number of crystallization water present.[9,91,112]. It is however important to mention that the water amount determined by TGA, which corresponds to 6 molecules per $H_3PW_{12}O_{40}$ molecule does not match the diffractograms found in the literature for this amount of water.[92] The HPW diffractogram however shows some similarities with the diffractogram obtained by Alotabi *et al.*[113]and by Xiao *et al.*[114] that reported three main peak groups that can also be observed, with a slight shift to lower angles, in Figure 19: between 7 and 10 º, 18 and 24 º and 26 and 30 º. For the $Cs_{2.5}$ material, diffractograms are in agreement with some authors.[93,113] The most intense peak appears at around 26 º. This slight shift from 25.3 º (expected for HPW with a cubic phase) to a higher angle (26 º for the $Cs_{2.5}$ salt) is commonly seen in Group B salts[111], such as the case for Cs salts. The diffractogram in question was yet compared with another cesium heteropoly acid salt, $Cs_6ZnW_{12}O_{40}\cdot 8H_2O$ (PDF 43-0001), and confirmed a cubic structure, that can be observed in the diffractogram of Figure 20. Also, when comparing of Figure 19 and Figure 20 it is possible to observe a peak broadening for the $Cs_{2.5}$ salt material which might be attributed to a decrease of the particle size when the HPW is transformed into $Cs_{2.5}$ salt. Also, it was observed an alteration on the unit cell parameters which can be attributed to the bond length variation that occurs when there is a change on the heteropoly acid counter cation.[9]

3.1.1.2 Optical Properties

UV-VIS DRS was carried out for the $Cs_{2.5}$ salt and for the HPW and the results can be seen in Figure 21. The spectra presented are very similar. Both have a peak at 260 nm that can be attributed to the presence of the $PW_{12}O_{40}^{3-}$ anion.[115,116] The cesium salt presents a peak at 305 nm that resembles the HPW peak at 307 nm but with a slight blue shift. The HPW spectrum shows yet a shoulder at around 350 nm due to the presence of octahedral tungsten species like the species present in the heteropoly acid's Keggin structure.[116,117]

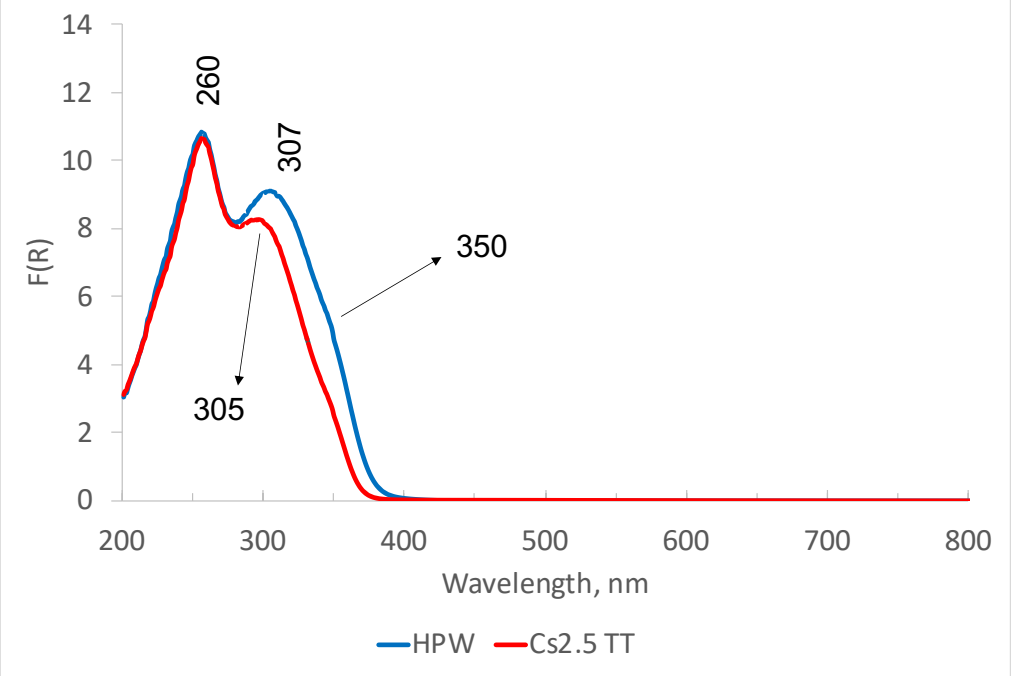

Figure 21: UV-Vis DRS spectra of HPW and thermal treated Cs2.5 salt.

In order to study the behavior of HPW on alumina, which is present on all nine catalysts prepared, the UV-Vis DRS analysis of HPW/PURAL SB calc. at 600 ºC, a γ-Al_2O_3 support, was done. The 305 nm peak is lost when the HPW is impregnated onto calcined PURAL, Figure 22. This was also reported by Sudhakar *et al.*[115] when this research group supported HPW on a mesoporous silica material. A shoulder at around 210 nm can be observed and is attributed to the presence of γ-Al_2O_3[118]. However, the characteristic Keggin structure can still be seen at 260 nm, confirming the presence of this structure onto the support.

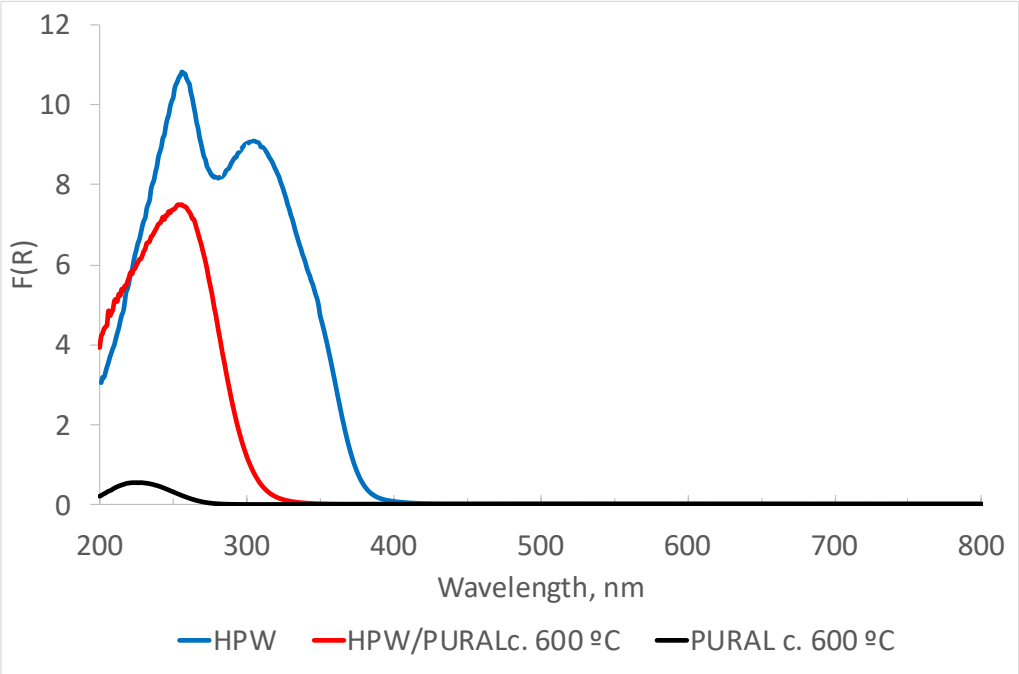

Figure 22: UV-Vis DRS spectra of HPW and HPW/PURALc. 600 ºC.

Regarding Infrared Spectroscopy, the spectra for HPW and $Cs_{2.5}$ salt can be seen in Figure 23. As it can be observed, both the HPW and $Cs_{2.5}$ salt present bands at relatively same wavenumbers. These are at 1078, 981 cm^{-1} for both materials, 908 and 783 cm^{-1} for HPW and 885 and 771 cm^{-1} for the $Cs_{2.5}$ salt. These are in fact in agreement with the literature[9,119,120], with all the fingerprints of the Keggin units, below 1100 cm^{-1}, as it ca be seen from Table 7.

Table 7: IR bands for $H_3PW_{12}O_{40}$ (HPW).From ref. 82.

Vibrational Frequency	**P-O**	**W=O**	**W-O-W**	**W-O-W**
Wavenumber (cm^{-1})	1080	982	893	812

The bands at 1600 cm^{-1} for HPW (more intense) and 1625 cm^{-1} for $Cs_{2.5}$ salt (less intense) are attributed to the bending vibration of crystallization water. Koyano *et al.*[121] attributed the bands at 3570 cm^{-1} for the HPW and 3395 cm^{-1} for $Cs_{2.5}$ salt to $H_5O_2^+$. From the spectra of both materials, it can be concluded that the HPW is more hydrated than the $Cs_{2.5}$ salt.

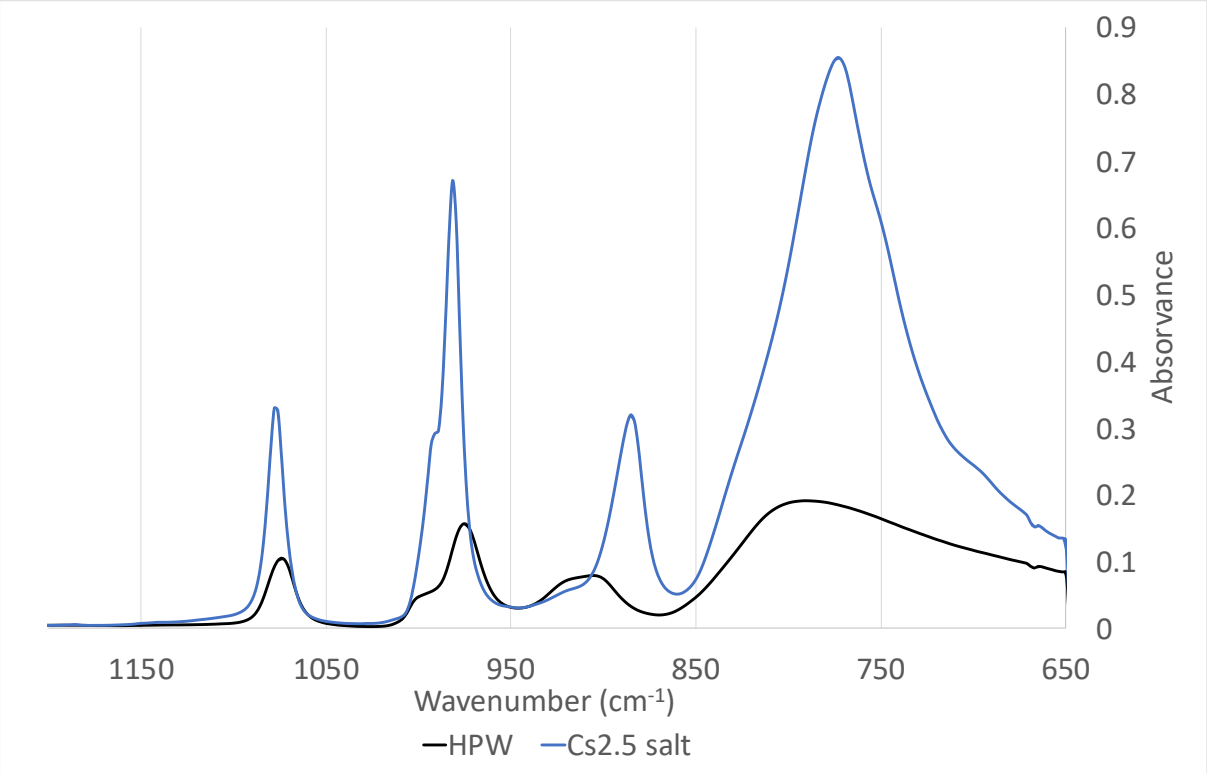

Figure 23: IR spectra for HPW and its cesium salt.

In Figure 24 the spectrum of HPW/PURAL SB calcined at 600 ºC is presented, together with spectra of sample HWP and PURAL SB calcined. The broad band at around 3500 cm^{-1} corresponds to the O-H vibrations of surface hydroxyl groups from water, so as the band at 1640 cm^{-1}.[122,123] There were also smaller bands at around 1500 and 1375 cm^{-1}, with the latter being attributed to the overtones of Al-O-Al groups. There is also a broad characteristic band of γ-Al_2O_3 between 900 and 300 cm^{-1} (which is this case is only visible until 650 cm^{-1}).[124] For the HPW/PURAL calcined at 600 ºC, the spectrum is very similar to the alumina but with a few new bands and shoulders which can be attributed to the heteropoly acid, a band at 1095 cm^{-1}, a shoulder at around 930 cm^{-1} and a small band at around 784 cm^{-1}. The band at 1095 cm^{-1} might relate with the P-O vibration of the HPW, the band at 930 cm^{-1} with the W=O groups and band at 784 cm^{-1} is probably the W-O-W vibration (in the case of HPW it appears at shifted at 812 cm^{-1}). This shift might be a confirmation of the partial decomposition of the HPW on basic supports, such as alumina.[9,125]

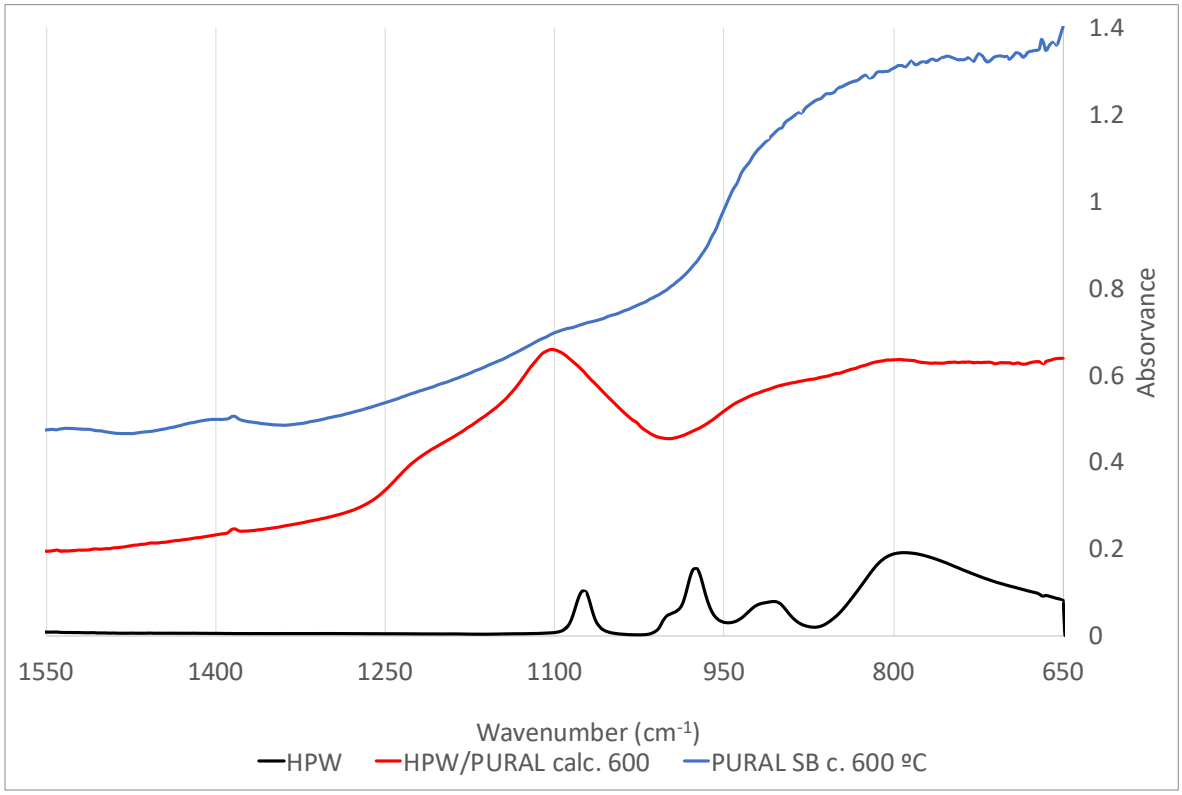

Figure 24: IR spectra for HPW, PURAL SB calcined at 600 ºC and HPW/PURAL c. 600 ºC.

In summary, the XRD diffractogram for the HPW does not agree neither with literature nor with the TGA results, in what concerns the quantity of crystallization water. Regarding HPW IR spectrum, the results match spectra found in literature for the tungsten heteropoly acid. The $Cs_{2.5}$ salt is arranged in a cubic Keggin structure and this was confirmed by XRD analysis. UV-Vis DRS and Infrared spectroscopies confirm the presence of the Keggin anion $PW_{12}O_{40}^{3-}$ in the cesium salt. Furthermore, it was possible to confirm the presence of HPW on PURAL SB calcined at 600 ºC but with some signs of HPW degradation.

3.1.2 Catalysts with Pt-Al_2O_3 as support

3.1.2.1 Structural Analysis

The X-ray diffractogram for Pt-Al_2O_3 and HPW impregnated on Pt-Al_2O_3 (HPW/Pt-Al_2O_3) can be seen in Figure 25. The presence of Pt phase cannot be seen for two probable and complementary reasons: the first one being that the Pt loading is only 1 wt. % and the second reason is that the Pt particles are well dispersed. The same observations for platinum alumina catalysts have been reported.[126] This is in agreement with the H_2/O_2 titration performed, that allowed to show a value for metal dispersion of 35 %, which is slightly higher than the values reported by some authors.[7,53]. Moreover, with the metal dispersion, and considering that the Pt particles are spherical[108] it is possible to calculate the particles size of Pt, which was about 3.2 nm. With N_2 sorption it was possible to calculate,

for Pt-Al_2O_3 sample, a BET surface area of 154 $m^2 \cdot g^{-1}$ and a pores volume of 0.45 $cm^3 \cdot g^{-1}$. The Pt-Al_2O_3 isotherm obtained is typical of mesoporous materials, which is in agreement with a material partially amorphous and presenting very small particles, such as been seen. However, here the value of the surface area is slightly lower than the values for alumina materials, which range from 200 to 250 $m^2 \cdot g^{-1}$.[81] Runnebaum *et al.*[7,53] reported for Pt-Al_2O_3 a surface area of 206 $m^2 \cdot g^{-1}$. The γ-Al_2O_3 phase obtained from COD database (COD 1101168) and used for comparison, can be seen in Figure 25 (closed diamond symbols). As it can be seen, some peaks from Pt-Al_2O_3 pattern are slightly deviated from the ones corresponding to the database result. This is thought to be due to the small particle size of the alumina, which can be related to the broad peaks and also because of its disorganized structure. However, the diffractogram obtained is in agreement with Brandão *et al.*[127]

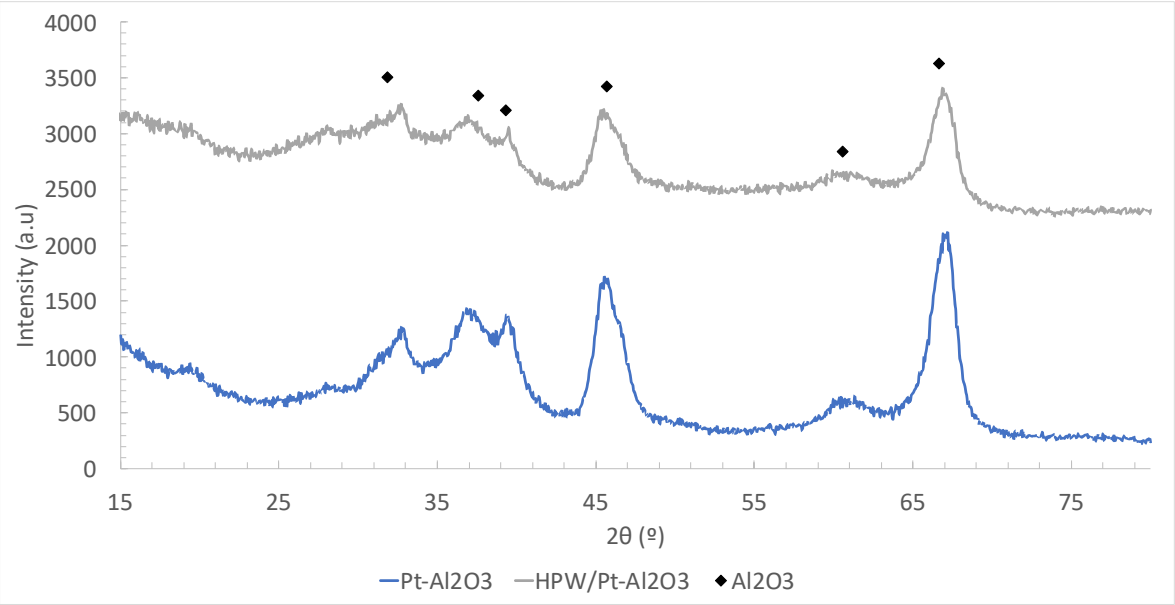

Figure 25: X-Ray Diffractogram of Pt- Al_2O_3, HPW/Pt- Al_2O_3 and comparison with gamma-Al_2O_3 (COD 1101168).

With respect to the HPW/Pt-Al_2O_3, its experimental pattern is very similar with the Pt-Al_2O_3 one. Here, the presence of HPW, which was dissolved in water and impregnated, cannot be detected and the same conclusion as for the case of platinum can possibly also be applied in this case: the HPW is probably well dispersed in the Pt-Al_2O_3 support. Caliman *et al.*[128] reported that the crystals of heteropoly acid were added to the alumina support as well dispersed and separated entities and thus cannot be detected by X-ray diffraction. On the other hand, the physical mixture of Pt-γ-Al_2O_3 and $Cs_{2.5}$ salt can be observed in Figure 26. The Pt-Al_2O_3/$Cs_{2.5}$ catalyst diffractogram consists of a sum of Pt-Al_2O_3 and $Cs_{2.5}$ salt patterns contribution, with a larger contribution from the $Cs_{2.5}$ salt but still with observable Pt-Al_2O_3 alumina peaks observable (large peak at around 46 º in 2θ).

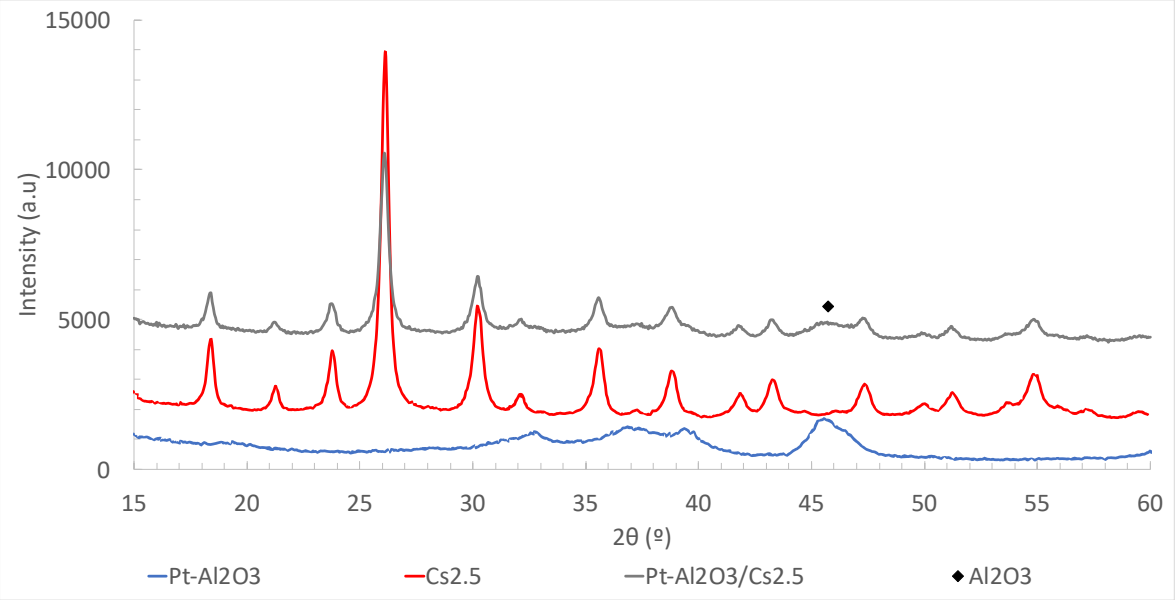

Figure 26: X-Ray Diffractograms of Pt-Al_2O_3 catalysts and $Cs_{2.5}$ salt and comparison with gamma-Al_2O_3 (COD 1101168).

3.1.2.2 Optical Properties

The UV-Vis DRS spectra of the different Pt-Al_2O_3 catalysts obtained are presented in Figure 27 and Figure 28. Concerning Pt-Al_2O_3 support, the respective spectrum is in agreement with literature[127], with a broad peak at 245 nm, expected for Pt-Al_2O_3 catalysts. It also presents a shoulder at around 210 nm, that can be attributed to γ-Al_2O_3.[118] The HPW/Pt - Al_2O_3 spectrum corresponds to the sum of both the HPW and Pt-Al_2O_3 contribution, with a shoulder around 245 nm and an intense peak at 260 nm, characteristic of the $PW_{12}O_{40}^{3-}$ ion, which confirms its presence in the Pt-Al_2O_3 support, a conclusion that could not be drawn from the X-Ray diffraction results.

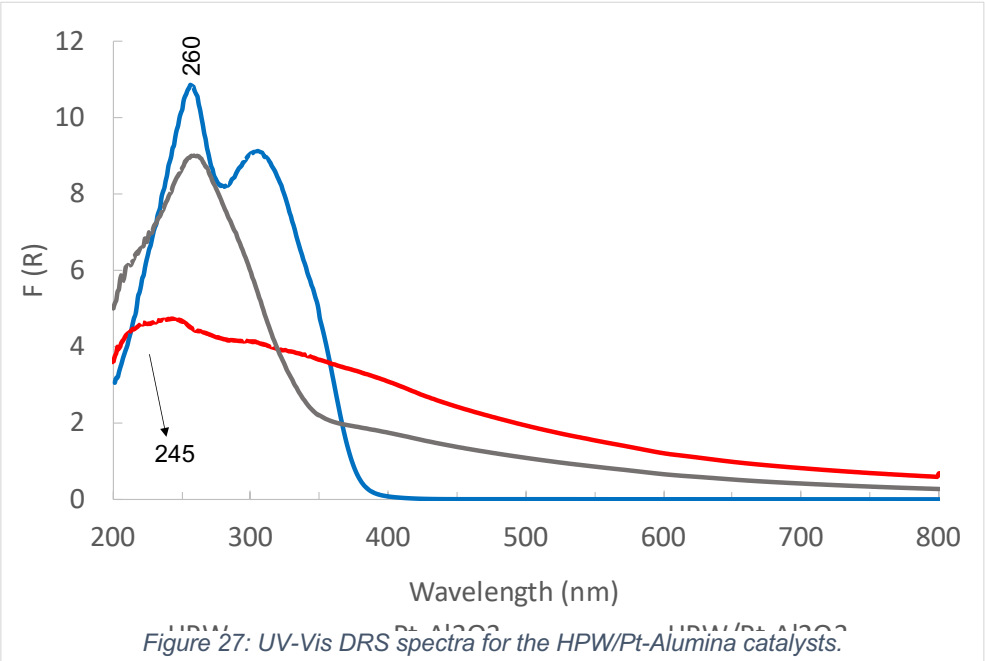

Figure 27: UV-Vis DRS spectra for the HPW/Pt-Alumina catalysts.

In Figure 28 it can be seen the spectrum for Pt-Al_2O_3/$Cs_{2.5}$, that presents a peak at 210 nm, probably from γ-Al_2O_3 support and also a peak at about 265 nm, coming from the heteropoly anion, but with a slight redshift deviation. However, here again, the peak at around 305 nm also disappears, in agreement with Sudhakar *et al.*[115] This might be due to the loss of the long-range order.

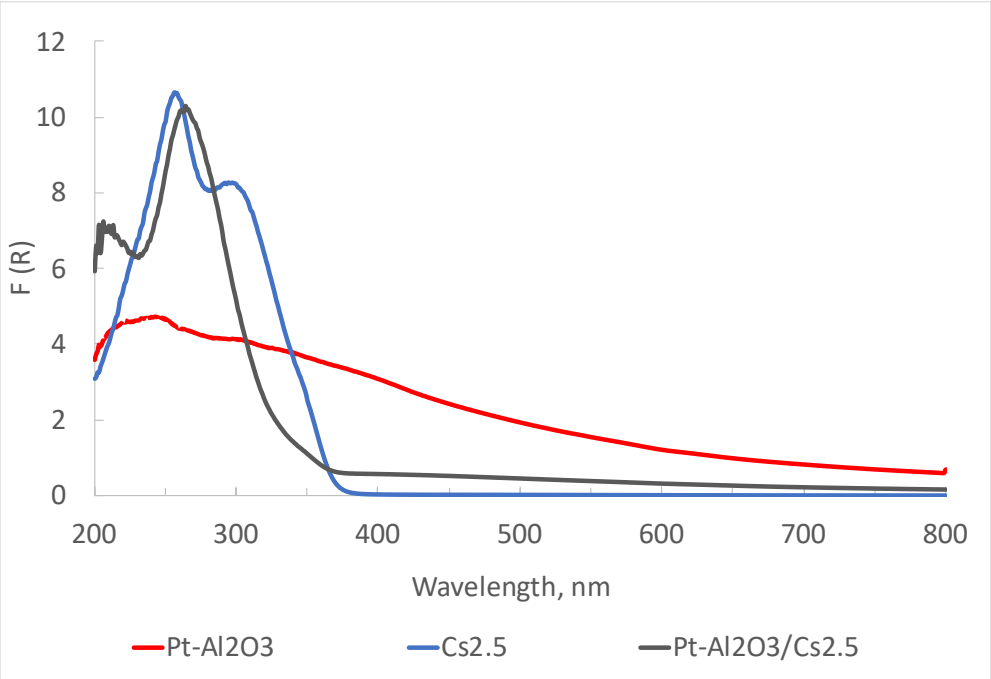

Figure 28: UV-Vis DRS spectra for the Pt-Alumina+Cs2.5 catalysts.

Regarding the Infrared results, the spectra for Pt-Al_2O_3 catalysts can be observed in Figure 29. The support presents bands at 1360, 1060, 811 and 740 cm^{-1}. As said above, the first three peaks can be attributed to Al-O-Al groups.[124] For all catalysts a broad band at around 3450 and a narrower band at 1630 cm^{-1} can be observed and are due to the presence of water.[122] All these bands can also be identified for the HPW and $Cs_{2.5}$ supported catalysts. In the case of HPW/Pt-Al_2O_3, the Keggin signature bands cannot be observed, as the spectrum resembles the Pt-Al_2O_3 support one. This is not the case for Pt-Al_2O_3/$Cs_{2.5}$ catalysts, where the Keggin bands are well defined at around 1080, 980, 870 and 810 cm^{-1}.

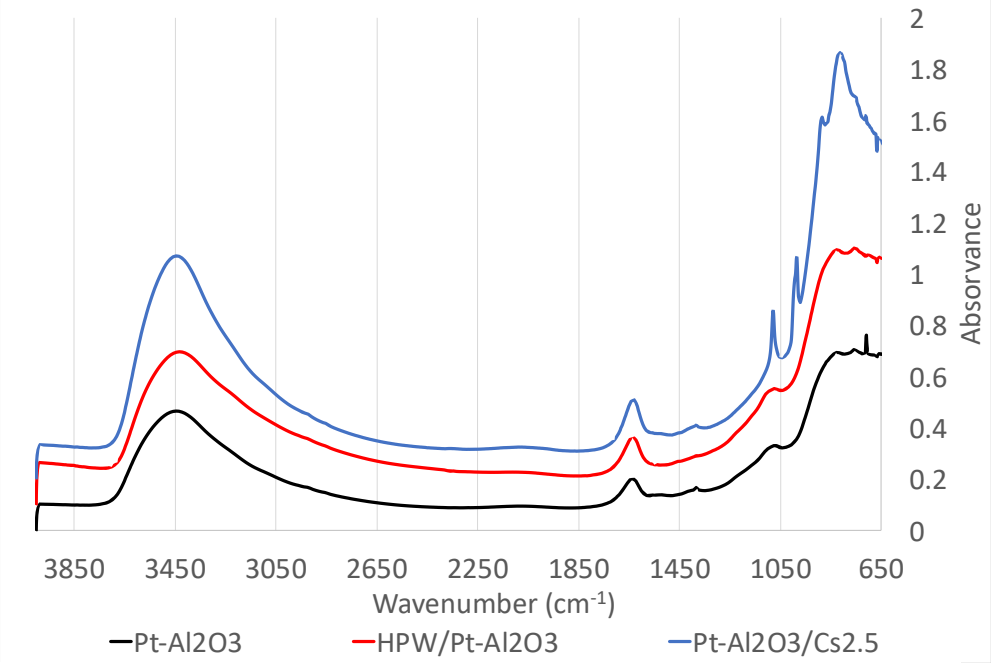

Figure 29: IR spectra for Pt-Al_2O_3 catalysts.

To summarize, concerning the Pt-Al_2O_3 supports, Pt cannot be identified in the X-Ray diffractograms because it is well dispersed (35 % metal dispersion from H_2/O_2 titration) and also because of the small particles size it presents (3.2 nm calculated from metal dispersion). The presence of Keggin anionic species cannot be identified in HPW/Pt-Al_2O_3 sample, neither by XRD nor IR spectroscopy, however, UV-Vis DRS confirms its presence in the support. On the contrary, for Pt-Al_2O_3/$Cs_{2.5}$ sample, the presence of $Cs_{2.5}$ phase can be detected by all techniques, where contributions of both the support and the $Cs_{2.5}$ salt are easily observed.

3.1.3 Catalysts with Ni28-Al_2O_3 as support

3.1.3.1 Structural Analysis

In Figure 30 powder X-Ray diffractograms of PURAL SB and PURAL SB calcined at 600 ºC can be observed. For the PURAL SB sample, prior to calcination, a boehmite phase, AlO(OH) (COD 9012247), can be observed but disappears after calcination at 600 ºC. It is, however, worth mentioning that a slight shift between the boehmite phase (COD 9012247) and the PURAL SB diffractogram can be observed, probably because PURAL SB is actually a pseudo-boehmite, meaning a boehmite with a higher water content. A γ-Al_2O_3 phase appears after calcination, seen by the match between the XRD pattern of the calcined PURAL and with the γ-Al_2O_3 (COD 1101168) from the database, as expected, represented by the dark blue dots. After calcination, a broadening of the peaks is observed. This is thought to be caused by the calcination of pseudo-boehmite, creating a poorly crystallized γ-Al_2O_3 with a large surface area.[81] In fact this was confirmed by a BET surface area (obtained from N_2 sorption measurements) of 218 $m^2 \cdot g^{-1}$ and a pores volume of 0.49 $cm^3 \cdot g^{-1}$. Here again, the isotherm obtained is typical of disorganized mesoporous materials.

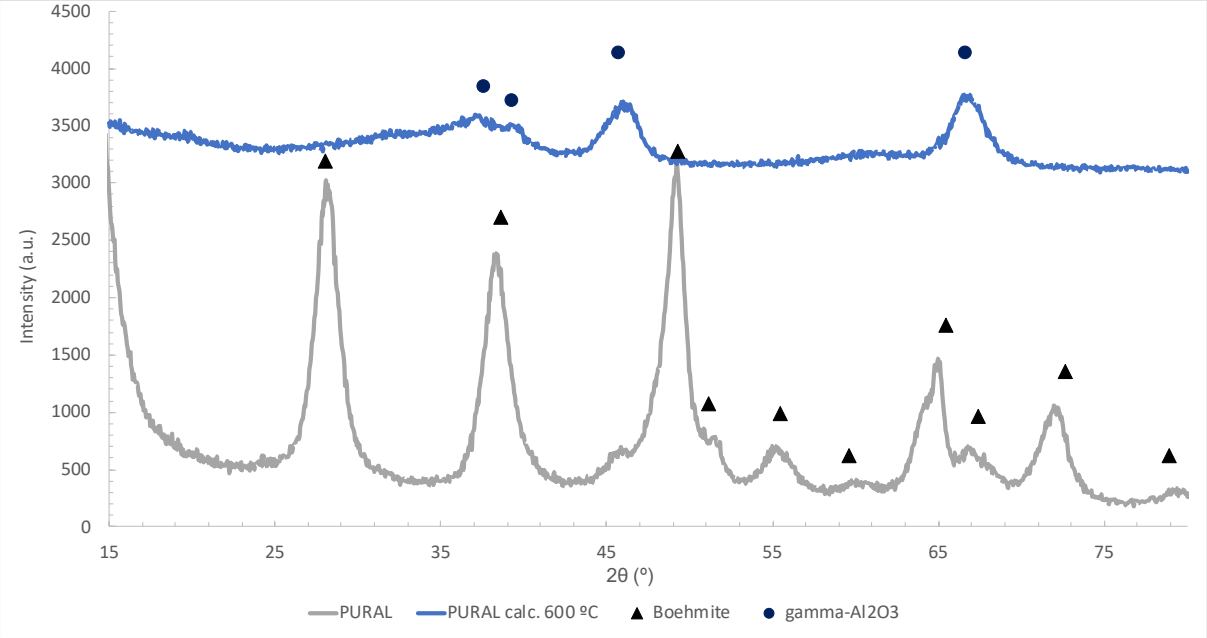

Figure 30: X-Ray Diffractograms of PURAL SB and PURAL SB calcined at 600 ºC. Comparison with boehmite (COD 9012247), gamma-Al_2O_3 (COD 1101168) from COD database.

The Ni28-Al_2O_3 diffractogram (Figure 31) is similar to PURAL SB calcined at 600 ºC although a metallic Ni phase can also be identified (see red squares symbols). As Ni phase peaks are very broad, one can say that Ni particles of very small size (Ni nanoparticles) are present in the support. On the other hand, no NiO phase could be identified for the Ni28-Al_2O_3 catalyst, meaning that, if present, NiO amount might be very low or NiO particles very small.

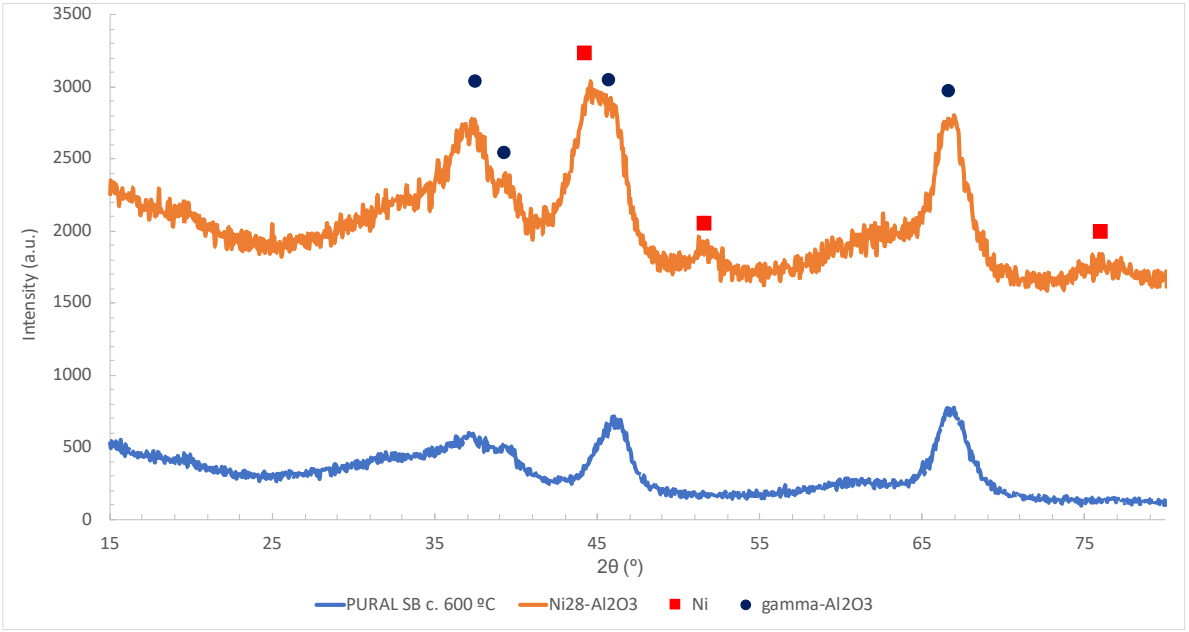

Figure 31: X-Ray Diffractogram of PURAL SB calcined at 600 ºC and Ni28-Al_2O_3 catalysts. Comparison with gamma-Al_2O_3 (COD 1101168) and Ni (COD 2100640) from COD database.

In Figure 32 the diffractograms of the Ni28-Al_2O_3, HPW/Ni28-Al_2O_3 and Ni28-Al_2O_3/$Cs_{2.5}$ can be seen. For the HPW/Ni28-Al_2O_3 catalyst, no HPW phase can be identified, with this diffractogram being very similar to the Ni28-Al_2O_3 one, probably due to a good HPW dispersion on Ni28-Al_2O_3, as also observed for previous HPW/Pt-Al_2O_3. Liu *et al.*[129], were also not able to identify HPW in Ni/alumina by XRD, agreeing with the results obtained here. For the Ni28-Al_2O_3/$Cs_{2.5}$ sample, and similarly to the Pt-Al_2O_3/$Cs_{2.5}$, its experimental pattern presents both Ni28-Al_2O_3 and $Cs_{2.5}$ salt pattern contributions, prevailing the latter over the Ni28-Al_2O_3 one.

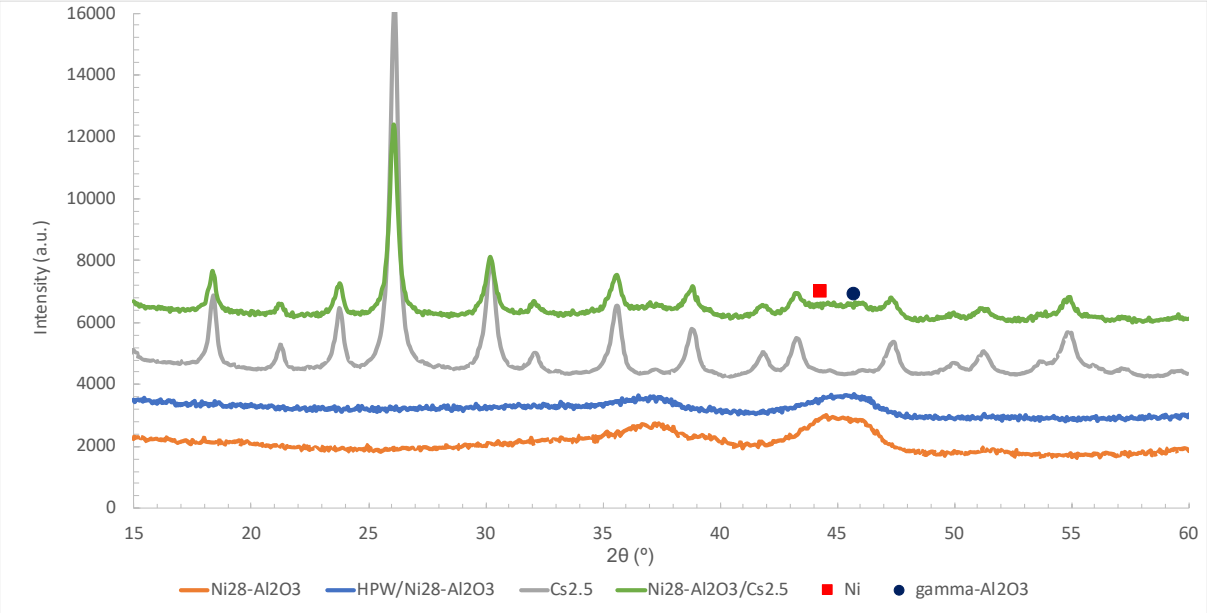

Figure 32: X-Ray Diffractogram of Ni28-Al_2O_3 /Cs2.5 and Cs2.5 salt, HPW/Ni28-Al_2O_3 catalyst. Comparison with Ni (COD 2100640) and Al_2O_3 (COD 1101168)

3.1.3.2 Optical Properties

It can be seen in Figure 33, the spectra of the starting materials, i.e. PURAL SB calcined, $Ni(NO_3)_2 \cdot 6H_2O$ and also Ni28-Al_2O_3 sample (after Ni nitrate impregnation but before calcination). Considering the $Ni(NO_3)_2 \cdot 6H_2O$, the spectrum on Figure 33 is in agreement with literature reports[130] with the three first peaks showing a slight shift to lower wavelengths (UV region). The peaks at 655 and 715 nm are characteristic of the presence of octahedral Ni^{2+} species. The Ni28-Al_2O_3 catalyst, before reduction, shows all the peaks of the precursor salt but with lower intensity., probably due to the matrix dilution effect.

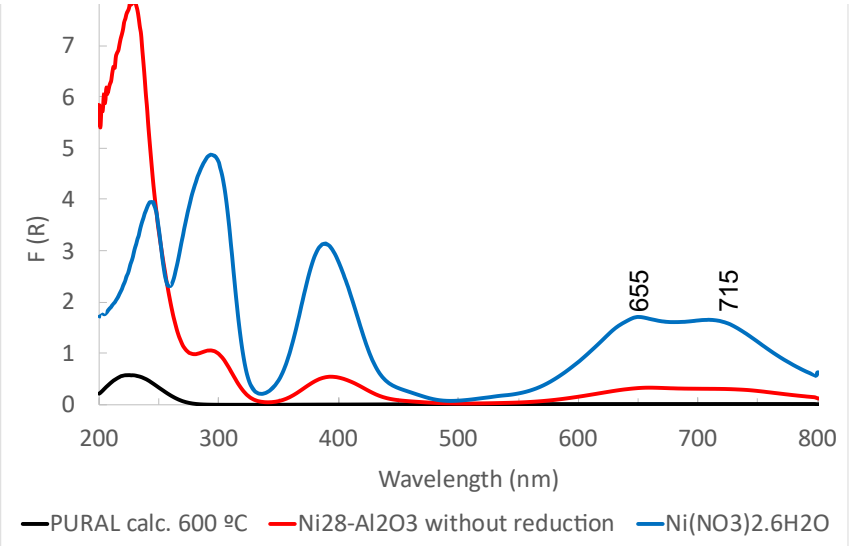

Figure 33: UV-Vis DRS spectra for the HPW, Ni28-Al_2O_3 and HPW/Ni28-Al_2O_3 samples

Figure 34 shows the spectrum of HPW impregnated on calcined Ni28-Al_2O_3 and compares it with the support and HPW samples. The peaks between 200 and 400 nm in the calcined Ni28-Al_2O_3 can be attributed to a nickel aluminate form.[130] A shoulder at around 634 nm can be seen not only for the Ni28-Al_2O_3 but also for HPW/Ni28-Al_2O_3 and it is not present for the HPW itself. The shoulder around 210 nm can be attributed to γ-Al_2O_3 .[118] Contrarily to what was seen for the HPW/Pt-Al_2O_3 case (see above), one cannot identify bands corresponding to HPW in the Ni28-Al_2O_3 support. This is thought to be because of the black color that HPW/Ni28- Al_2O_3 presents, that absorbs strongly the incident radiation.

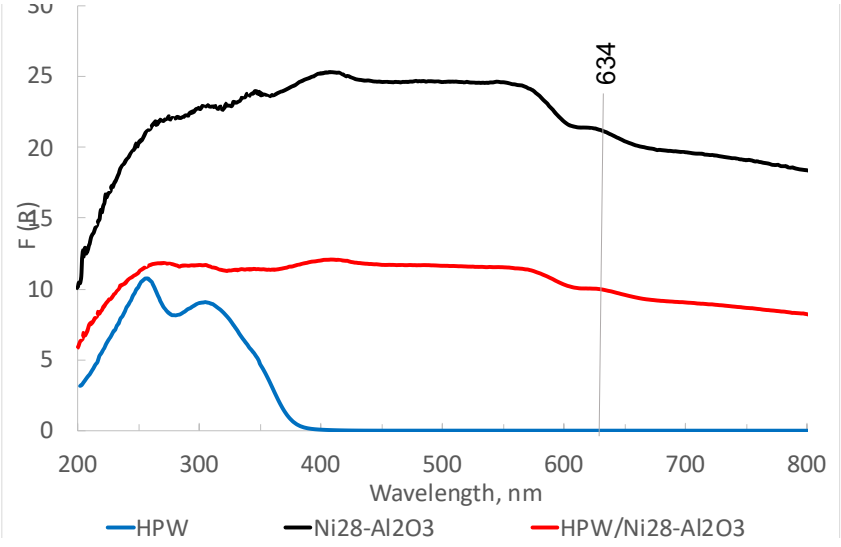

Figure 34: UV-Vis DRS spectra for the HPW/Ni28- Al_2O_3 catalysts

Considering the IR Spectra, Figure 35, it can be seen, once again, that in the HPW/Ni28-Al_2O_3 catalyst, the presence of the HPW cannot be detected, as none of the Keggin typical bands are present. The spectrum for this catalyst seems to present only the Ni28-Al_2O_3 support contribution. On the other hand, and also as seen before, the same does not happen with the Ni28-Al_2O_3/$Cs_{2.5}$ catalyst, where the

contribution of the two components is clearly observable. The bands attributed to water, at around 3400 and 1640 cm^{-1}, are also present for all three catalysts. The bands at around 1360, 1060, 811 and 740 cm^{-1} can be attributed to the Al-O-Al groups of the support, Al_2O_3.[124]

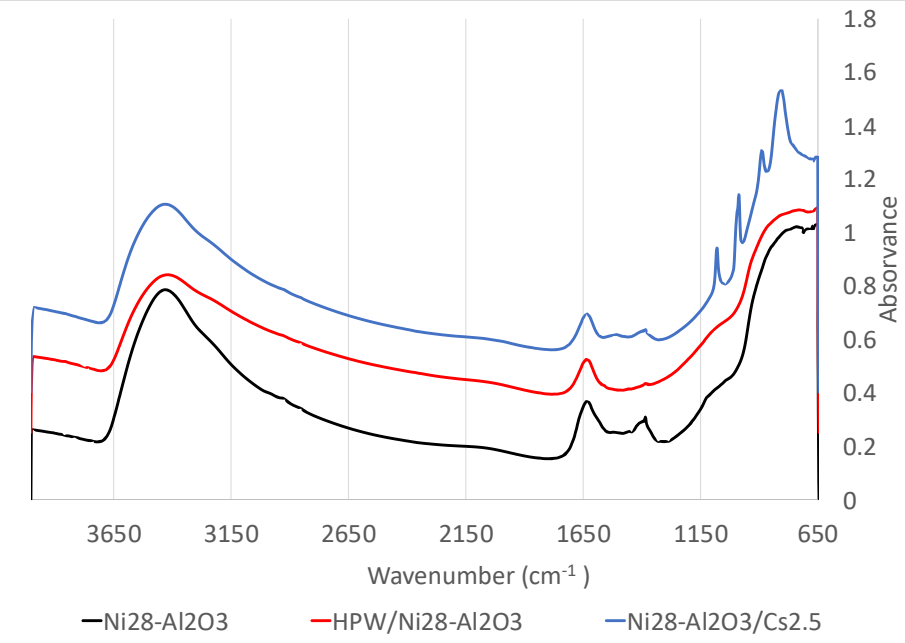

Figure 35: IR Spectra for Ni28-Al_2O_3 catalysts.

3.1.3.3 On the reducibility of Ni in Ni28-Al2O3

After the thermal treatment, this sample went through a H_2-TPR analysis, shown in blue, in Figure 36.

For comparison reasons, some of the Ni28-Al_2O_3 precursor was also calcined in air. Again, after this treatment, this sample went through a H_2-TPR analysis, shown in red, in Figure 36. Because this catalyst was prepared by impregnation, all the Ni that was added, with a solution of nickel nitrate, is in its Ni^{2+} form, initially. In the sample that was calcined with air, it is assumed that after the treatment, all of the Ni is in its oxide form, NiO, again, a Ni^{2+}species.

In an attempt to find a value of percentage of reduction of the Ni after the reductive thermal treatment, the TPR profiles of both thermal treatments employed were used. With the assumption that all of the Ni present in Ni28-Al_2O_3 after calcination in air is in its NiO form, the area of the NiO28-Al_2O_3 profile after reductive treatment was divided by the area of Ni28-Al_2O_3 profile after the oxidative treatment and a 60% reduction value was obtained.

The TPR profile of the reduced Ni28-Al_2O_3 (in blue in Figure 36) is in agreement with Zieliński[131] with a narrow peak appearance at around 200 ºC that can be attributed to the reduction of NiO to metallic Ni and a broader peak at around 540 ºC can be attributed to the reduction of $NiAl_2O_4$ species, meaning that part of Ni interacts strongly with alumina support to form a nickel aluminate phase.

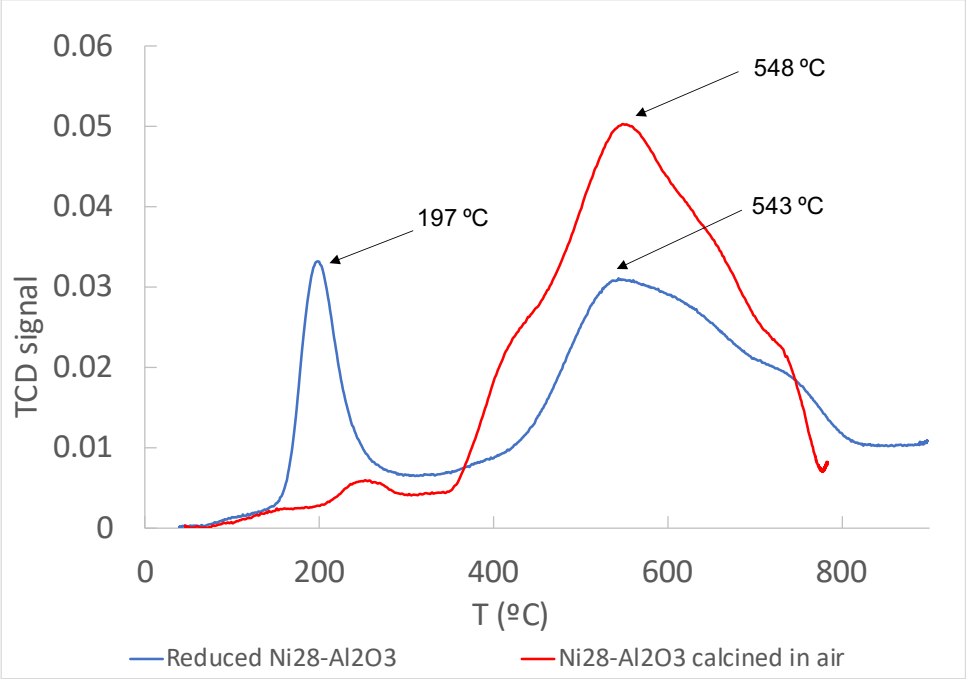

Figure 36: TPR profile of Ni28-Al_2O_3 catalyst, after thermal treatment in oxidative and reductive atmospheres.

In conclusion, in the X-Ray diffractograms, a change from pseudo-boehmite to gamma-alumina can be seen upon thermal treatment. In these catalysts it is possible to identify by XRD a Ni phase but not a NiO phase. This species, however, is present, which was confirmed by H_2-TPR. It was also possible to see, through H_2-TPR and UV-Vis DRS that a portion of the nickel interacts with the alumina support. The presence of impregnated HPW on Ni28-Al_2O_3 was not possible to be confirmed, neither from XRD, UV-Vis DRS nor IR spectroscopy. The presence of $Cs_{2.5}$ however, was confirmed by both XRD measurement and IR spectroscopy.

3.1.4 Catalysts with NiO25-Al_2O_3 as support

3.1.4.1 Structural Analysis

In Figure 37 and Figure 38 are presented the X-Ray diffractograms for NiO25-Al_2O_3, starting materials and compounds from the database. For this group of catalysts, it was possible to identify a considerable number of different phases. In Figure 37 it is possible to compare the reduced catalysts with non-reduced starting material. In the non-reduced NiO25-Al_2O_3, boehmite, doyleite (which is a polymorph of gibbsite[132]), $CaCO_3$, NiO phases can be observed, although some other unidentified peaks are present. For the reduced NiO25-Al_2O_3, it is possible to observe that the doyleite phase disappeared, probably due to the thermal treatment employed for this support. A γ-Al_2O_3 phase appeared, however the temperature applied at the thermal treatment was not high enough to fully transform into γ-Al_2O_3 phase, once it is still possible to observe a boehmite phase. Also, a metallic Ni phase appeared while NiO phase is still visible, although with lower intensity and broader peaks.

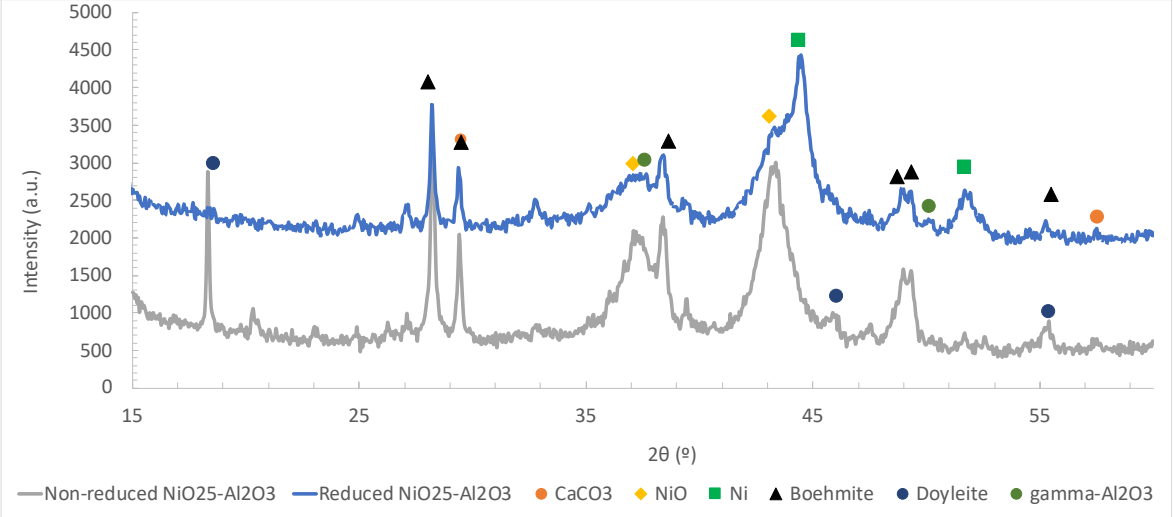

Figure 37: Powder X-Ray diffractograms for NiO25-Al_2O_3 non-reduced and reduced, $CaCO_3$ (COD 1010928), NiO (COD 4320505), Ni (COD 2100640), boehmite (COD 9012247), doyleite (COD 9011512) and gamma-Al_2O_3 (COD 1101168)

In Figure 38 the diffractograms for HPW/NiO25-Al_2O_3 and NiO25- Al_2O_3/$Cs_{2.5}$ are shown and compared with NiO25-Al_2O_3 and $Cs_{2.5}$ salt ones. For the HPW/NiO25-Al_2O_3 sample, the peaks that correspond to the NiO25-Al_2O_3 support pattern can be seen and also some peaks that seem to correspond to the $Cs_{2.5}$ salt pattern.

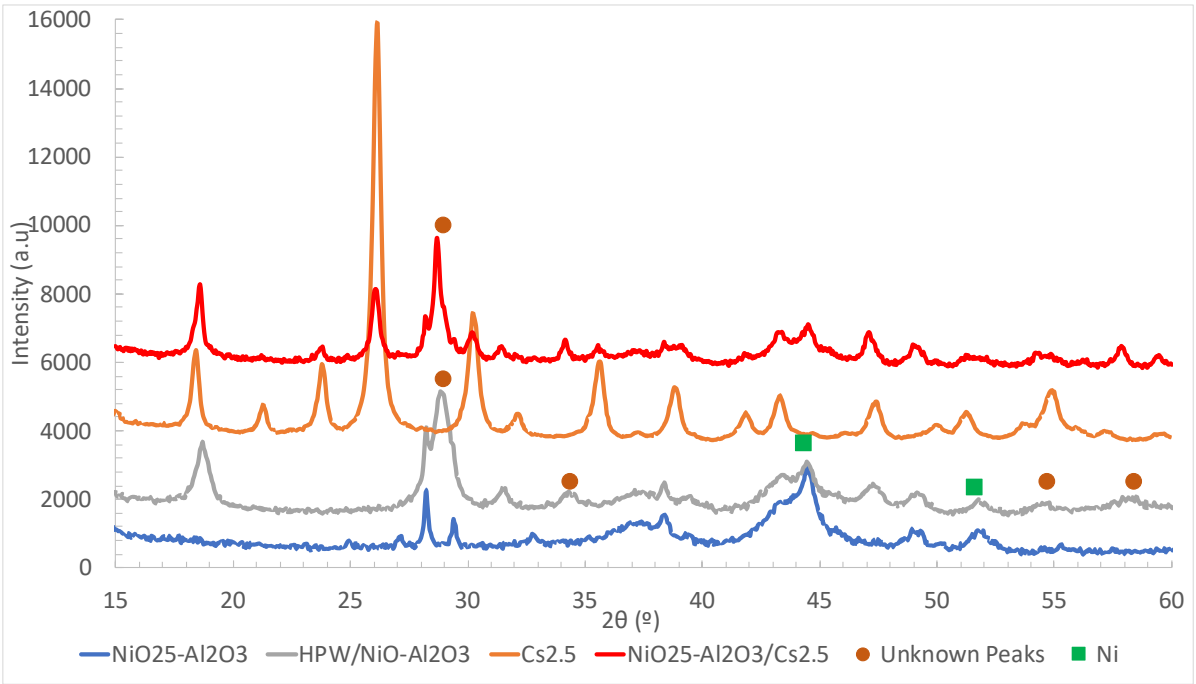

Figure 38: X-Ray Diffractogram of NiO25-Al_2O_3 catalysts in their heteropolyacid forms and comparison with $Cs_{2.5}$.

The metallic Ni phase can be observed for the HPW/NiO25-Al_2O_3, however, it also contains peaks unidentified that do not belong to anyone of both these structures (see close dots symbols). There is also the contribution of an intense peak, at around 29 º, that is present in both HPW/NiO25-Al_2O_3 and NiO25-Al_2O_3/$Cs_{2.5}$ patterns but is not present in the support one. This peak has not been observed for any other HPA catalysts. Regarding the NiO25-Al_2O_3/$Cs_{2.5}$ catalyst the observations are very similar to the observed for the other $Cs_{2.5}$ physically mixed catalysts: the diffractogram is very similar to the $Cs_{2.5}$ salt pattern although a support contribution can also be observed. However, there is the presence of an unknown peak, at around 29 º in 2 theta, which is only present in the HPW patter, not in the $Cs_{2.5}$ salt pattern nor in the NiO-Al_2O_3.

3.1.4.2 Vibrational Properties

For the NiO25-Al_2O_3, due to its black color, IR spectroscopy was the only spectroscopic method that could be used, Figure 39. This is due to the black color that these catalysts present, that strongly absorb light in the visible region, making it practically impossible to analyze using UV-Vis DRS.

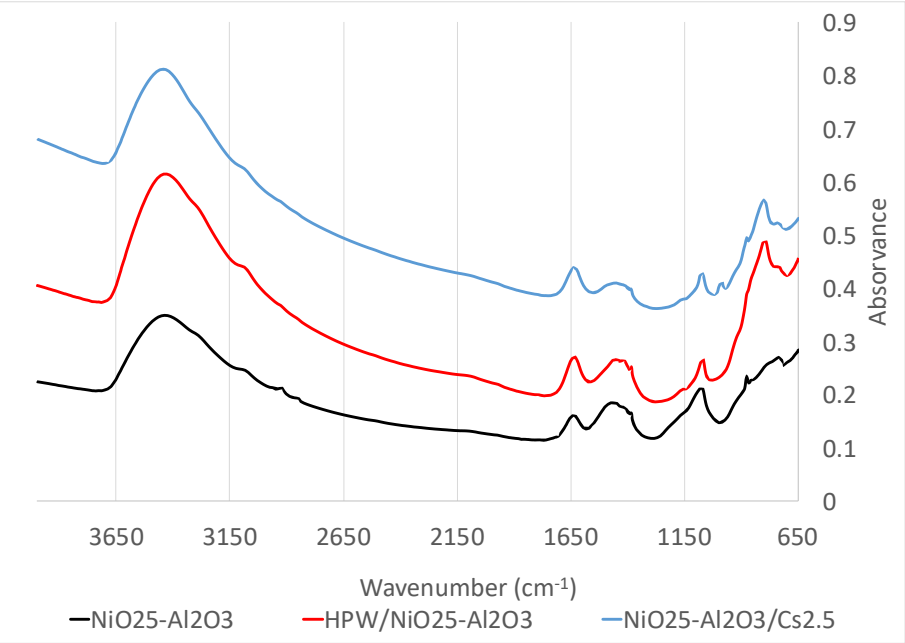

Figure 39: IR Spectra for NiO25-Al_2O_3 catalysts.

Two bands at around 3430 and 1620 cm^{-1} were identified and attributed to water. A band at 3080 cm^{-1} can be seen in all the catalysts and is probably a contribution from the support. The same can be said over the bands at around 1400 and 1060 cm^{-1} (Al-O-Al groups). As opposite to what has been seen for the other catalysts, a band and around 780 cm^{-1}, characteristic for HPW, can be seen for both HPW and $Cs_{2.5}$ salt. In this case, the presence of $Cs_{2.5}$ salt on the support is not so obvious. In fact, for the $Cs_{2.5}$ salt only the bands at 780, 870 and 983 cm^{-1} can be seen, as opposite to the band at 1080 cm^{-1} that is usually visible for the heteropoly compounds. This is probably due to the marked presence of the support band at 1060 cm^{-1}.

3.1.4.3 On the reducibility of NiO25-Al_2O_3 support

The NiO25-Al_2O_3 is an industrial catalyst, where Ni is present in its oxide form, NiO. For it to have hydrogenation capacity, it is necessary to reduce the catalyst. H_2-TPR analysis was done before reduction, meaning, in its NiO form, and after reduction and the profiles can be seen in Figure 40.

Once again, using the TPR analysis profiles, and considering that all the Ni is in its NiO form in the NiO25-Al_2O_3 prior to reduction, an attempt to calculate the percentage of reduction from the thermal treatment was done by dividing the area of the reduced sample by the non-reduced one. The value obtained was 49.6%.

Looking at Figure 36 (Ni28-Al_2O_3 TPR) a similarity of TPR profiles can be observed an it is probable that the two catalysts contain similar species, with the exception of the peak at 384 ºC, in Figure 40. This might be due to the large number of phases identified for the NiO25- Al_2O_3 that were not identified for the Ni28- Al_2O_3 catalyst. However, the same conclusions that were obtained for Ni28- Al_2O_3 can also be applied to the NiO25-Al_2O_3: the narrow peak appearance at lower temperatures can be attributed to the reduction of NiO to metallic Ni while the broader peak at higher temperatures can be attributed to the reduction of Ni that interacts strongly with the Al_2O_3 support.

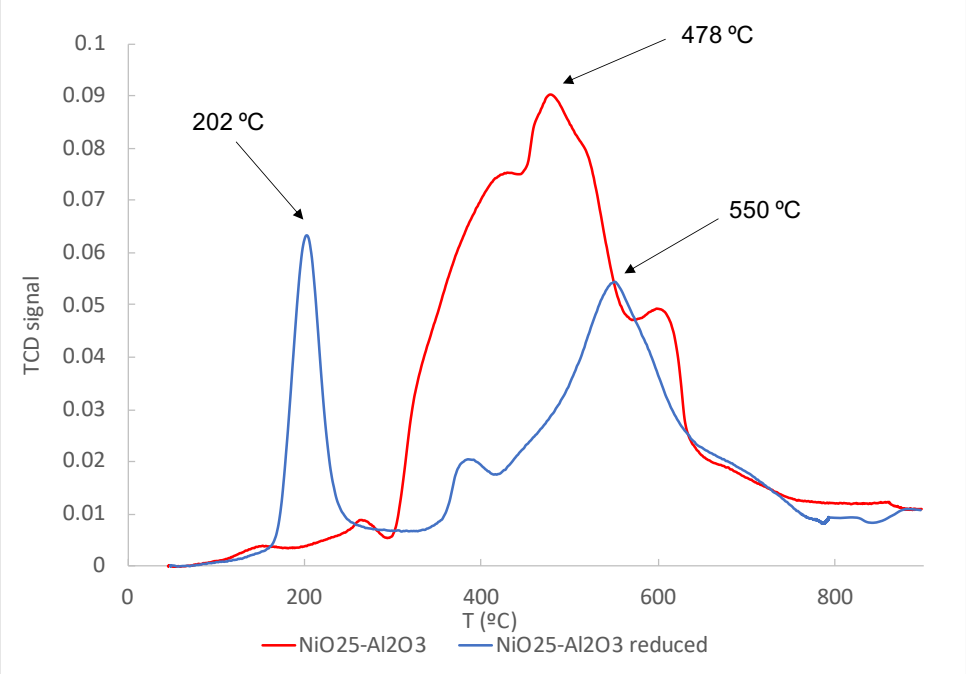

Figure 40: TPR profile of NiO non-reduced and reduced industrial catalyst.

To summarize, the NiO25-Al_2O_3 catalyst support has a lot more crystalline phases in its constitution when compared with the other two supports, which can be verified by the large number of identified phases in the X-Ray diffractogram of these catalysts (Figure 37). It can be seen by XRD both Ni NiO phases, which could not be seen in Ni28-Al_2O_3. This might mean that the NiO particles in the NiO25-Al_2O_3 catalysts are probably bigger in size or/and worse dispersed when compared with the Ni28-Al_2O_3 catalysts. The presence of NiO was confirmed by H_2-TPR and with this technique it was also possible to verify that this catalyst has also a nickel aluminate phase. Once again, the presence of HPW

on the supports was unable to be confirmed by XRD but the presence of $Cs_{2.5}$ was. Like the other two groups of catalysts studied, the pattern of Ni28-Al_2O_3/ $Cs_{2.5}$ is the sum of the contributions of the support and of the $Cs_{2.5}$ salt. Because of its black color, UV-Vis DRS was not performed although IR spectroscopy was successfully used. For the first time, it was possible to see evidence of HPW presence in the support, with one of the characteristic Keggin bands present in both HPW/NiO25-Al_2O_3 and NiO25-Al_2O_3/$Cs_{2.5}$ samples.

3.2 Catalysts evaluation in HDO reaction with guaiacol

In this section, the results of the catalytic tests will be shown and discussed. The division will be made by metal used. In this way, the results of the Pt-Al_2O_3 catalysts will be shown first and the results for both Ni28-Al_2O_3 and NiO25-Al_2O_3 will be shown simultaneously, once the discussion will fall on the properties and literature finds of Ni catalysts. For all catalytic tests the experimental conditions were previously presented in the Chapter 2.3.2 (HDO Reaction) and are summarized in Table 8.

Table 8: Reaction Conditions.

Feed flow rate ($mL \cdot h^{-1}$)	3.0
GUA flow rate ($mL \cdot h^{-1}$)	0.15
n-heptane flow rate ($mL \cdot h^{-1}$)	2.85
Catalyst Load (mg)	100
Molar ratio H_2/Gua	50
Reaction temperature (ºC)	300
Pressure (atm)	1

The 1 wt. % Pt-Al_2O_3 is a well-studied HDO catalyst.[7,53,54,62] Ni based catalysts are also applied usually supported on acidic supports such as USY[66] or HZSM-5[8] or in the presence of other metals.[56,133] To summarize, three supports were tested by themselves, and for each support HPW or $Cs_{2.5}$ was added, resulting in nine different catalysts. The effects of the introduction of the heteropoly acid or salt (by impregnation or by physical mixture) will be analyzed in the following sections.

3.2.1 Catalysts based on Pt-Al_2O_3 support

Figure 41 shows the evolution of total conversion of Pt-Al_2O_3 catalysts as a function of reaction time. The dashed lines that will be shown in some of the Figures are only present for auxiliary purposes, to guide the eyes for tendencies that otherwise might be missed. None of these lines have physical meanings. Empty dots represent the discarded points for the construction of the auxiliary lines.

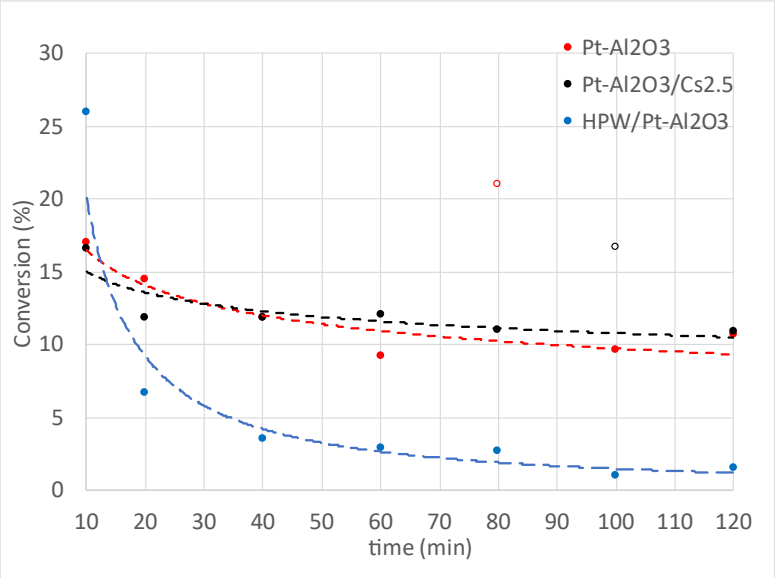

Figure 41: Guaiacol conversion as a function of time for Pt-Al_2O_3 support-based catalysts.

For Pt-Al_2O_3 sample alone (in red) there is no significant variation of the conversion values with time, being situated between 10 and 15 % for all reaction times. The addition of $Cs_{2.5}$ salt (in black) does not change this tendency. The addition of HPW (in blue) however, yields a higher initial conversion (26 %) but it decreases faster when compared with the other two catalysts, originating lower conversions for longer reaction times, probably due to the occurrence of deactivation phenomena.

In Table 9 a list of reaction products formed for each individual catalyst can be seen. It should be mentioned that there were also unidentified products present, which were called unknowns. As it can be observed, there are no deoxygenated products.

Table 9:Identified products for Pt-Al_2O_3 catalysts.

Catalyst	Identified Products
Pt-Al_2O_3	phenol, cyclohexanone
Pt-Al_2O_3/$Cs_{2.5}$	phenol, anisole, cyclohexanone
HPW/Pt-Al_2O_3	phenol, anisole, cyclohexanone

Concerning phenol selectivity (Figure 42), it decreases with time for Pt-Al_2O_3, being undoubtably one of the major reaction products. The results obtained for Pt- Al_2O_3 are in agreement with the results obtained by Runnebaum *et al.*[134], who also obtained conversions in the same range (up to 13 %) with phenol being one of the major products. Along with phenol, catechol and 3-methylcatechol were also classified as major products but were not identified in the present work.

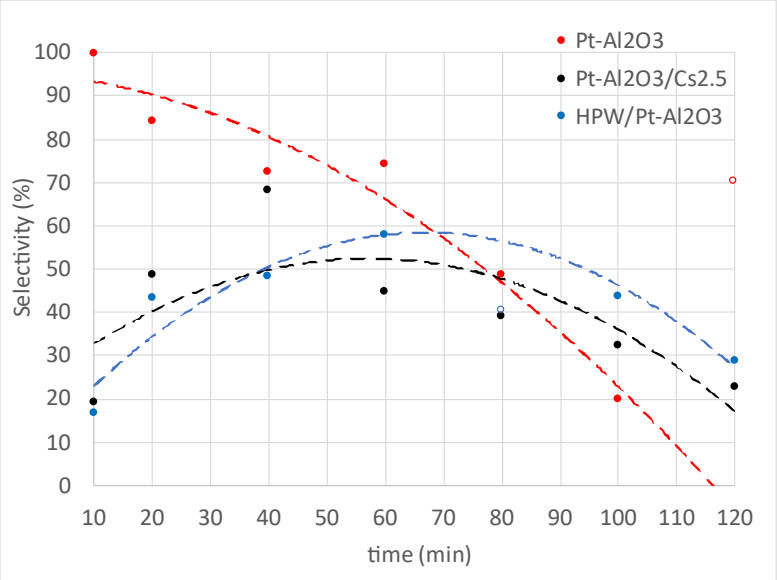

Figure 42: Selectivity of phenol for Pt-Al_2O_3 catalysts with time on stream.

This research group[134] used the same exact Pt- Al_2O_3 from Sigma-Aldrich at similar conditions (300 ºC, 140 kPa, H_2/GUA = 10 molar) and was yet able to identify anisole, cyclohexanone and benzene as minor products in their work. In our work, however, it was only possible to identify, for Pt-Al_2O_3 alone, cyclohexanone, which according to the proposed mechanism presented in Figure 43, suggests the occurrence of phenol hydrogenation. The cyclohexanone selectivity can be analyzed in Figure 44. Neither benzene nor cyclohexane were identified for Pt-Al_2O_3 tough these were minor products detected in the work of Runnebaum *et al.*[134]

For the HPW and $Cs_{2.5}$ salt catalysts the same trend for phenol selectivity is observed: it increases until it reaches a maximum and then decreases. By using different experimental conditions than the ones applied for the reaction in question (120 ºC, 7 atm, 9 h on stream), Itagaki *et al.*[68], using a Pt supported on $Cs_{2.5}$ support (Pt/$Cs_{2.5}$ = 1/100 molar *versus* Pt/$Cs_{2.5}$ = 1/1.56 molar in this work) obtained mainly cyclohexane, a fully deoxygenated product. In the HDO reaction of anisole with also a Pt supported on $Cs_{2.5}$ (95 wt. % of the latter), Alharbi *et al.*[135] (100 ºC, atmospheric pressure) also obtained also cyclohexane as the primary product, although a methanol selectivity ranging between 80 and 99 % was obtained. Interestingly, none of these authors reported a significant amount of phenol when using the $Cs_{2.5}$ salt as the support for Pt. Alharbi *et al.*[136] reported a 10 wt. % Pt on activated carbon (Pt/C) physically mixed with $Cs_{2.5}$ salt catalyst (also 95 wt. % of $Cs_{2.5}$ salt) used for the hydrodeoxygenation of acetophenone (100 ºC, atmospheric pressure). They discovered that this catalyst has a better stability for the hydrogenation of the reagent, with less deactivation when compared with the supported Pt on $Cs_{2.5}$ salt. In fact, in both studies, a considerably higher amount of $Cs_{2.5}$ salt than the one used is the present work (which was 20 wt. %) was used, and cyclohexane was obtained as the major product. Although the metal function is indispensable for hydrogenolysis[7], the acid function brought by the acid sites of the $Cs_{2.5}$ salt shifts the product distribution to a larger amount of deoxygenated and hydrogenated products. Anderson *et al.*[58] reported, for the HDO of anisole (1.01 bar

and 320 ºC, with a 10 wt. % molybdenum heteropoly acid (HPMo) supported on TiO_2 catalyst) benzene as the primary product, but also phenol, alkylated oxygenated (mainly cresol) and alkylated aromatics (mainly toluene) in some extent.

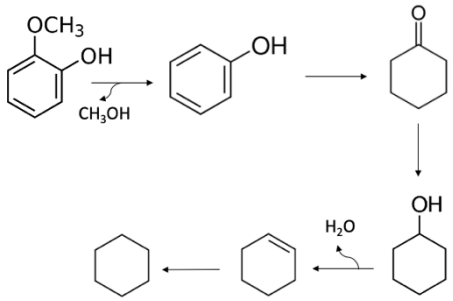

Figure 43: Proposed mechanism for the production of cyclohexanone. Adapted from ref. 103.

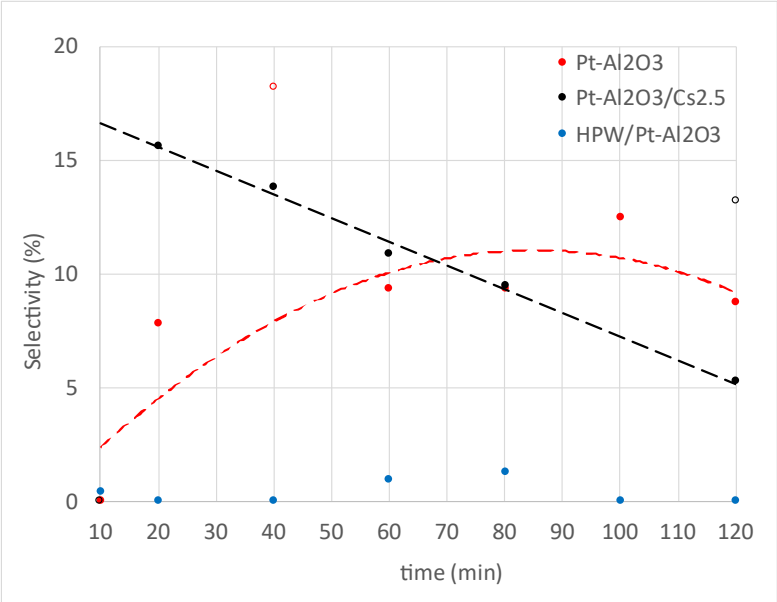

Figure 44: Selectivity of cyclohexanone for Pt-Al_2O_3 catalysts with time on stream.

On the other hand, anisole was identified for the HPW/Pt- Al_2O_3 catalysts (Figure 45). This means that HPW/Pt-Al_2O_3 was able to cleave the much energetic $C_{aromatic}$-OH bond before the $C_{aromatic}$-OCH_3 one, nonetheless with a lower overall selectivity when compared with phenol. In this case, no trend lines are shown because: a) in the case of Pt/γ-Al_2O_3 and Pt/γ-Al_2O_3/Cs2.5 salt, selectivity to anisole is almost zero and b) in the case of HPW/ Pt/γ-Al_2O_3, no definitive trend can be observed.

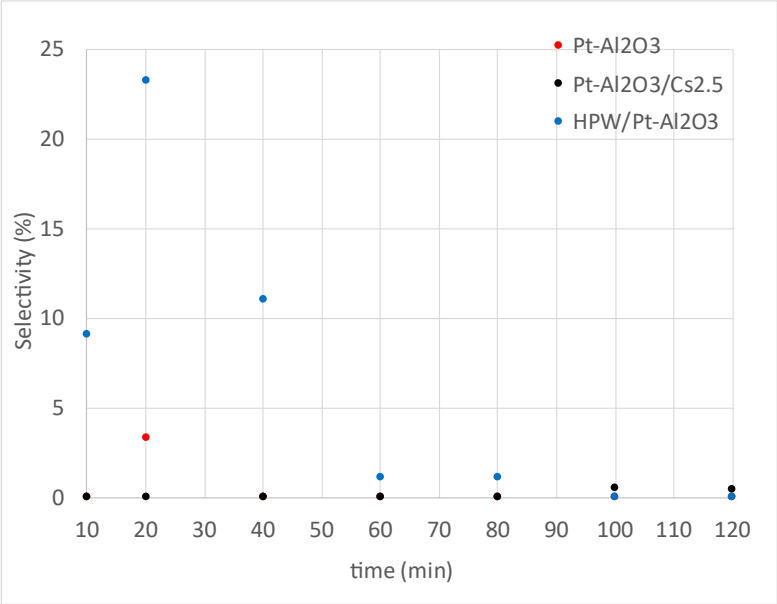

Figure 45: Selectivity of anisole for Pt-Al_2O_3 catalysts with time on stream.

Besides the main reaction products that were possible to identify using GC standards, some amount of other reaction products, designated as “unknowns” or U were also detected and their selectivity can be observed in Figure 46. Concerning the selectivity values obtained for the unknown products, a relationship between these values and the selectivity obtained for phenol (Figure 42) can be proposed. In fact, it was observed that when phenol selectivity reaches its maximum, the selectivity for unknowns, on the other hand, reaches its minimum.

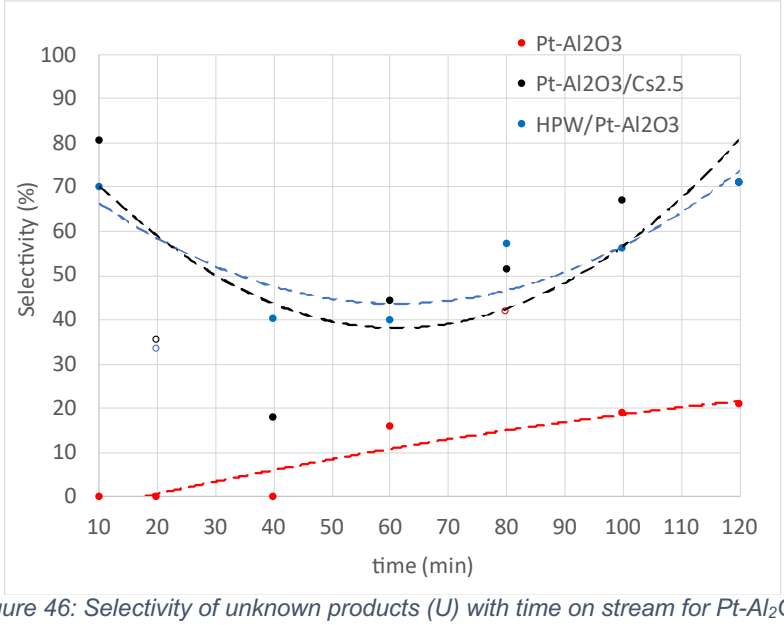

Figure 46: Selectivity of unknown products (U) with time on stream for Pt-Al_2O_3 catalysts.

This might indicate that phenol is suffering secondary reactions. Because the unknown products have longer retention times, and it was noticed that deoxygenated compounds tend to have lower RT, it is expected that the unidentified products are oxygenated aromatics (See Appendix E, Table 15 and

Table 16). According to the following statements: i) the trend of phenol selectivity is the opposite of the unknowns one, ii) acid sites are responsible for methyl transfer[7] and iii) Anderson *et al.*[58] reported a synergetic effect between Lewis acid sites (from alumina) and Brønsted acid sites (from HPW or $Cs_{2.5}$ salt) for alkylation, it can be speculated that the unknown products are probably alkylated phenolic compounds or compounds with more than one -OH group. For Pt- Al_2O_3 and HPW/Pt-γ-Al_2O_3, the number of unknowns remain relatively constant with time however, for Pt- Al_2O_3 /$Cs_{2.5}$ it increases slightly.

Figure 47 presents a summary of the results obtained for the different Pt-Al_2O_3 catalysts at the beginning (10 min TOS), or at the end of the reaction (120 min TOS). For all catalysts, since the main reaction product is always phenol, it can be concluded that the main reaction pathway is the direct deoxygenation over hydrogenation (Figure 7).

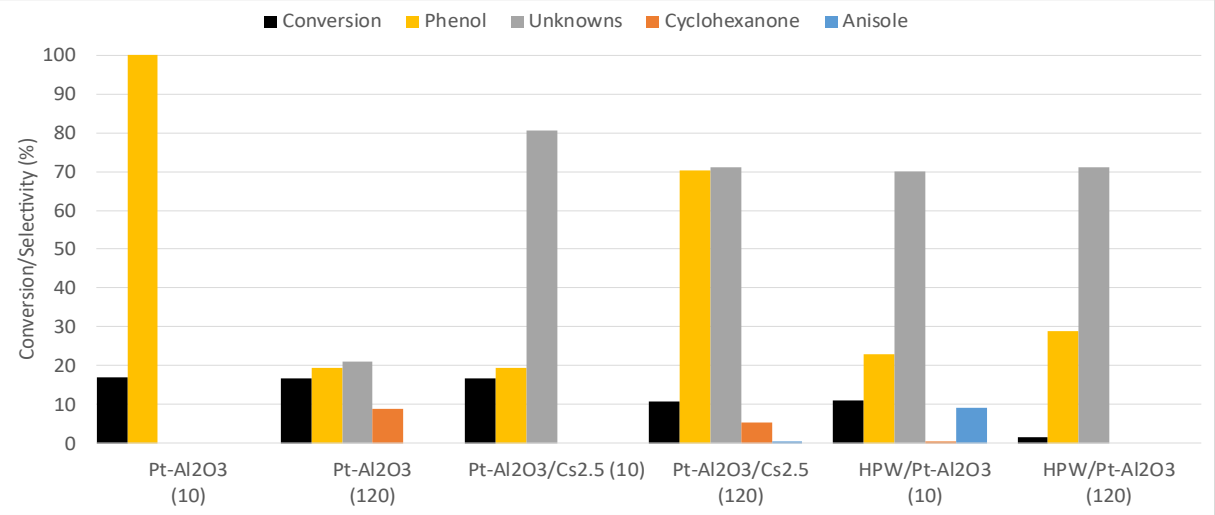

Figure 47: Summary of the results of the HDO of guaiacol for Pt-Al_2O_3. In parenthesis is shown TOS, in minutes.

3.2.2 Catalytic tests with Ni catalysts

Because both Ni28-Al_2O_3 and NiO25-Al_2O_3 are nickel catalysts, the catalytic results will be presented and discussed simultaneously. Once again, the dashed lines that will be shown in some of the figures are only present for auxiliary purposes, to guide the eyes for tendencies that otherwise might be missed. None of these lines have physical meanings. Empty dots represent the discarded points for the construction of the auxiliary lines.

For Ni28-Al_2O_3 and NiO25-Al_2O_3 catalysts, when compared with Pt-Al_2O_3 ones, the conversions are significantly higher, especially for Ni28-Al_2O_3 and HPW/Ni28-Al_2O_3, as it can be seen in Figure 48 and for all the NiO25-Al_2O_3 catalysts. The latter are the catalysts with the higher initial conversions (Figure 49) with the physical mixture with $Cs_{2.5}$ (NiO25-Al_2O_3/$Cs_{2.5}$) showing the highest initial conversion. In both cases HPW impregnated catalysts suffer a decrease in conversion over time faster when compared with the support itself or with the physical mixtures with $Cs_{2.5}$. This might be due to the formation of carbonaceous deposits on the acid sites, as reported by Boahene *et al.*[137] for molybdenum heteropoly acid and nickel catalysts. Overall, the conversion of guaiacol is higher for the NiO25-Al_2O_3 catalysts than it is for the Ni28-Al_2O_3 ones.

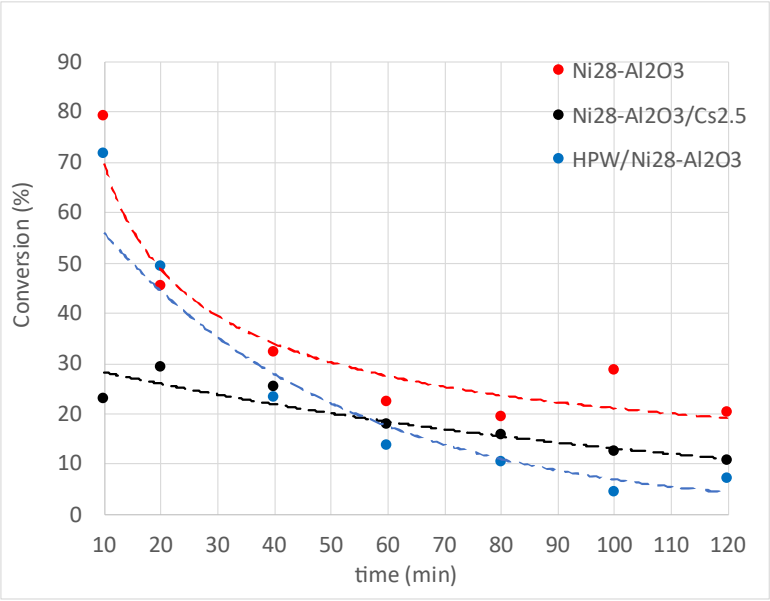

Figure 48: Guaiacol conversion as a function of time for Ni28-Al_2O_3 catalysts.

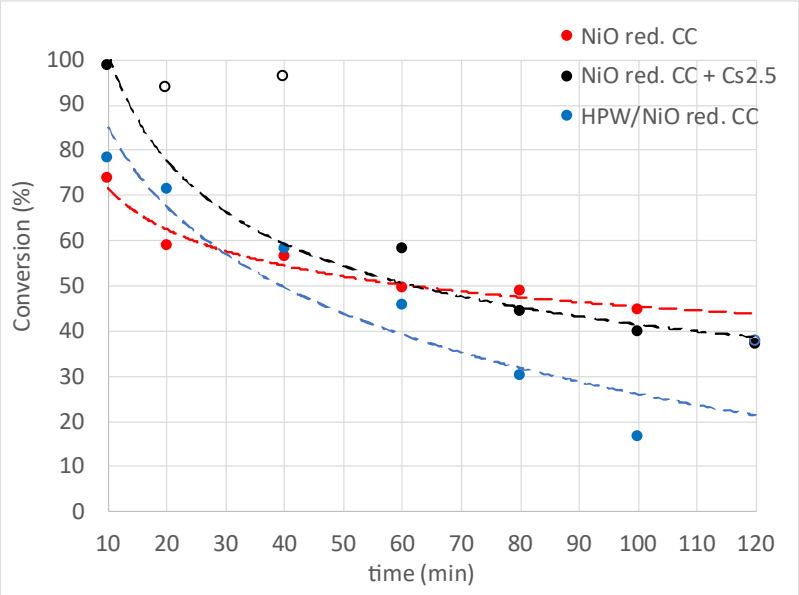

Figure 49: Guaiacol conversion as a function of time for NiO25-Al_2O_3 catalysts.

In Table 10 is shown a list of products formed for each catalyst, besides unknowns, and in contrast to the Pt-Al_2O_3 catalysts, here it was possible to detect deoxygenated products, mainly benzene. The deoxygenated product, in this case, is benzene and the selectivity for this product, obtained for each group of catalysts can be observed in Figure 50 and Figure 51. Benzene is one of the target products since a) it is totally deoxygenated, b) it is not hydrogenated, meaning that there is no H_2 "wasted" in hydrogenating the aromatic ring.

Table 10: Identified products for Ni28- Al_2O_3 and NiO25- Al_2O_3 catalysts.

Catalyst	Identified Products
Ni28- Al_2O_3	benzene, phenol, cyclohexanone
NiO25- Al_2O_3	benzene, phenol, cyclohexanone
Ni28- Al_2O_3 / $Cs_{2.5}$	benzene, phenol, anisole, cyclohexanone
NiO25- Al_2O_3/ $Cs_{2.5}$	benzene, phenol, anisole, cyclohexanone
HPW/Ni28- Al_2O_3	phenol, anisole, cyclohexanone
HPW/NiO25- Al_2O_3	benzene, phenol, cyclohexanone

The HPW/Ni28-Al_2O_3 catalyst is the one which led to a higher content of benzene in the products. However, the benzene selectivity decreased with time for these catalysts. Song *et al.*[8] reported a synergetic effect between Ni active sites and Bronsted acid sites in the presence of H_2. Indeed, it is observed a more pronounced production of benzene for HPW/Ni28-Al_2O_3 but this is not the case for Ni28-Al_2O_3/ $Cs_{2.5}$.

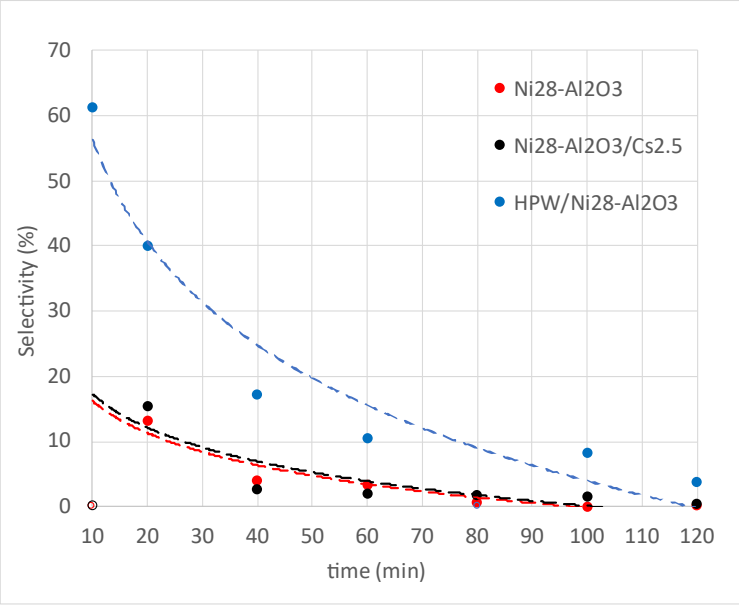

Figure 50: Selectivity of benzene with time on stream for Ni28-Al_2O_3 catalysts.

Although Figure 51 shows a 0 % benzene selectivity for initial times for NiO25-Al_2O_3/ $Cs_{2.5}$, it is believed that is not. However, as it can be seen in Appendix D, with this catalysts and under the reaction conditions applied, a transformation of *n*-heptane occurs, whose GC peaks overlap with the benzene GC peak. This was the only catalyst where *n*-heptane transformation was readily observed. Thus, considering that one cannot distinguish between the products from solvent or from benzene, benzene cannot be precisely accounted for, for this specific catalyst. For the case of NiO25-Al_2O_3 by itself, the selectivity for benzene decreases with reaction time (seen in red). Ardiyanti *et al.*[138] reported benzene as the main product for the HDO of anisole (300 ºC, 10 bar), with 72.5 % selectivity to benzene and only

2.2 % phenol selectivity over Ni/δ-Al_2O_3. In fact, although it is possible to produce benzene with the support without heteropoly acids, benzene selectivity is much lower and phenol selectivity is much greater in the present work than the reported by this research group. However, it is important to highlight that guaiacol has one more oxygen containing group than anisole, the support is slightly different (δ-Al_2O_3 Vs. γ-Al_2O_3) and the pressure is ten times higher than the one applied in this work. Although the values of benzene selectivity are not very high for the HPW/NiO25-Al_2O_3 catalyst, they remained in the same range of values throughout the whole reaction time.

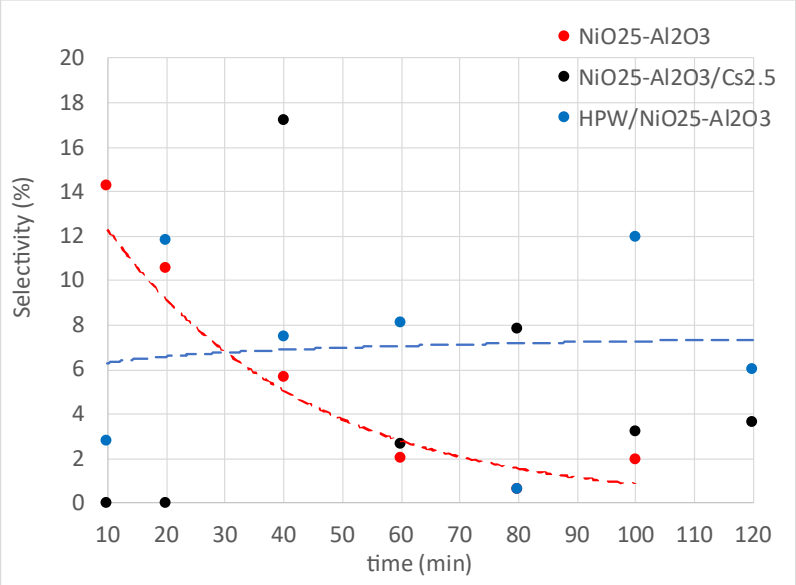

Figure 51: Selectivity of Benzene with time on stream for NiO25-Al_2O_3 catalysts.

The phenol selectivity followed the same tendency for all Ni-based catalysts (Figure 52 and Figure 53). It increased with time until values ranged from 60 to 80 %, depending on the catalyst. For the Ni28-Al_2O_3 catalysts, Ni28-Al_2O_3/ $Cs_{2.5}$ (in black in Figure 52) is the catalyst in which phenol selectivity suffered the smallest increase which is the opposite of what happens with the NiO25-Al_2O_3/ $Cs_{2.5}$ (in black Figure 53), that is the catalyst where the largest increase in phenol selectivity is observed. The trend of the selectivity to phenol is the same for Ni28-Al_2O_3 and HPW/Ni28-Al_2O_3. It can be seen, however, that as benzene selectivity decreases, phenol selectivity increases meaning that there is probably a loss in hydrodeoxygenation capacity.

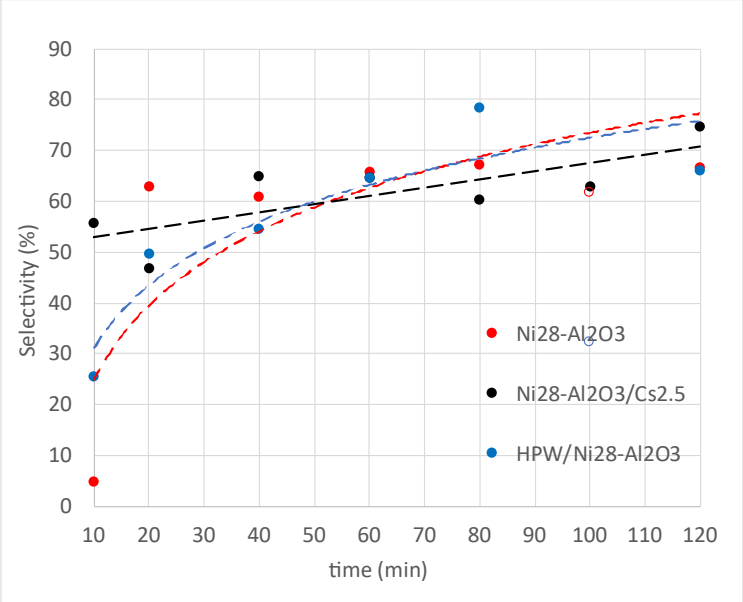

Figure 52: Selectivity of Phenol with time on stream for Ni28-Al_2O_3 catalysts.

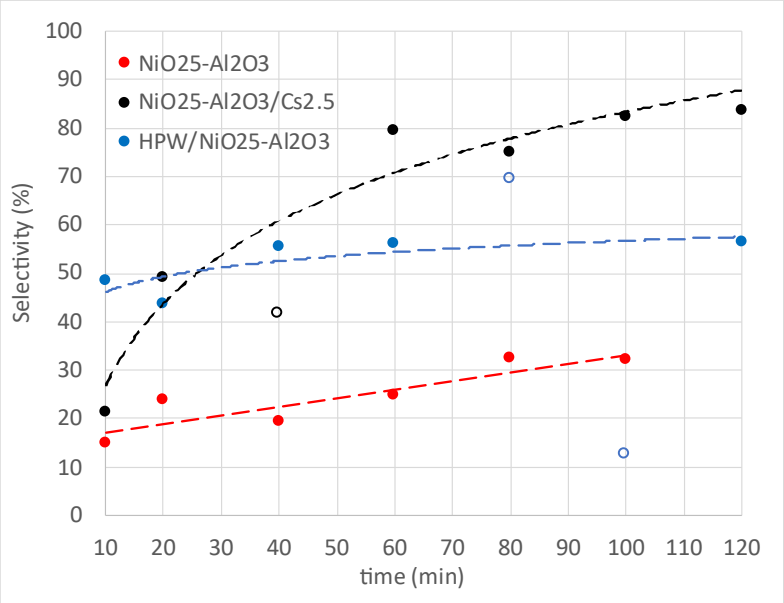

Figure 53: Selectivity of Phenol with time on stream for NiO25-Al_2O_3 catalysts.

For HPW/NiO25-Al_2O_3 (Figure 53, blue), the selectivity to phenol follows the same trend of the selectivity to benzene, being almost constant for all TOS values. For the support alone, there is a slight increase of phenol selectivity with time. Peters *et al.*[139] reported, for two commercial hydrotreating Ni catalysts, 24.3 % phenol selectivity for one of them and 42.0 % for the second one, at 400 ºC and 1.7 bar. Interestingly, this research group studied the effect of pressure and verified, in agreement with other authors[7] that increasing pressures increase the selectivity to deoxygenated products. Alharbi[140] reported on her thesis a 10 wt. % Ni supported $Cs_{2.5}$ salt catalyst (100 ºC and 1 atmospheric pressure) in which the anisole conversion was 10 %, considerably lower than the value obtained for both Ni catalysts but also at a lower temperature, with 40 % selectivity to phenol,, which is in agreement with

the results of the present work. Moreover, in Alharbi's work, cyclohexane selectivity was 22 %, which is a fully deoxygenated and hydrogenated product.

Cyclohexanone selectivity (Figure 54) is always less than 10 % for all Ni28-Al_2O_3 catalysts and it remains relatively constant with time.

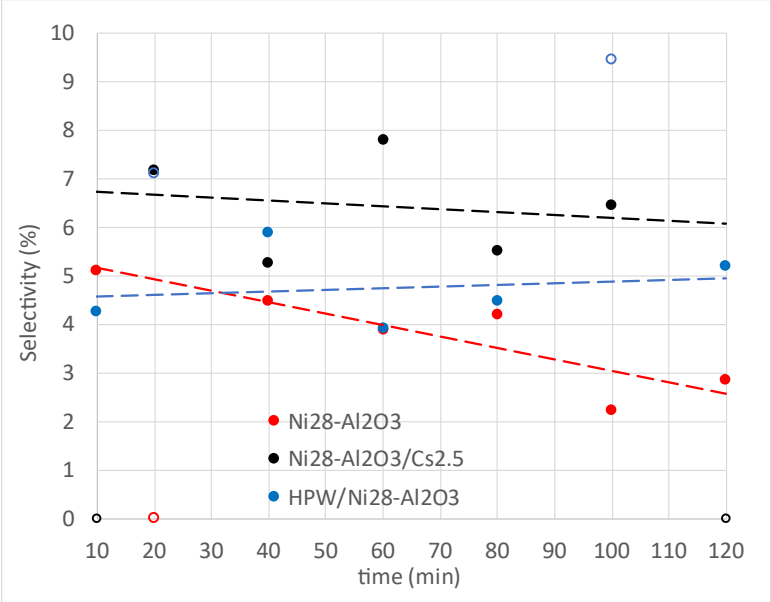

Figure 54:Selectivity of cyclohexanone in function of time for Ni28- Al_2O_3 catalysts.

NiO25-Al_2O_3 catalysts group has rather high selectivity cyclohexanone values, which might indicate the occurrence of hydrogenation (Figure 55). The selectivity however decreases with time, as opposite to the phenol selectivity, which might indicate a decrease in hydrogenation capacity with the reaction time.

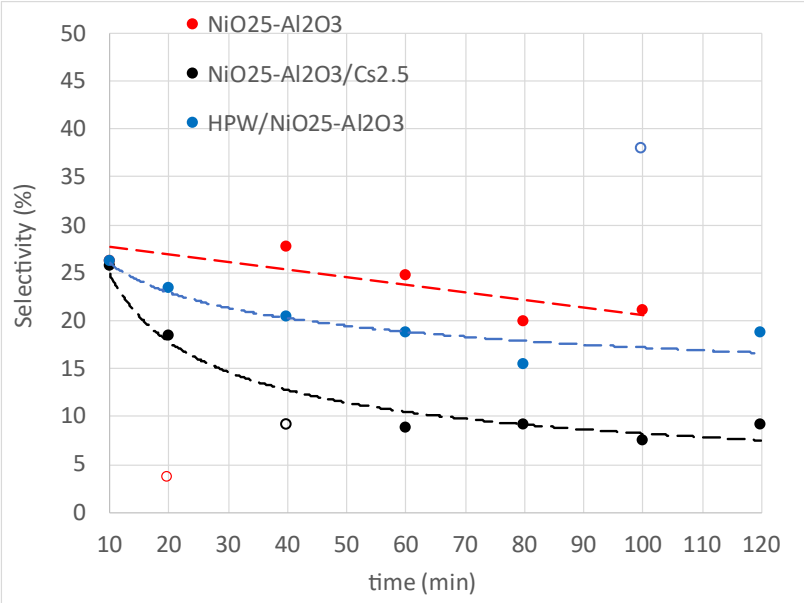

Figure 55: Selectivity of cyclohexanone in function of time for NiO25- Al_2O_3 catalysts.

Anisole was also identified for Ni28-Al_2O_3 based catalysts, with a tendency of decreasing selectivity with increasing reaction time for all catalysts, as it can be seen in Figure 56. However, for NiO25-Al_2O_3 catalysts group, anisole was only found for $Cs_{2.5}$ salt catalyst and in only two of the seven samples, with selectivity values that did not reach 1 %, meaning that this catalysts groups, in comparison with the other groups studies, did not led to the production of anisole.

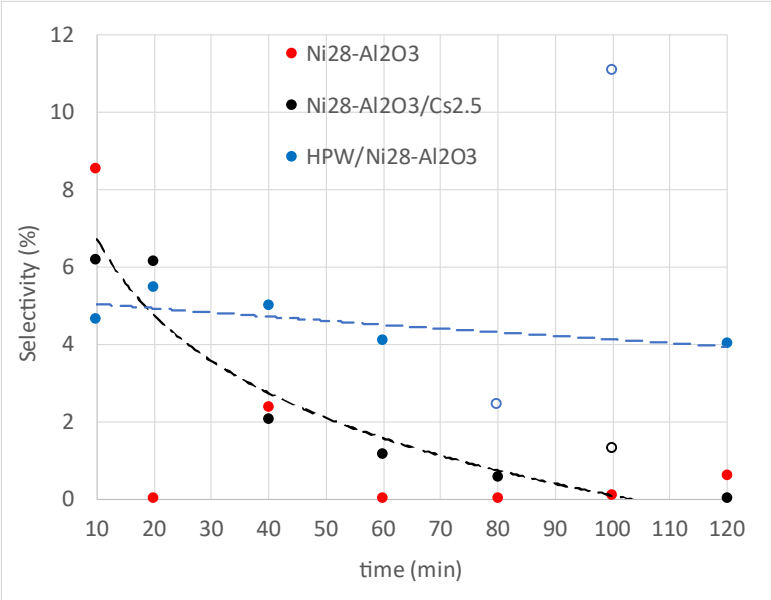

Figure 56: Selectivity of Anisole as a function of TOS for Ni28- Al_2O_3 catalysts.

Concerning transformation of guaiacol into anisole, the much energetic $C_{aromatic}$-OH bond must be broken. As it can be seen in Figure 56, the catalysts that yields a higher anisole amount is HPW/Ni28-Al_2O_3, the same catalysts thar yields a higher benzene amount. This indicates the capacity for this catalyst to eliminate $C_{aromatic}$-OR bonds, with R being either hydrogen or a methyl group, without ring hydrogenation.

Concerning unknown products selectivity (Figure 57 and Figure 58), it follows the same trend of phenol for Ni28-Al_2O_3 catalysts, with a marked increase of selectivity for initial reaction times. The exception is Ni28-Al_2O_3/$Cs_{2.5}$ whose selectivity remains roughly constant. The number of unknown species increases with time (See Appendix E, Table 15 and Table 16) for Ni28-Al_2O_3 but remains constant for both Ni28-Al_2O_3/ $Cs_{2.5}$ and HPW/Ni28-Al_2O_3. With Ni28- Al_2O_3 catalyst alone the number of unknowns products is higher, and the retention times are longer, which might be an indicator of heavier products.

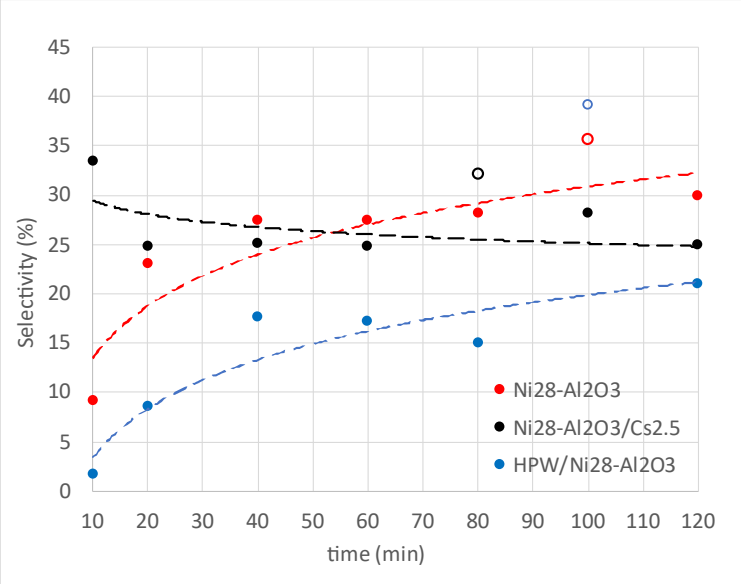

Figure 57: Selectivity of Unknowns (U) as a function of time on stream for Ni28- Al_2O_3 catalysts.

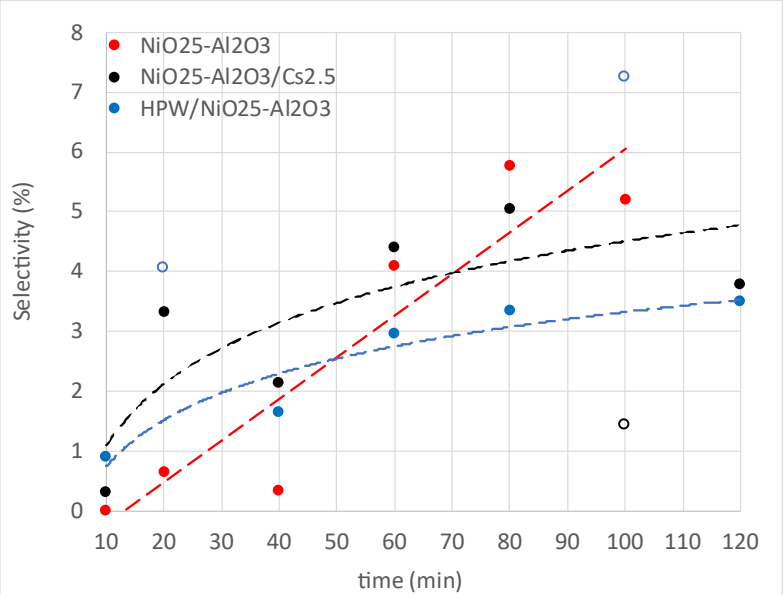

Figure 58: Selectivity of unknowns (U) as a function of time on stream for NiO25- Al_2O_3 catalysts.

For NiO25-Al_2O_3, selectivity to unknown products globally increases with reaction time however, values are always below 10 %, being a considerably lower amount when compared with the other two catalyst groups. Just like for Ni28-Al_2O_3 catalysts, the number of unknowns increases with time (See Appendix E) for the NiO25-Al_2O_3 support alone but remains constant for HPW/NiO25-Al_2O_3 and NiO25-Al_2O_3/ $Cs_{2.5}$. It was also observed that the retention times of the unknowns for NiO25-Al_2O_3 are generally shorter when compared with the Ni28-Al_2O_3 unknowns.

Figure 59 and Figure 60 show, for initial (10 min) and final times (120 min apart from NiO25-Al_2O_3, which is 100 min), the conversion and selectivity for the identified products and unknowns. It can be seen, in all cases, a decrease in conversion between 10 and 120 (or 100) min. For Ni28-Al_2O_3 catalysts (Figure 59), phenol is the main product, and its selectivity increases with time. The catalyst

that yields the higher benzene selectivity is HPW/Ni28-Al_2O_3 and it is also one of the catalysts with the higher initial conversion, however, both conversion and benzene selectivity decrease significantly with time.

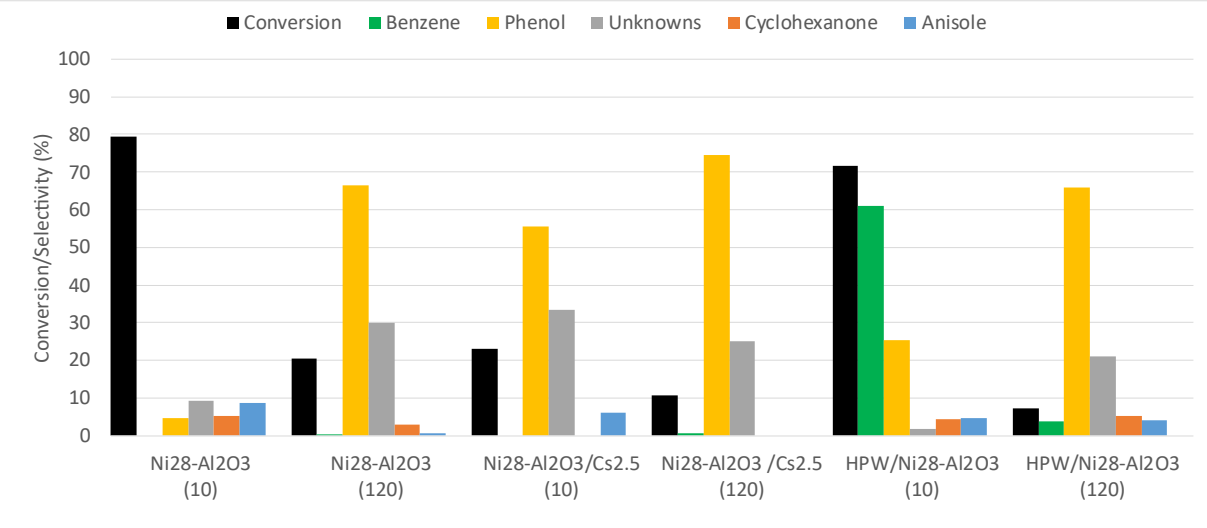

Figure 59: Summary of the results of the HDO of guaiacol for Ni28-Al_2O_3. In parenthesis TOS values, in minutes.

Considering NiO25-Al_2O_3 catalysts, Figure 60 ,it can be seen that the conversion decreases with time for all catalysts and that phenol and cyclohexanone are the major reaction products.

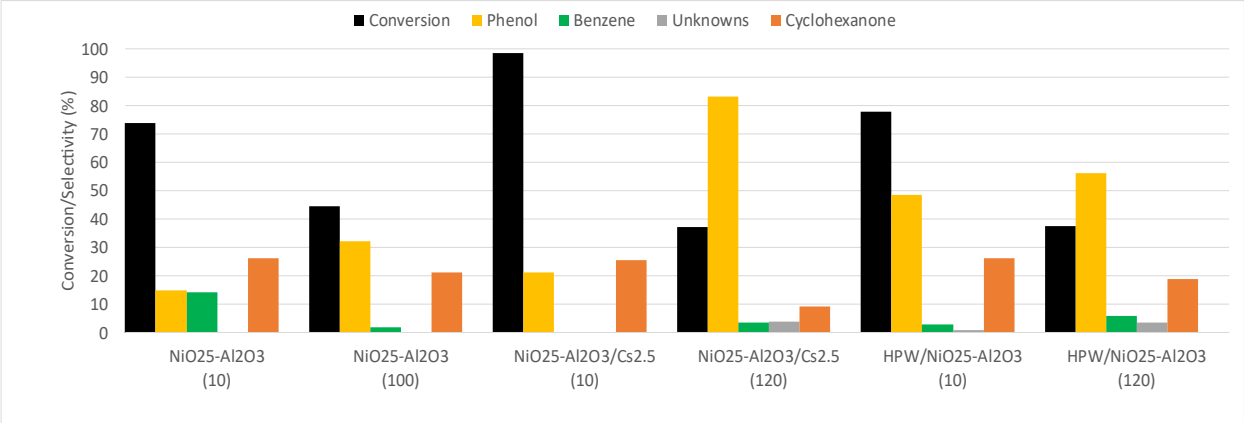

Figure 60: Summary of the results of the HDO of guaiacol for NiO25-Al_2O_3. In parenthesis TOS values, in minutes.

As for the case of Pt-Al_2O_3 based catalysts, the main reaction pathway for Ni-Al_2O_3 based catalysts is the direct deoxygenation (DDO) over the hydrogenation (HYD) pathway once phenol is one of the major products of the reaction. Indeed these results are in agreement with literature, for Ni catalysts based in acid supports.[8,141] For instance, Zhao *et al.*[141] reported that DDO is the preferred pathway when low pressures are applied (the pressures studied are between 5 and 20 bar) and Song *et al.*[8] reported that DDO pathway accounted for 75 % of guaiacol HDO while HYD accounted for the other 25 % (200 ºC, 30 bar H_2). This happens due to the steric effect of the methoxy group of the guaiacol molecule, making co-planar adsorption of guaiacol on the support a more difficult process leading to a

direct deoxygenation pathway. This research group obtained significantly lower conversions (0 to 18 % for 2 h of reaction time) when compared with both Ni based catalysts groups tested in this work, with the main product being phenol, but having identified also cyclohexanol, cyclohexanone, anisole and 2-methoxycyclohexanol. In fact, the results of this work mainly agree with the results of Song *et al.*[8] once that, for both catalysts, cyclohexane was obtained, which is a sign of the preferred hydrogenation-deoxygenation pathway for phenol molecules.

With all, in Table 11 the impregnated HPW catalysts, that were the ones that showed to be the most effective for the HDO of guaiacol, are compared with some catalysts for HDO reactions found on literature.

Table 11: Summary of HPW supported catalysts and comparison HDO reaction from literature.

Entry	Catalyst	Description	Reagent	Reaction Conditions, T (ºC), pressure (bar)	Conversion (%), initial (final) **	Major Products (initial selectivity, final selectivity (%))**
1	**HPW/Pt-Al_2O_3**	**HPW impregnated on Al_2O_3**	**GUA***	**300, 1**	**26 (1.54)**	**Phenol (16.7, 28.9), Anisole (9.09, 0)**
2[7]	Pt/Al_2O_3	Pt/ Al_2O_3 Sigma-Aldrich	GUA	300, 1.4	13	Phenol (12,12) Catechol (52,49)
3[68]	Pt/ $Cs_{2.5}$		GUA	120, 7	---	Cyclohexane (68 % yield)
4	**HPW/Ni28-Al_2O_3**	**HPW impregnated in Ni (previously) impregnated on Al_2O_3**	**GUA**	**300,1**	**71.8 (7.21)**	**Benzene (61.1, 3.83), Phenol (25.4, 66)**
5[140]	10%Ni/ $Cs_{2.5}$	Ni impregnated on $Cs_{2.5}$ salt and calcined at 400 ºC	ANI*	100, 1	10	Phenol (40), Cyclohexane (22)
6[8]	Ni/HZSM-5		GUA	200, 30	18	Phenol (44), Cyclohexanol (22)

7	**HPW/NiO25-Al_2O_3**	**HPW impregnated in NiO industrial catalyst**	**GUA**	**300, 1**	**78.1 (37.6)**	**Phenol (28.5, 56.4), Cyclohexanone (26.2, 18.8)**
8[64]	Ni/Al_2O_3	Ni impregnated on Al_2O_3	ANI	290, 3	99	Cyclohexane (54), Benzene (27)
9[66]	Ni/USY	IWI of Ni in USY and calcined at 550 ºC	ANI	200, 52	75	Cyclohexane (70)
10[142]	15% wt. Ni/ Al_2O_3	----	GUA	300, 50	26	Deoxygenated products (23)
*GUA stands for guaiacol and ANI for anisole. ** initial and final values when applicable. In **bold** are the catalysts tested in this work.						

3.2.3 Spent catalysts characterization

Due to the high degree of deactivation of all catalysts, seen from the decrease in the conversion of guaiacol, the spent catalysts were characterized to try to understand the reason for this fast deactivation. For that purpose, the techniques used were powder XRD, to analyze structural changes, TGA, to quantify the weight loss of each catalyst and IR Spectroscopy, to evaluate the presence of organic species (e.g., coke) in the catalysts.

The experimental X-ray patterns of fresh and spent catalysts show no differences, leading to the conclusion that the catalyst deactivation is not due to catalysts structural changes.

The IR analysis was carried out on the catalysts, in an attempt to understand the cause of the deactivation of the catalysts. For all the spent catalysts, new bands can be observed. Popov *et al.*[73] studied the adsorption of phenolic molecules on alumina supports (among others). They discovered that guaiacol interacts strongly with the alumina support, through chemisorption of doubly anchored phenate. This means that when guaiacol is contacted with the alumina support, it attaches easily to the support with, not one, but actually both oxygens, when temperatures exceed 250 ºC (in this work, the reaction was done at 300 ºC), Figure 61. Moreover, Jongerius *et al.*[143] reported that this guaiacol adsorption on alumina supports is reversible and that there is a competitive adsorption between water molecules and aromatic oxygenates onto the alumina surface.

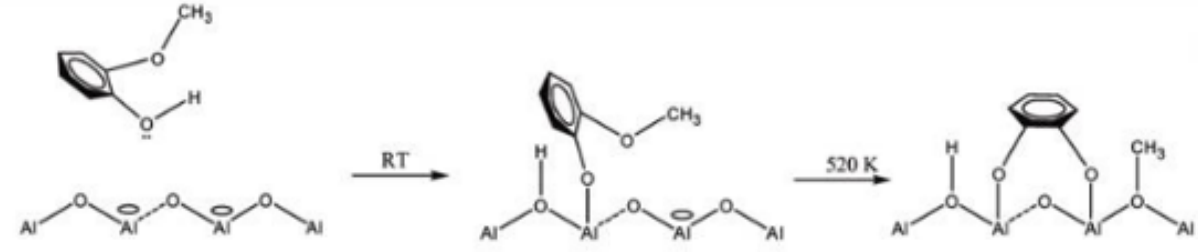

Figure 61Formation of doubly anchored phenate species between guaiacol and alumina support. From ref. 74.

When analyzing all the spectra for all the spent catalysts (Figure 62, Figure 63 andFigure 64), it becomes evident the appearance of two new bands: the former at around 1480 cm^{-1} and the latter at around 1250 cm^{-1}. The first band can be associated with the aromatic ring vibrations with an -OH contribution and the second band is also attributed to also aromatic ring vibrations with a C-O contribution.[73] Both these bands are characteristic of guaiacol and, in this case, confirm its presence on the catalysts, being, as reported above, a possible cause of deactivation of all the catalysts, which agrees with the findings of Popov *et al.*[73]

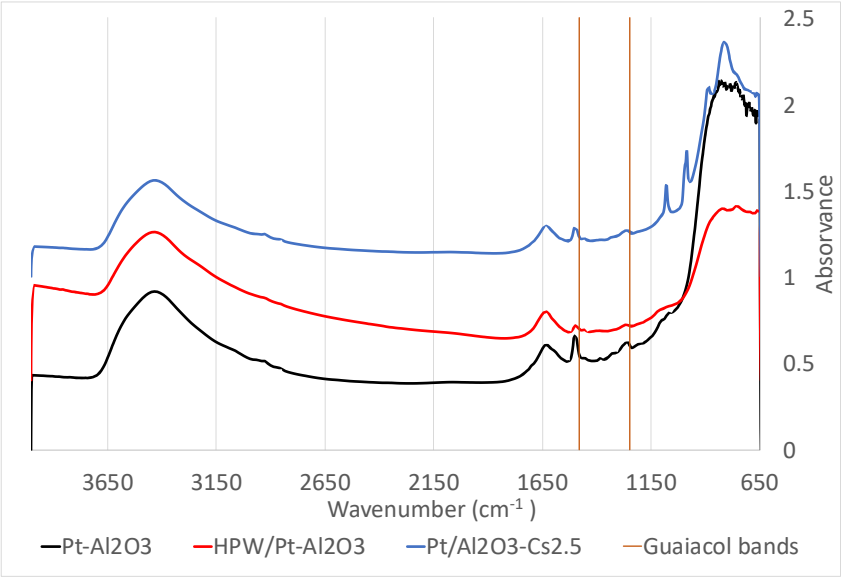

Figure 62: IR spectra for spent Pt/Al_2O_3 catalysts.

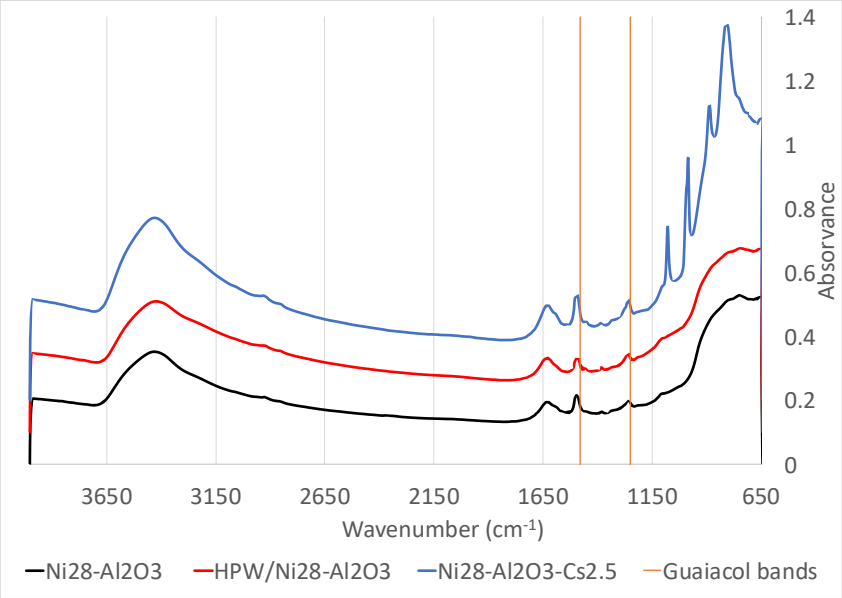

Figure 63: IR spectra for spent Ni28-Al_2O_3 catalysts.

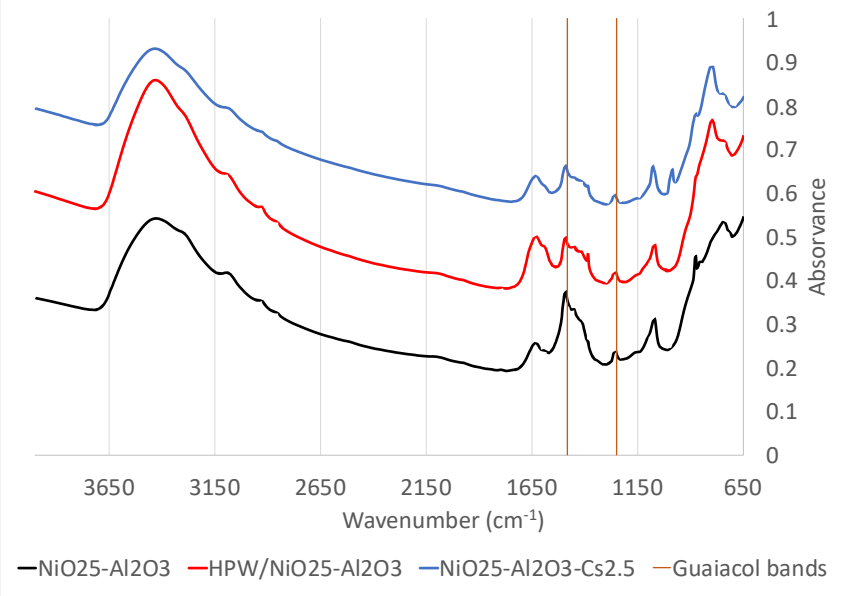

Figure 64: IR spectra for spent NiO25- Al_2O_3 catalysts.

The thermogravimetric (TGA) results can be seen in Table 12 and Table 13. The first loss, which is endothermic for all catalysts and situated around 100 ºC, can be easily attributed to water desorption. The second weight loss observed is exothermic and ranges from 160 to 550 ºC for Ni catalysts and 140 to 640 ºC for Pt catalysts. NiO25-Al_2O_3 catalysts group showed yet two more endothermic weight losses at higher temperatures. It is important to mention that the TG-DSC analysis was done using air, and after the experiments, the nickel catalysts presented a greenish NiO typical color. This means that although only weight losses are considered, some gain loss might occur, due to the oxidation of the Ni species.

Coke is known as one of the most common causes of catalyst deactivation. There are two types of coke, soft and hard, and the formation of one or another depends mainly on the reaction's

temperature.[144,145] Although the temperatures ranges are not well established, Guisnet *et al.*[145] proposed that formation of light or soft coke is done for reaction temperatures below 200 ºC and for hard or heavy coke, formation is done for temperatures above 350 ºC. For intermediate temperatures, which is our case (300 ºC), the coke is formed by the mechanisms of both soft and hard coke. The soft coke is produced by condensation and rearrangement reactions and it depends highly on the reagent. In this case, and because the reagent is an oxygenated molecule, guaiacol, the soft coke is probably composed of polymethyl phenols or anisoles. On the other hand, for the case of hard coke, regardless of the reagent, the coke is composed by polyaromatics that, besides condensation and rearrangement reactions, go through hydrogen transfer reactions on the acid sites and through dehydrogenation reactions, on the metal sites, in the case of bifunctional catalysts.[145] Thus, the carbonaceous deposits formed for the guaiacol HDO reactions are probably a mixture of these two types. Because the oxidation of coke is accompanied by exothermic TGA peaks[146], the two higher temperatures weight losses for the NiO25-Al_2O_3 are probably not caused by carbonaceous deposits. These two endothermic weight losses however, might be caused by the transformation of boehmite into γ-Al_2O_3, as seen, between 450 and 700 ºC and also $CaCO_3$ decomposition is endothermic and occurs around 750 ºC.[147,148]

For the Pt-Al_2O_3 catalysts, although HPW/Pt-Al_2O_3 suffers a higher degree of deactivation (seen by the decrease in conversion as a function of TOS in Figure 41), the catalyst that has a higher (second) weight loss observed is Pt-Al_2O_3 (10.3 %). Although the conversion value of Pt-Al_2O_3 alone and Pt-Al_2O_3/ $Cs_{2.5}$ are similar, the former catalyst presents a higher weight loss. For the Pt-Al_2O_3 support, at higher reaction times, the RT of unknowns are longer, thus it is speculated that products are maybe multi-oxygenated compounds. In fact, the TGA weight loss for this catalyst is the highest and as aforementioned, non-desorbed carbonaceous compounds of phenolic reagents tend to be polymethyl phenols or anisoles. For the Ni28-Al_2O_3, once again, the catalyst that deactivates faster, HPW/Ni28-Al_2O_3 is not the one with the higher weight loss, which in this case is Ni28- Al_2O_3/$Cs_{2.5}$.

Table 12: TGA results summary for Pt-Al_2O_3 and Ni28-Al_2O_3 catalysts.

Samples	Weight loss (%)	Weight loss (%)	TOTAL WEIGHT LOSS (%)
ΔT (ºC)	**25-200**	**200 - 640**	
Pt-Al_2O_3	2.4	**10.3**	**12.7**
HPW/Pt-Al_2O_3	2.6	**6.9**	**9.5**
Pt-Al_2O_3 / $Cs_{2.5}$	2.4	**8.5**	**10.9**
Ni28- Al_2O_3	2.0	**7.0**	9.0
HPW/ Ni28- Al_2O_3	4.0	**6.1**	10.1
Ni28- Al_2O_3/ $Cs_{2.5}$	2.4	**7.4**	9.8

The TGA results for the NiO25- Al_2O_3 are shown in Table 13. The higher weight losses occur between 500 and 560 ºC, contrarily to what happens for the other two groups of catalysts, where the weight loss between 200 and 500 ºC is the most significant. However, because these losses are

endothermic ones, they are probably not carbonaceous deposits. Thus, these were the catalysts that yielded the less coke.

Table 13: TGA results summary for NiO25-Al_2O_3 catalysts.

Samples	Weight loss (%)	Weight loss (%)	Weight loss (%)	Weight loss (%)	TOTAL WEIGHT LOSS (%)
ΔT (ºC)	**25-160**	**160 - 500**	**500 - 560**	**600 - 700**	
NiO25- Al_2O_3	3.4	**2.0**	3.6	3.3	12.3
HPW/NiO25- Al_2O_3	2.5	**1.6**	3.7	1.6	9.4
NiO25- Al_2O_3 / $Cs_{2.5}$	2.3	**2.2**	3.1	2.2	9.8

Considering the results abovementioned, one can say that part of the deactivation of the catalysts might come from carbonaceous deposits. It is known that not only guaiacol (that binds with both oxygens), but also phenolic compounds, such as phenol and anisole (reaction products), interact strongly with the alumina support and can act as "coke" precursors.[73] Jongerius *et al.*[143] showed that a Pt-Al_2O_3 treated with guaiacol in an autoclave at 225 ºC shows a mass loss of 14 to 17 %, with a peak at around 450 ºC, which is in agreement with the results. Indeed, "coke" deposits might be the main cause of deactivation for both the supports and the physical mixtures. However, is not thought to be the case for HPW catalysts, once these suffer the most important deactivation over time, although they do not present the highest weight losses. Because the HPW structure could not be seen in the diffractograms of fresh catalysts, a more thorough analysis should be done to investigate if the structure of the HPW impregnated on the supports is still unaltered or if it has decomposed. Because there is only one exothermic weight loss at considerably low temperatures for all catalysts, the deposits are probably guaiacol.

Overall, the conversions obtained follow the order NiO25-Al_2O_3> Ni28-Al_2O_3 ≫ Pt-Al_2O_3 (on a support basis). This is probably because Pt loading in Pt catalysts is 1 wt. % and in Ni catalysts it is always higher than 10 wt. %. The main product obtained was, with no doubt, phenol, whose selectivity increases with time for all Ni catalysts. However, for Pt catalysts it reaches a maximum and decreases afterwards. Concerning HPW supported catalysts, all of them deactivate faster. Carbonaceous deposits seem to be the main cause of deactivation for supports and physically mixed catalysts, however, it was ruled out as the main cause of deactivation of the HPW impregnated catalysts. As seen by IR spectroscopy analysis, guaiacol is probably one of the main species strongly adsorbed on the surface of the catalysts. The HPW structure could not be identified by XRD, UV-Vis DRS nor IR spectroscopy, so other techniques should be applied to try to understand if, in fact, the cause of deactivation of these catalysts originates from HPW structural changes. These catalysts, however, showed very good selectivity to deoxygenated products, especially regarding the cleavage of $C_{aromatic}$-O bonds. This can

be seen not only because selectivity of benzene is higher, but also due to higher anisole selectivity values, for the Pt-Al_2O_3 and Ni28-Al_2O_3 catalysts. Considering NiO25-Al_2O_3 catalysts, the benzene production is difficult to evaluate, due to the overlap of the GC peaks of benzene and *n*-heptane transformation products, mainly for the physically mixed catalyst, although it seems that there is a decreasing trend overtime. The low selectivity to cyclohexanone in HPW catalysts shows that, along with the high selectivity for aromatic product (whether these are oxygenated, ex. phenol, or not, ex. benzene), the reaction follows mainly a direct deoxygenation (DDO) pathway. In a less pronounced way, this conclusion can be drawn for all catalysts tested. This is thought to be caused by the steric effect of the methoxy group of guaiacol.[8] For the physically mixed catalysts the conversion is usually similar to the support conversion, with the exception for the NiO25-Al_2O_3, where the conversion is higher. When compared with the results for the support alone, it can be seen that physically mixed catalysts do not bring any significant benefit on a first glance. However, with the knowledge that this catalyst leads to solvent transformation, it would be interesting to repeat this reaction with some changes. For example, changing the GC column temperature configuration to a slower heating rate, in order to obtain larger difference between RT of the products and being able to distinguish between the GC peaks of benzene and of the products of the *n*-heptane transformation. Along with that, increasing the $Cs_{2.5}$ salt fraction content would be interesting, as some authors[68,136] use much higher $Cs_{2.5}$ loadings than the ones applied in this work. The loadings in the present work were chosen so as to have the same weight percentage of both the heteropoly acid and the $Cs_{2.5}$ salt on the catalysts.

It would also be interesting to perform GC-MS (Mass Spectrometry) in order to characterize the unknown compounds. Although for Pt-Al_2O_3 with heteropoly acids it can be speculated that these unknowns are probably alkylated phenolic compounds or compounds with more than one -OH group, due to the increasing RT with TOS and acidity of the catalyst, for Ni catalysts this hypothesis is more unlikely, once the catalysts that led to a higher amount of unknowns with longer RT are the supports alone, specially Ni28-Al_2O_3. Liquid Chromatography-Mass Spectrometry (LC-MS) has been performed to try to identify the unknown products, however, these products are probably composed of small molecules that cannot be ionized by the electrospray ionization technique and thus no conclusion could be obtained from this analysis.

Conclusions and perspective

The objective of this work was to study heteropoly acids combined with metal-based alumina supports in the HDO of oxygenated molecules. Guaiacol, in this case, was chosen as a model compound once it has not one, but two $C_{aromatic}$-O functional groups. For that purpose, several catalysts were prepared based on three supports, 1 wt. % Pt-Al_2O_3, Ni28-Al_2O_3 and an industrial NiO25-Al_2O_3. The heteropoly acid was added to the support in two different ways. The first one was incipient wetness impregnation of an aqueous solution of 12-tungstophosphoric acid ($H_3PW_{12}O_{40}$, HPW). The second one was a mechanical mixture of $Cs_{2.5}H_{0.5}PW_{12}O_{40}$ ($Cs_{2.5}$ salt) with the support. In both cases, the heteropoly acid or salt content was kept constant (20 wt. %). The $Cs_{2.5}$ salt was synthetized by adding the appropriate amount of a cesium precursor to an aqueous solution of HPW. The catalysts tested were: Pt-Al_2O_3, HPW/ Pt-Al_2O_3 and Pt-Al_2O_3/$Cs_{2.5}$ (with 1 wt. % Pt-Al_2O3 as support); Ni28-Al_2O_3, HPW/Ni28-Al_2O_3 and Ni28-Al_2O_3/$Cs_{2.5}$ (with Ni28-Al_2O_3 as support) and finally NiO25-Al_2O_3, HPW/NiO25-Al_2O_3 and NiO25-Al_2O_3/$Cs_{2.5}$ (with NiO25-Al_2O_3 as support).

Using different characterization techniques, it was possible to confirm the presence of $Cs_{2.5}$ salt in all the “mixture” catalysts. However, for the HPW impregnated catalysts, the only catalyst where presence of the heteropoly acid on the support was confirmed was HPW/Pt-Al_2O_3 (UV-Vis DRS results). It is worth mentioning, however, that it was possible to confirm the presence of the HPW impregnated on alumina only by UV-Vis DRS.

The guaiacol HDO reaction was carried out at 300 ºC, under atmospheric pressure and with a H_2/guaiacol molar ratio of 50. The conversion results followed the group order NiO25-Al_2O_3 > Ni28-Al_2O_3 >> Pt-Al_2O_3. It is, however, difficult to compare Ni catalysts with Pt one, once the metal loading of Pt is only 1 wt % while the Ni loadings are much higher (about 25 %). The main product for all catalysts was phenol. For Pt catalysts, anisole and cyclohexanone were also identified. For the Ni catalysts, all these products were identified. However, benzene, a fully deoxygenated products, was also identified for these catalysts. From the catalytic tests results, it can be seen that NiO25-Al_2O_3/$Cs_{2.5}$ catalyst has a lot of potential, being the catalyst with the highest initial conversion, however its results could not be properly analyzed due to the occurrence of solvent transformations, that made the distinction between guaiacol transformation products and *n*-heptane transformation products a difficult task. HPW impregnated on Ni catalysts led to high initial conversions with also high selectivity to benzene. There was also a large amount of products that could not be identified. Based on the main reaction product, phenol, it was possible to conclude that the main reaction pathway was the direct deoxygenation of guaiacol, instead of the hydrogenation-deoxygenation pathway.

Although a decrease of conversion as a function of time on stream was observed for all catalysts, it was much more pronounced on the HPW impregnated catalysts. To understand the cause for this behavior, the spent catalysts were characterized by XRD, TGA and IR Spectroscopy. The XRD results showed no structural changes in all the catalysts after reaction. Thus, the cause of deactivation of the catalysts is thought to be caused by the strong adsorption of guaiacol on the catalysts surface. TGA and IR Spectroscopy results were in agreement. The weight losses for all catalysts are comprised between 9 and 12.7 % and occur at rather low temperatures, not commonly seen in coke oxidation.

Hence it is thought to be the oxidation of lighter carbonaceous deposits. IR spectroscopy results show the appearance of mainly two new bands, which are characteristic of guaiacol, confirming the presence of this species on the catalysts. This result, however, does not explain the reason for the faster deactivation of the HPW catalysts once the maximum weight loss is generally observed for $Cs_{2.5}$ catalysts and not for HPW catalysts. Thus, this deactivation might be also caused by a decomposition of the heteropoly acid on the support, which cannot be seen because, even in the fresh catalysts, the HPW presence could not be confirmed.

There is still a lot of work in perspective. First of all, it would be important to definitely confirm the presence of the heteropoly acid impregnated on the various supports. A textural analysis would be interesting to understand the changes in the surface of the catalysts with the addition of both the heteropoly acid or its $Cs_{2.5}$ salt. Pyridine sorption (followed by Infrared) or NH_3 TPD would be interesting techniques to be used in order to understand how heteropoly acid or salt influence the catalysts acidity properties. Moreover, it would be interesting to perform H_2 chemisorption to the Ni based catalysts and TEM to all catalysts for a better understanding of their dispersion. Because it was seen that guaiacol adsorbs strongly on alumina, trying new supports, such as the $Cs_{2.5}$ salt itself or even physical mixtures of this salt with other supports, such as zeolites could be also an alternative. Finally, regarding the HDO reaction, it would be interesting to perform it under different reaction conditions, such as varying temperatures and contact times for optimization purposes. For a better comparison of the supports, in particular for the comparison between Pt and Ni supports, these should be done by comparing the different under the same conditions of conversion, i.e. iso-conversion.

References

1. Ahmad, T. & Zhang, D. A critical review of comparative global historical energy consumption and future demand: The story told so far. *Energy Reports* **6**, 1973–1991 (2020).
2. Yildiz, L. *Fossil Fuels*. *Comprehensive Energy Systems* vols 1–5 (2018).
3. Zhong, J., Pérez-Ramírez, J. & Yan, N. Biomass valorisation over polyoxometalate-based catalysts. *Green Chem.* **23**, 18–36 (2021).
4. Attia, M., Farag, S. & Chaouki, J. Upgrading of oils from biomass and waste: Catalytic hydrodeoxygenation. *Catalysts* **10**, 1–30 (2020).
5. Huber, G. W., Iborra, S. & Corma, A. Synthesis of transportation fuels from biomass: Chemistry, catalysts, and engineering. *Chem. Rev.* **106**, 4044–4098 (2006).
6. Bridgwater, A. V. Review of fast pyrolysis of biomass and product upgrading. *Biomass and Bioenergy* **38**, 68–94 (2012).
7. Runnebaum, R. C., Lobo-Lapidus, R. J., Nimmanwudipong, T., Block, D. E. & Gates, B. C. Catalytic Conversion of Guaiacol Catalyzed by Platinum Supported on Alumina: Reaction Network Including Hydrodeoxygenation Reactions. *Energy and Fuels* **25**, 3417–3427 (2011).
8. Song, W., Liu, Y., Baráth, E., Zhao, C. & Lercher, J. A. Synergistic effects of Ni and acid sites for hydrogenation and C-O bond cleavage of substituted phenols. *Green Chem.* **17**, 1204–1218 (2015).
9. Misono, M. *Heterogeneous Catalysis of Mixed Oxides Perovskite and Heteropoly Catalysts*. vol. 176 (Elsevier, 2013).
10. Okuhara, T., Kasai, A., Hayakawa, N., Misono, M. & Yoneda, Y. the Important Role of the Bulk of 12-Tungustophosphoric Acid in the Catalytic Dehydration of Alcohols To Olefins. *Chem. Lett.* **10**, 391–394 (1981).
11. Shonnard, D. R. & Allen, D. T. *Green Engineering: Environmentally Conscious Design and Chemical Processes*. (2002).
12. World Population @ Population.Un.Org. https://population.un.org/wpp/. - 6th of april 2021
13. The World Bank Group. GDP @ data.worldbank.org. *2010* - 6th april 2021http://data.worldbank.org/indicator/NY.GDP.MKTP.KD.ZG (2010).
14. bp. *Energy Outlook 2020 edition*.
15. Action on Climate and SDGs @ unfccc.int. https://unfccc.int/topics/action-on-climate-and-sdgs/action-on-climate-and-sdgs. - 3rd of april 2021
16. The Paris Agreement @ unfccc.int. https://unfccc.int/process-and-meetings/the-paris-agreement/the-paris-agreement. - 3rd of april 2021
17. Antar, M. *et al.* Biomass for a sustainable bioeconomy: An overview of world biomass production and utilization. *Renew. Sustain. Energy Rev.* **139**, 110691 (2021).
18. Biomass Resources @ www.energy.gov. https://www.energy.gov/eere/bioenergy/biomass-resources. - 14th of april 2021
19. Headey, D. *Causes of the 2007-2008 global food crisis identified*. (2011).
20. Rutz, D. & Janssen, R. Feedstock Production. *BioFuel Technol. Handb.* 72 (2007).
21. Stokke, D. D., Wu, Q. & Han, G. Lignocellulosic Materials. *Introd. to Wood Nat. Fiber Compos.*

19–59 (2013) doi:10.1002/9780470711804.ch2.

22. Graça, I., Lopes, J. M., Cerqueira, H. S. & Ribeiro, M. F. Bio-oils upgrading for second generation biofuels. *Ind. Eng. Chem. Res.* **52**, 275–287 (2013).
23. Wang, X., Arai, M., Wu, Q., Zhang, C. & Zhao, F. Hydrodeoxygenation of lignin-derived phenolics-a review on the active sites of supported metal catalysts. *Green Chem.* **22**, 8140–8168 (2020).
24. Hossain, M. A. *et al.* Catalytic cleavage of the B-O-4 aryl ether bonds of lignin model compounds by Ru/C catalyst. *Appl. Catal. A Gen.* **582**, 117100 (2019).
25. Zhang, C. *et al.* Cleavage of the lignin β-O-4 ether bond: Via a dehydroxylation-hydrogenation strategy over a NiMo sulfide catalyst. *Green Chem.* **18**, 6545–6555 (2016).
26. Saidi, M. *et al.* Upgrading of lignin-derived bio-oils by catalytic hydrodeoxygenation. *Energy Environ. Sci.* **7**, 103–129 (2014).
27. Nag, A. *Biofuels Refining and Performance*. (2008).
28. Bridgwater, A. V. & Peacocke, G. V. C. Fast pyrolysis processes for biomass. *Renew. Sustain. energy Rev.* **4**, 1–73 (2000).
29. Mortensen, P. M., Grunwaldt, J. D., Jensen, P. A., Knudsen, K. G. & Jensen, A. D. A review of catalytic upgrading of bio-oil to engine fuels. *Appl. Catal. A Gen.* **407**, 1–19 (2011).
30. WebBook, N. C., Editions), (various, O. E. I. & International Gas Union, N. G. C. G. Heat-Values-of-Various-Fuels @ World-Nuclear.Org. https://world-nuclear.org/information-library/facts-and-figures/heat-values-of-various-fuels.aspx.- 14th of july 2021
31. Ribeiro, F. *Petroleum (Oil), Classification and Properties*.
32. Speight, J. G. *The Chemistry and Technology of Petroleum*. *The Chemistry and Technology of Petroleum* (2014). doi:10.1201/b16559.
33. Zeman, F. S. & Keith, D. W. Carbon neutral hydrocarbons. *Philos. Trans. R. Soc. A Math. Phys. Eng. Sci.* **366**, 3901–3918 (2008).
34. Si, Z., Zhang, X., Wang, C., Ma, L. & Dong, R. An Overview on Catalytic Hydrodeoxygenation of Pyrolysis Oil and Its Model Compounds. *Catalysts* vol. 7 1–22 (2017).
35. Maggi, R. & Delmon, B. A review of catalytic hydrotreating processes for the upgrading of liquids produced by flash pyrolysis. *Stud. Surf. Sci. Catal.* **106**, 99–113 (1997).
36. Axelsson, L. *et al.* Perspective: Jatropha cultivation in southern India: Assessing farmers' experiences. *Biofuels, Bioprod. Biorefining* **6**, 246–256 (2012).
37. Furimsky, E. Chemistry of Catalytic Hydrodeoxygenation. *Catal. Rev. - Sci. Eng.* **25**, 421–458 (1983).
38. Sirous-Rezaei, P. *et al.* Mild hydrodeoxygenation of phenolic lignin model compounds over a FeReOx/ZrO2 catalyst: zirconia and rhenium oxide as efficient dehydration promoters. *Green Chem.* **20**, 1472–1483 (2018).
39. Gonçalves, V. O. O., Brunet, S. & Richard, F. Hydrodeoxygenation of Cresols Over Mo/Al2O3 and CoMo/Al2O3 Sulfided Catalysts. *Catal. Letters* **146**, 1562–1573 (2016).
40. Furimsky, E. Catalytic hydrodeoxygenation. *Appl. Catal. A Gen.* **199**, 147–190 (2000).
41. Mortensen, P. M., Grunwaldt, J. D., Jensen, P. A. & Jensen, A. D. Screening of catalysts for

hydrodeoxygenation of phenol as a model compound for bio-oil. *ACS Catal.* **3**, 1774–1785 (2013).

42. Hong, D. Y., Miller, S. J., Agrawal, P. K. & Jones, C. W. Hydrodeoxygenation and coupling of aqueous phenolics over bifunctional zeolite-supported metal catalysts. *Chem. Commun.* **46**, 1038–1040 (2010).
43. Alharbi, K., Alharbi, W., Kozhevnikova, E. F. & Kozhevnikov, I. V. Deoxygenation of Ethers and Esters over Bifunctional Pt-Heteropoly Acid Catalyst in the Gas Phase. *ACS Catal.* (2016) doi:10.1021/acscatal.6b00096.
44. Ambursa, M. M. *et al.* A review on catalytic hydrodeoxygenation of lignin to transportation fuels by using nickel-based catalysts. *Renew. Sustain. energy Rev.* (2021) doi:https://doi.org/10.1016/j.rser.2020.110667.
45. Elliott, D. C. Historical Developments in Hydroprocessing Bio-oils. *Energy and Fuels* **21**, 1792–1815 (2007).
46. Patil, M. L., Lali, A. M. & Dalai, A. K. Catalytic hydrodeoxygenation of bio-oil model compound for production of fuel grade oil. *Asia-Pacific J. Chem. Eng.* **14**, 1–14 (2019).
47. Kim, S. *et al.* Recent advances in hydrodeoxygenation of biomass-derived oxygenates over heterogeneous catalysts. *Green Chem.* **21**, 3715–3743 (2019).
48. Rinaldi, R. *Catalytic Hydrogenation for Biomass Valorization*. (Royal Society of Chemistry, 2015).
49. Silva, N. K. G., Ribas, R. M., Monteiro, R. S., Barrozo, M. A. de S. & Soares, R. R. Thermodynamic equilibrium analysis of the vapor phase hydrodeoxygenation of guaiacol. *Renew. Energy* **147**, 947–956 (2020).
50. Robinson, A. M., Hensley, J. E. & Will Medlin, J. Bifunctional Catalysts for Upgrading of Biomass-Derived Oxygenates: A Review. *ACS Catal.* **6**, 5026–5043 (2016).
51. Zhang, J., Sun, J. & Wang, Y. Recent advances in the selective catalytic hydrodeoxygenation of lignin-derived oxygenates to arenes. *Green Chem.* **22**, 1072–1098 (2020).
52. Fang, H. *et al.* Product tunable behavior of carbon nanotubes-supported Ni–Fe catalysts for guaiacol hydrodeoxygenation. *Appl. Catal. A Gen.* **529**, 20–31 (2017).
53. Runnebaum, R. C., Lobo-Lapidus, R. J., Nimmanwudipong, T., Block, D. E. & Gates, B. C. Conversion of anisole catalyzed by platinum supported on alumina: The reaction network. *Energy and Fuels* **25**, 4776–4785 (2011).
54. Fisk, C. A. *et al.* Bio-oil upgrading over platinum catalysts using in situ generated hydrogen. *Appl. Catal. A Gen.* **358**, 150–156 (2009).
55. Pichaikaran, S. & Arumugam, P. Rh/Ni wet-impregnated Ia3d mesostructured aluminosilicate and r-GO catalysts for hydrodeoxygenation of phenoxybenzene. *New J. Chem.* **41**, 7893–7907 (2017).
56. Han, Q. *et al.* The synergistic effect between Ni sites and Ni-Fe alloy sites on hydrodeoxygenation of lignin-derived phenols. *Appl. Catal. B Environ.* **253**, 348–358 (2019).
57. Xu, X. & Jiang, E. “BTX” from Guaiacol HDO under Atmospheric Pressure: Effect of Support and Carbon Deposition. *Energy & Fuels* **31**, 2855–2864 (2017).

58. Anderson, E., Crisci, A., Murugappan, K. & Román-Leshkov, Y. Bifunctional Molybdenum Polyoxometalates for the Combined Hydrodeoxygenation and Alkylation of Lignin-Derived Model Phenolics. *ChemSusChem* **10**, 2226–2234 (2017).
59. Ju, C., Li, M., Fang, Y. & Tan, T. Efficient hydro-deoxygenation of lignin derived phenolic compounds over bifunctional catalysts with optimized acid/metal interactions. *Green Chem.* **20**, 4492–4499 (2018).
60. Lee, C. R. *et al.* Catalytic roles of metals and supports on hydrodeoxygenation of lignin monomer guaiacol. *Catal. Commun.* **17**, 54–58 (2012).
61. Gutierrez, A., Turpeinen, E. M., Viljava, T. R. & Krause, O. Hydrodeoxygenation of model compounds on sulfided CoMo/γ-Al2O3 and NiMo/γ-Al2O3 catalysts; Role of sulfur-containing groups in reaction networks. *Catal. Today* **285**, 125–134 (2017).
62. Gutierrez, A., Kaila, R. K., Honkela, M. L., Slioor, R. & Krause, A. O. I. Hydrodeoxygenation of guaiacol on noble metal catalysts. *Catal. Today* **147**, 239–246 (2009).
63. Zhu, X., Lobban, L. L., Mallinson, R. G. & Resasco, D. E. Bifunctional transalkylation and hydrodeoxygenation of anisole over a Pt/HBeta catalyst. *J. Catal.* **281**, 21–29 (2011).
64. Yang, Y. *et al.* Effect of metal-support interaction on the selective hydrodeoxygenation of anisole to aromatics over Ni-based catalysts. *Appl. Catal. B Environ.* **145**, 91–100 (2014).
65. Zhong, J., Pérez-Ramírez, J. & Yan, N. Biomass valorisation over polyoxometalate-based catalysts. *Green Chem.* **23**, 18–36 (2021).
66. Gamliel, D. P., Karakalos, S. & Valla, J. A. Liquid phase hydrodeoxygenation of anisole, 4-ethylphenol and benzofuran using Ni, Ru and Pd supported on USY zeolite. *Appl. Catal. A Gen.* **559**, 20–29 (2018).
67. Li, S. *et al.* One-pot hydrodeoxygenation of biomass furan derivatives into decane under mild conditions over Pd/C combined with phosphotungstic acid. *Green Chem.* **22**, 2889–2900 (2020).
68. Itagaki, S., Matsuhashi, N., Taniguchi, K., Yamaguchi, K. & Mizuno, N. Efficient hydrodeoxygenation of ketones, phenols, and ethers promoted by platinum-heteropolyacid bifunctional catalysts. *Chem. Lett.* **43**, 1086–1088 (2014).
69. Zhang, M. *et al.* A review of bio-oil upgrading by catalytic hydrotreatment: Advances, challenges, and prospects. *Mol. Catal.* **504**, 111438 (2021).
70. Han, Y. *et al.* Hydrotreatment of pyrolysis bio-oil: A review. *Fuel Process. Technol.* **195**, (2019).
71. Sulfur Dioxide @ Www.Epa.Gov. https://www.epa.gov/so2-pollution/sulfur-dioxide-basics.- 30th of august 2021
72. Viljava, T. R., Komulainen, R. S. & Krause, A. O. I. Effect of H2S on the stability of CoMo/Al2O3 catalysts during hydrodeoxygenation. *Catal. Today* **60**, 83–92 (2000).
73. Popov, A. *et al.* Bio-oils Hydrodeoxygenation: Adsorption of Phenolic Molecules on Oxidic Catalyst Supports. *J. Catal.* **297**, 176–186 (2010).
74. Vasilevich, A. V., Baklanova, O. N. & Lavrenov, A. V. Hydrodeoxygenation of Guaiacol with Molybdenum-Carbide-Based Carbon Catalysts. *ChemistrySelect* **5**, 4575–4579 (2020).
75. Laurent, E. & Delmon, B. Influence of water in the deactivation of a sulfided NiMo γ-Al2O3

catalyst during hydrodeoxygenation. *J. Catal.* **146**, (1994).

76. Badawi, M. *et al.* Effect of water on the stability of Mo and CoMo hydrodeoxygenation catalysts: A combined experimental and DFT study. (2011) doi:10.1016/j.jcat.2011.06.006.
77. Laurent, E. & Delmon, B. Study of the hydrodeoxygenation of carbonyl, car□ylic and guaiacyl groups over sulfided CoMo/γ-Al2O3 and NiMo/γ-Al2O3 catalysts: I. Catalytic reaction schemes. *Appl. Catal. A Gen.* **109**, 77–96 (1994).
78. Hurff, S. J. & Klein, M. T. Reaction pathway analysis of thermal and catalytic lignin fragmentation by use of model compounds. *Ind. Eng. Chem. Fundam.* **22**, 426–430 (2002).
79. Huuska, M. & Rintala, J. Effect of catalyst acidity on the hydrogenolysis of anisole. *J. Catal.* **94**, 230–238 (1985).
80. Massoth, F. E. *et al.* Catalytic Hydrodeoxygenation of Methyl-Substituted Phenols: Correlations of Kinetic Parameters with Molecular Properties. *J. Phys. Chem. B* **110**, 14283–14291 (2006).
81. Marcilly, C. *ACIDO-BASIC CATALYSIS Application to Refining and Petrochemistry - Volume 1*. vol. 1 (2006).
82. Prins, R. On the structure of γ-Al2O3. *J. Catal.* **392**, 336–346 (2020).
83. Erlt, G., Knozinger, H., Schuth, F. & Weitkamp, J. *Handbook of Heterogeneous Catalysis*. vol. 66 (Wiley, 1994).
84. Mizuno, N. & Misono, M. Heteropolyanions in catalysis. *J. Mol. Catal.* **86**, 319–342 (1994).
85. Misono, M. *Characterization of Acidic Properties of Heteropoly Compounds in Relation to Heterogeneous Catalysis*. *Studies in Surface Science and Catalysis* vol. 20 (1985).
86. Tsigdinos, G. A. Heteropoly compounds of molybdenum and tungsten. *Top. Curr. Chem.* **76**, 1–64 (1978).
87. Niiyama, H., Saito, Y. & Echigoya, E. *Acid-type catalysis by metal cation-substituted hetero-poly compounds*. *Studies in Surface Science and Catalysis* vol. 7 http://dx.doi.org/10.1016/S0167-2991(08)64752-7 (1981).
88. Misono, M. Acid catalysts for clean production. Green aspects of heteropolyacid catalysts. *Comptes Rendus l'Academie des Sci. - Ser. IIc Chem.* **3**, 471–475 (2000).
89. Kozhevnikov, I. V. Sustainable heterogeneous acid catalysis by heteropoly acids. *J. Mol. Catal. A Chem.* **262**, 86–92 (2007).
90. Wu, Y. *et al.* Heterogenization of Heteropolyacids: A General Discussion on the Preparation of Supported Acid Catalysts. *Ind. Eng. Chem. Res.* **35**, 2546–2560 (1996).
91. Okuhara, T., Mizuno, N. & Misono, M. Catalytic Chemistry of Heteropoly Compounds. in *Advances in Catalysis* vol. 41 113–252 (1996).
92. Mizuno, N. & Misono, M. Pore Structure and Surface Area of CsxH3-xPM12O40(x= 0-3, M= W, Mo). *Chem. Lett.* **53**, 967–970 (1987).
93. Okuhara, T., Watanabe, H., Nishimura, T., Inumaru, K. & Misono, M. Microstructure of cesium hydrogen salts of 12-tungstophosphoric acid relevant to novel acid catalysis. *Chem. Mater.* **12**, 2230–2238 (2000).
94. Okuhara, T. & Nakato, T. Catalysis by porous heteropoly compounds. *Catal. Surv. from Japan* **2**, 31–44 (1998).

95. Mizuno, N. & Misono, M. Heterogeneous catalysis. *Chem. Rev.* **98**, 199–217 (1998).
96. Okuhara, T., Masayuki, Y., Kyutae, N. & Makoto, M. Alkylation of Isobutane with Butenes Catalyzed by a Cesium Hydrogen Salt of 12-Tungstophosphoric Acid. *Chem. Lett.* **23**, (1994).
97. Kresge, C., Marler, D. O., Rav, G. S. & Rose, B. H. Supported heteropoly acid catalysts for isoparaffin-olefin alkylation reactions. (1993).
98. Guisnet, M., Bichon, P., Gnep, N. S. & Essayem, N. Transformation of propane, n-butane and n-hexane over H3PW12O40 and cesium salts. Comparison to sulfated zirconia and mordenite catalysts. *Top. Catal.* **11**–**12**, 247–254 (2000).
99. Liu, Y., Koyano, G. & Misono, M. *Hydroisomerization of n-hexane and n-heptane over platinum-promoted Cs 2.5 H 0.5 PW 12 O 40 (Cs2.5) studied in comparison with several other solid acids*. *Topics in Catalysis* vol. 11 (2000).
100. Anastas, P. & Warner, J. 12 Principles of Green Chemistry @ www.Acs.Org. - 5th of october 2021 https://www.acs.org/content/acs/en/greenchemistry/what-is-green-chemistry/principles/12-principles-of-green-chemistry.html.
101. Poole, O., Alharbi, K., Belic, D., Kozhevnikova, E. F. & Kozhevnikov, I. V. Hydrodeoxygenation of 3-pentanone over bifunctional Pt-heteropoly acid catalyst in the gas phase: Enhancing effect of gold. *Appl. Catal. B Environ.* **202**, 446–453 (2017).
102. Alotaibi, M. A., Kozhevnikova, E. F. & Kozhevnikov, I. V. Efficient hydrodeoxygenation of biomass-derived ketones over bifunctional Pt-polyoxometalate catalyst. *Chem. Commun.* **48**, 7194–7196 (2012).
103. Chemicals, S. *PURAL CATAPAL High-purity alumina hydrates*.
104. Figueiredo, J. L. & Ribeiro, F. R. *Catálise Heterogénea*. (2015).
105. Bartholomew, C. H. & Farrauto, R. J. Chemistry of nickel-alumina catalysts. *J. Catal.* **45**, 41–53 (1976).
106. Hammond, C. *The Basics of Crystallography and Diffraction*. (2015).
107. Micromeritics. *Temperature-Programmed Reduction Using the AutoChem*. *Temperature-Programmed Reduction Using AutoChem* www.micromeritics.com.
108. Bergeret, G. & Gallezot, P. Chapter 3: Characterization of Solid Catalysts. in *Handbook of Heterogeneous Catalysis* 738–765 (2008).
109. Kortum, G. *Reflectance Spectroscopy: Principles, Methods, Applications*. (Springer, 1969).
110. Stuart, B. H. *INFRARED SPECTROSCOPY: FUNDAMENTALS AND APPLICATIONS*. (John Wiley & Sons, Ltd, 2004).
111. Santos, J. S. *et al.* Mixed salts of cesium and ammonium derivatives of 12-tungstophosphoric acid: Synthesis and structural characterization. *Appl. Catal. A Gen.* **394**, 138–148 (2011).
112. Fournier, M., Feumi-Jantou, C., Rabia, C., Hervé, G. & Launay, S. Polyoxometalates catalyst materials: X-ray thermal stability study of phosphorus-containing heteropolyacids H3+xPM12-xVxO40·13-14H 2O (M=Mo,W; x=0-1). *J. Mater. Chem.* **2**, 971–978 (1992).
113. Alotaibi, M. A. *et al.* Facile preparation of cesium salt of tungstophosphoric acid for catalytic synthesis of one-pot two-component 1,3,4-oxadiazole derivatives in water: A doubly green approach. *Sustain. Chem. Pharm.* **17**, 100279 (2020).

114. Xiao, Z. *et al.* Biochemical coupling strategy promotes saccharification of bamboo leaves biomass via xylanase and heteropolyacids. *Biomass Convers. Biorefinery* **10**, 1007–1020 (2020).
115. Sudhakar, P. & Pandurangan, A. Heteropolyacid (H3PW12O40)-impregnated mesoporous KIT-6 catalyst for green synthesis of bio-diesel using transesterification of non-edible neem oil. *Mater. Renew. Sustain. Energy* **8**, 1–11 (2019).
116. Lizama, L. & Klimova, T. Highly active deep HDS catalysts prepared using Mo and W heteropolyacids supported on SBA-15. *Appl. Catal. B Environ.* **82**, 139–150 (2008).
117. Méndez, F. J. *et al.* Mesoporous catalysts based on Keggin-type heteropolyacids supported on MCM-41 and their application in thiophene hydrodesulfurization. *Fuel* **110**, 249–258 (2013).
118. Kousi, K. *et al.* Glycerol steam reforming over modified Ni-based catalysts. *Appl. Catal. A Gen.* **518**, 129–141 (2016).
119. Southward, B. W. L., Vaughan, J. S. & O'Connor, C. T. Infrared and thermal analysis studies of heteropoly acids. *Journal of Catalysis* vol. 153 293–303 (1995).
120. Nakato, T., Kimura, M., Nakata, S. I. & Okuhara, T. Changes of surface properties and water-tolerant catalytic activity of solid acid Cs2.5H0.5PW12O40 in water. *Langmuir* **14**, 319–325 (1998).
121. Koyano, G., Saito, T., Hashimoto, M. & Misono, M. In situ infrared spectroscopic investigation of 12-tungstphosphoric acid and its cesium hydrogen salts in relation to catalytic activity. *Stud. Surf. Sci. Catal.* **130 D**, 3077–3082 (2000).
122. NIST. Water @ Webbook.Nist.Gov. *National Institute of Standards and Technology* https://webbook.nist.gov/cgi/cbook.cgi?Name=Decane&Units=SI (2017). - 27th of october 2021
123. Dabbagh, H. A., Yalfani, M. & Davis, B. H. An XRD and Fourier-transformed infrared spectroscopy investigation of single and mixed γ-alumina and thorium oxide. *J. Mol. Catal. A Chem.* **238**, 72–77 (2005).
124. Boumaza, A. *et al.* Transition alumina phases induced by heat treatment of boehmite: An X-ray diffraction and infrared spectroscopy study. *J. Solid State Chem.* **182**, 1171–1176 (2009).
125. Kraleva, E. *et al.* Solid acid catalysts for dehydration of glycerol to acrolein in gas phase. *J. Mater. Sci.* **46**, 7160–7168 (2011).
126. Ju, C., Li, M., Fang, Y. & Tan, T. Efficient hydro-deoxygenation of lignin derived phenolic compounds over bifunctional catalysts with optimized acid/metal interactions. *Green Chem.* **20**, 4492–4499 (2018).
127. Brandão, D. S. *et al.* Pt and Pd catalysts supported on Al2O3 modified with rare earth oxides in the hydrogenation of tetralin, in the presence of thiophene. *Catal. Today* **133**–**135**, 324–330 (2008).
128. Caliman, E., Dias, J. A., Dias, S. C. L. & Prado, A. G. S. Solvent effect on the preparation of H3PW12O 40 supported on alumina. *Catal. Today* **107**–**108**, 816–825 (2005).
129. Liu, J. *et al.* Hydroprocessing of Jatropha Oil for Production of Green Diesel over Non-sulfided Ni-PTA/Al2O3 Catalyst. *Sci. Rep.* **5**, 1–13 (2015).
130. Scheffer, B., Heijeinga, J. J. & Moulijn, J. A. An electron spectroscopy and x-ray diffraction

study of nickel oxide/alumina and nickel-oxide-tungsten trioxide/alumina catalysts. *J. Phys. Chem.* **91**, 4752–4759 (1987).

131. Zieliński, J. Morphology of nickel/alumina catalysts. *J. Catal.* **76**, 157–163 (1982).
132. Chao, G. Y., Baker, J., Sabina, A. P. & Roberts, A. C. DOYLEITE, A NEW POLYMORPH OF Al(OH)3, AND ITS RELATIONSHIP TO BAYERITE, GIBBSITE AND NORDSTRANDIT. *Can. Mineral.* **23**, 21–28 (1985).
133. Wang, H. *et al.* One-Pot Process for Hydrodeoxygenation of Lignin to Alkanes Using Ru-Based Bimetallic and Bifunctional Catalysts Supported on Zeolite Y. *ChemSusChem* **10**, 1846–1856 (2017).
134. Runnebaum, R. C., Lobo-Lapidus, R. J., Nimmanwudipong, T., Block, D. E. & Gates, B. C. Catalytic Conversion of Guaiacol Catalyzed by Platinum Supported on Alumina: Reaction Network Including Hydrodeoxygenation Reactions. *Energy and Fuels* **25**, 3417–3427 (2011).
135. Alharbi, K., Alharbi, W., Kozhevnikova, E. F. & Kozhevnikov, I. V. Deoxygenation of Ethers and Esters over Bifunctional Pt-Heteropoly Acid Catalyst in the Gas Phase. *ACS Catal.* (2016) doi:10.1021/acscatal.6b00096.
136. Alharbi, K., Kozhevnikova, E. F. & Kozhevnikov, I. V. Hydrogenation of ketones over bifunctional Pt-heteropoly acid catalyst in the gas phase. *Appl. Catal. A Gen.* **504**, 457–462 (2015).
137. Boahene, P. E., Soni, K., Dalai, A. K. & Adjaye, J. Hydrotreating of coker light gas oil on Ti-modified HMS supports using Ni/HPMo catalysts. *Appl. Catal. B Environ.* **101**, 294–305 (2011).
138. Ardiyanti, A. R., Khromova, S. A., Venderbosch, R. H., Yakovlev, V. A. & Heeres, H. J. Catalytic hydrotreatment of fast-pyrolysis oil using non-sulfided bimetallic Ni-Cu catalysts on a δ-Al 2O 3 support. *Appl. Catal. B Environ.* **117**–**118**, 105–117 (2012).
139. Peters, J. E., Carpenter, J. R. & Dayton, D. C. Anisole and guaiacol hydrodeoxygenation reaction pathways over selected catalysts. *Energy and Fuels* **29**, 909–916 (2015).
140. Alharbi, K. Hydrodeoxygenation of bio-derived oxygenates over bifunctional metal-acid catalysts in the gas phase Hydrodeoxygenation of bio-derived oxygenates over. (2017).
141. Zhao, Y. P. *et al.* Hydrodeoxygenation of lignin model compounds to alkanes over Pd–Ni/HZSM-5 catalysts. *J. Energy Inst.* **93**, 899–910 (2020).
142. Broglia, F. *et al.* Guaiacol hydrodeoxygenation as a model for lignin upgrading. Role of the support surface features on Ni-based alumina-silica catalysts. *Fuel* **243**, 501–508 (2019).
143. Jongerius, A. L. *et al.* Stability of Pt/γ-Al2O3 catalysts in lignin and lignin model compound solutions under liquid phase reforming reaction conditions. *ACS Catal.* **3**, 464–473 (2013).
144. Karge, H. G. *COKE FORMATION ON ZEOLITES*. *Studies In Surface Science And Catalysis* vol. 5 (2001).
145. Guisnet, M. & Magnoux, P. Organic chemistry of coke formation. *Appl. Catal. A Gen.* **212**, 83–96 (2001).
146. Almeida, R., Ribeiro, M. F., Fernandes, A. & Lourenço, J. P. Gas-phase conversion of glycerol to allyl alcohol over vanadium-supported zeolite beta. *Catal. Commun.* **127**, 20–24 (2019).
147. Bilton, M., Brown, A. P. & Milne, S. J. Investigating the optimum conditions for the formation of

calcium oxide, used for CO2 sequestration, by thermal decomposition of calcium acetate. *J. Phys. Conf. Ser.* **371**, (2012).

148. Wang, Y., Lin, S. & Suzuki, Y. Experimental study on CO2 capture conditions of a fluidized bed limestone decomposition reactor. *Fuel Process. Technol.* **91**, 958–963 (2010).

149. Perry, R. H. *Perry's Chemical Engineers' Handbook*. *Perry's Chemical Engineers' Handbook* (1999).

Appendix

Appendix A – Metal dispersion and mean particle size calculations

The values used for the calculating both metal dispersion and mean particle size are present in Table 14.

Table 14: Data used for metal dispersion and mean particle size calculation.

Property	MM_{Pt}	V_{H2}	Sample mass	V_{molar}	x_{Pt}	Stoich H_2:Pt	v_{Pt}	a_{Pt}
Value	195.084	0.0965	19.77	22400	0.01	1.5	15.10	8.07
Units	$g \cdot mol^{-1}$	cm^3	mg	$cm^3 \cdot mol^{-1}$			$Å^3$	$Å^2$

Appendix B – Thermogravimetric Temperature Profiles

Thermogravimetric temperature profiles for the analysis of the HPW and of the spent catalysts can be seen in Figure 65 and Figure 66.

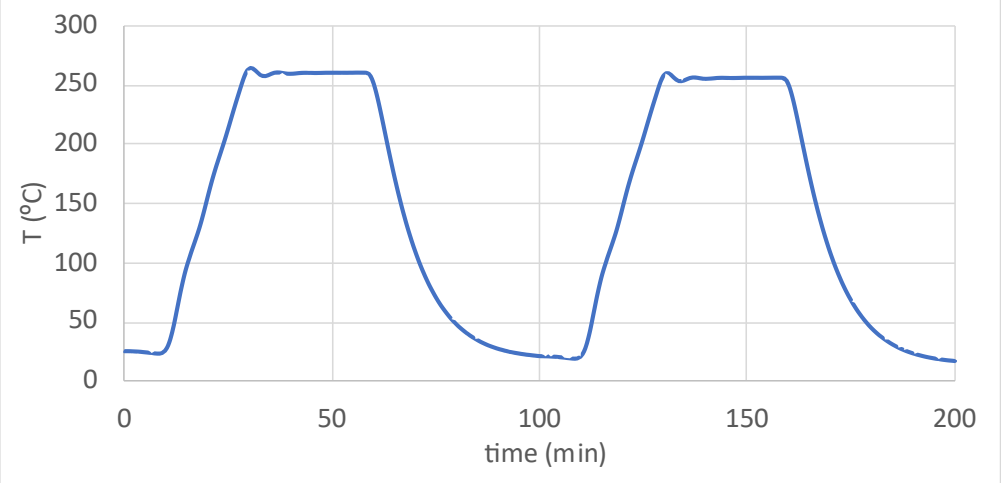

Figure 65: TGA temperature profile as a function of time for the analysis of HPW.

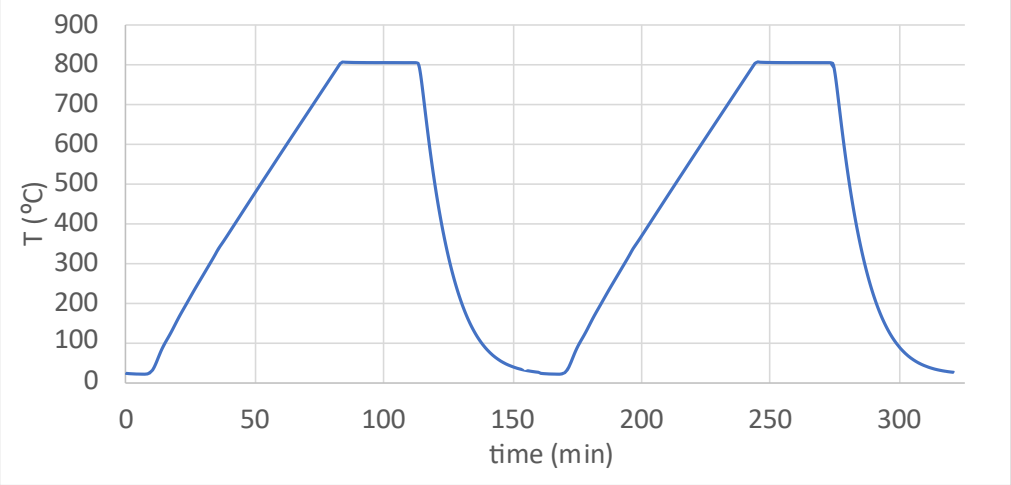

Figure 66: TGA temperature profile as a function of time for the analysis of the spent catalysts.

Appendix C – Reaction set-up

The reaction set-up can be seen in Figure 67.

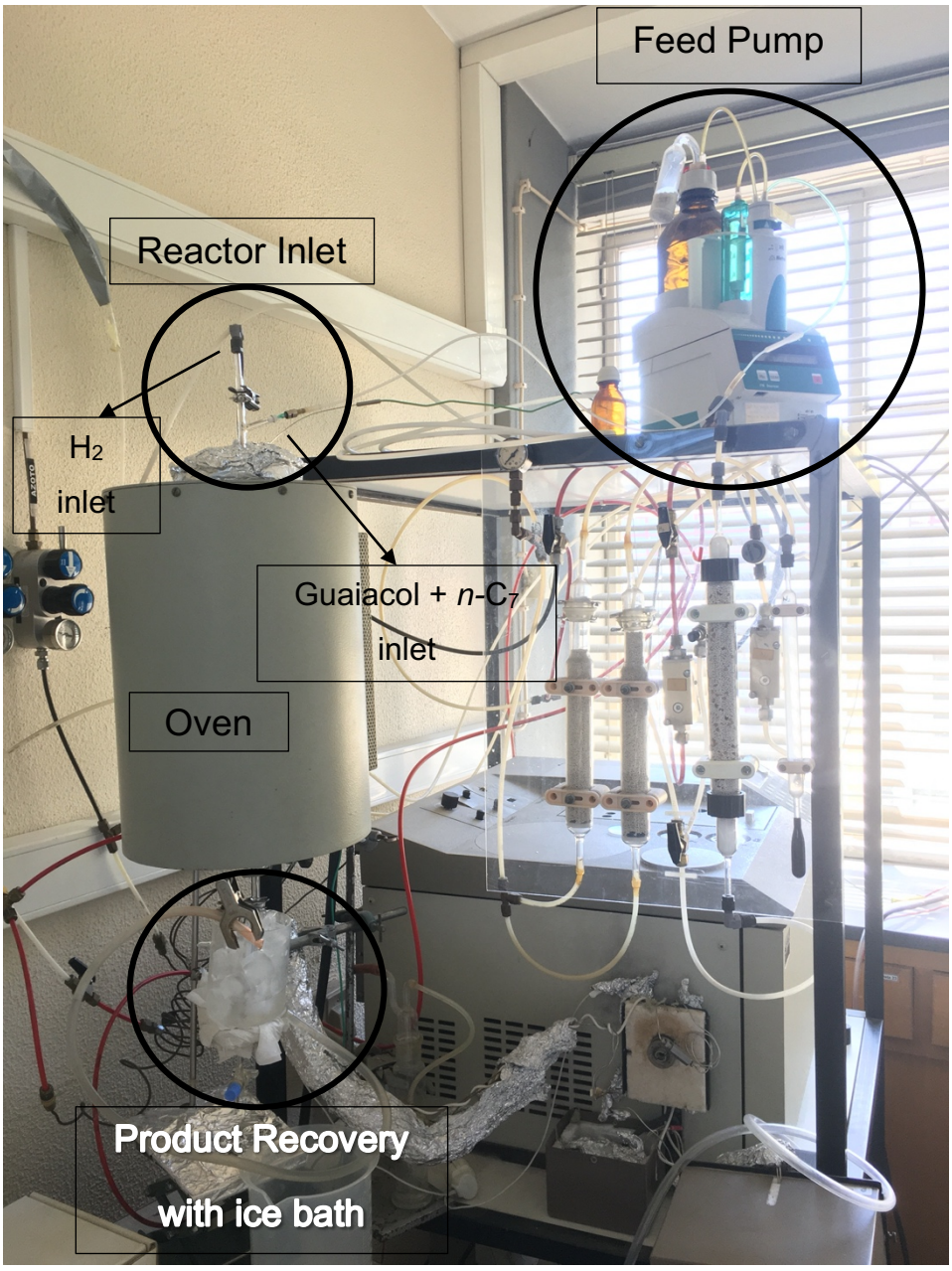

Figure 67: HDO reaction set-up.

Appendix D – Control Reaction

The chromatogram for the control reaction with the solvent (*n*-heptane), can be seen in Figure 68.

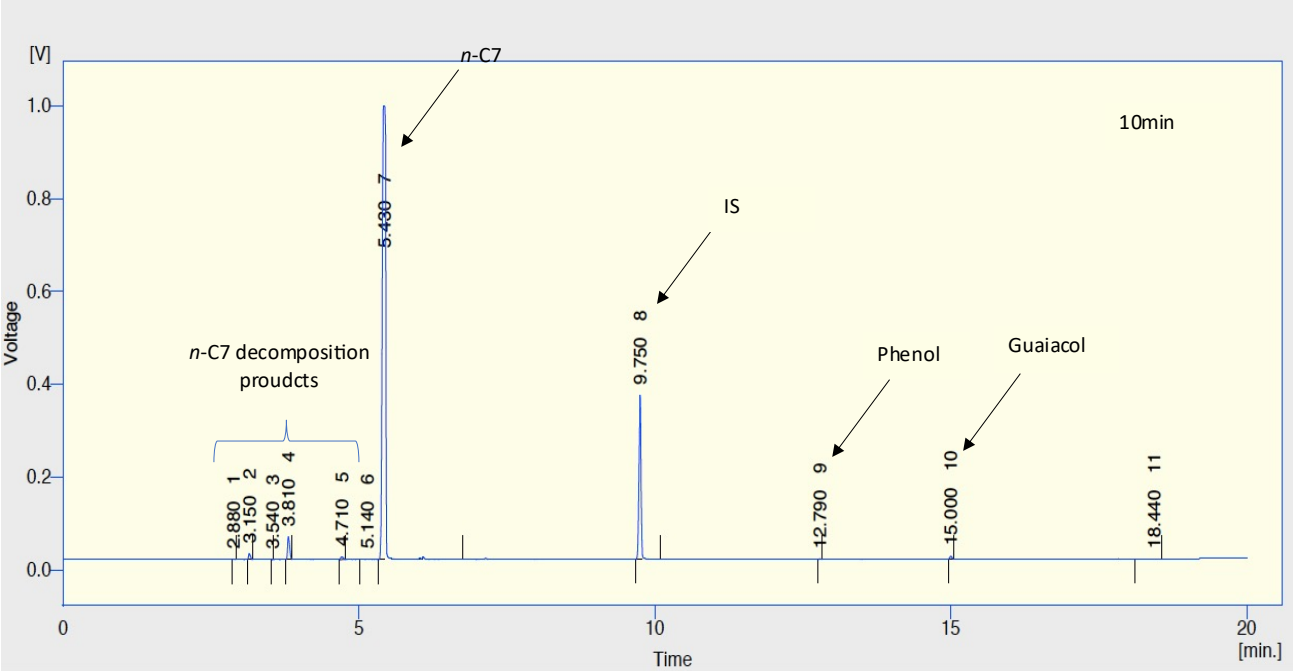

Figure 68: Gas Chromatogram for the control reaction with NiO25- Al_2O_3. 10 min of reaction; n-C7 is n-heptane.

Appendix E – Retention time and response factor determination

The RT of various compounds can be seen in Table 15 and the number and RT of the unknowns for the different catalysts are present in Table 16.

Table 15: Retention times and boiling points of identified and unidentified compounds.

Compound	Retention Time (min)	Boiling Point (ºC)[149]
Guaiacol	15.00	205
Anisole	11.10	154
Benzene	4.58	80.1
Cyclohexanone	10.51	155
Phenol	12.70	172
Ethylbenzene (IS)	9.63	136.2
U1	9.88	
U2	14.35	
U3	17.06	
U4	7.58	
U5	18.25	

U6	19.20	
Compound	**Retention Time (min)**	**Boiling Point (ºC)[149]**
U7	16.02	
U8	16.75	
U9	11.87	
U10	13.07	
U11	13.45	
U12	20.93	
U13	10.29	
U14*	4.80	
U15	13.66	
U16*	3.70	
U17*	3.07	
U18	14.78	
U19	16.55	
U20	17.76	
Unknown products with * marked are probably *n*-heptane cracking products		

Table 16: Retention time range and number of unknowns for the catalysts tested.

Catalyst	TOS (min)	RT range, min (compound)	Number of unknowns
Pt-Al_2O_3	10	---	0
	20	---	0
	40	---	0
	60	14.38, 16.79 (U2, U3)	2
	80	9.89, 14.35, 17.16, 18.28, 19.21 (U1, U2, U3, U5, U6)	5
	100	14.37, 19.26 (U2, U6)	2
	120	9.94 (U1)	1
HPW/Pt-Al_2O_3	10	9.86, 13.6, 15.98, 17.89 (U1, U11, U7, U5)	4
	20	14.94, 15.98, 16.69 (U2, U7, U8)	3
	40	9.82, 15.96, 16.69 (U1, U7, U8)	3
	60	9.85, 14.31, 15.97, 17.13 (U1, U2, U7, U3)	4
	80	14.32, 15.99, 17.15 (U2, U7, U3)	3
	100	13.95, 15.62 (U2, U7)	2
	120	14.34, 16 (U2, U7)	3

Catalyst	TOS (min)	RT range, min (compound)	Number of unknowns
Pt-Al_2O_3/$Cs_{2.5}$	10	16.00, 16.73, 17.98 (U7, U8, U5)	3
	20	9.90, 14.36, 16.03, 16.76, 18.32 (U1, U2, U7, U8, U5)	5
	40	16.01, 17.18, 18.28, 19.2 (U7, U3, U5, U6)	4
	60	9.89, 14.34, 16.01, 17.17, 18.28, 19.21 (U1, U2, U7, U3, U5, U6)	6
	80	9.88, 13.45, 14.34, 16.01, 17.13, 18.27, 19.2 (U1, U11, U2, U7, U3, U5, U6)	7
	100	9.82, 11.87, 13.04, 13.42, 15.99, 16.72, 17.02, 18.22, 19.17 (U1, U9, U10, U11, U2, U7, U8, U3, U5, U6)	10
	120	9.88, 13.07, 13.45, 14.35, 16.02, 16.75, 17.06, 18.25, 19.2 (U1, U10, U11, U2, U7, U8, U3, U5, U6)	9
Ni28-Al_2O_3	10	14.96 (U2)	1
	20	14.34 (U2)	1
	40	14.33, 16.02, 16.75 (U2, U7, U8)	3
	60	14.3, 15.98, 16.71, 19.11 (U2, U7, U8, U6)	4
	80	14.33, 16.94(U2, U3)	2
	100	14.33, 14.78, 16.01, 16.75, 17.12, 18.25, 19.19 (U2, U18, U7, U8, U3, U5, U6)	7
	120	14.42, 14.85, 16.06, 16.55, 16.79, 17.22, 18.31 (U2, U18, U7, U19, U8, U3, U5)	7
HPW/Ni28-Al_2O_3	10	10.36 (U13)	1
	20	14.35, 16.02, 16.76 (U2, U7, U8)	3
	40	14.34, 16.01, 16.74 (U2, U7, U8)	3
	60	14.33, 16.00, 16.73 (U2, U7, U8)	3
	80	14.34, 16.02 (U2, U7)	3
	100	14.37, 16.04, 16.77 (U2, U7, U8)	3
	120	14.39, 16.06 (U2, U7)	2

Catalyst	TOS (min)	RT range, min (compound)	Number of unknowns
Ni28-Al_2O_3/$Cs_{2.5}$	10	14.34, 16.02, 16.75 (U2, U7, U8)	3
	20	14.35, 16.03, 16.76 (U2, U7, U8)	3
	40	14.37, 16.05, 16.78 (U2, U7, U8)	3
	60	14.36, 16.03, 16.77 (U2, U7, U8)	3
	80	14.33, 16.01, 16.74, 17.76 (U2, U7, U8, U20)	4
	100	14.33, 16.01, 16.74 (U2, U7, U8)	4
	120	14.37, 16.04, 16.77 (U2, U7, U8)	3
NiO25-Al_2O_3	10	---	0
	20	11.85 (U9)	1
	40	16.03 (U7)	1
	60	13.54, 13.66, 16.00 (U11, U15, U7)	3
	80	13.5, 13.63, 14.3, 15.98, 16.71 (U11, U15, U2, U7, U8)	5
	100	13.55, 13.68, 14.35, 16.02 (U11, U15, U2, U7)	4
	120		
HPW/NiO25-Al_2O_3	10	14.33, 16.01 (U2, U7)	2
	20	14.34, 16.01 (U2, U7)	2
	40	14.33 (U2)	1
	60	14.37 (U2)	1
	80	14.33 (U2)	1
	100	14.37 (U2)	1
	120	14.3, 15.98 (U2, U7)	2
NiO25-Al_2O_3/$Cs_{2.5}$	10	14.31 (U2)	1
	20	14.34 (U2)	1
	40	14.35 (U2)	1
	60	14.34, 16.02 (U2, U7)	2
	80	14.32, 16.00 (U2, U7)	2
	100	14.32, 16.00 (U2, U7)	2
	120	14.36 (U2)	1

As internal standard results for guaiacol are shown already Figure 69 to Figure 72 present the calibration curves for anisole, benzene, cyclohexanone and phenol.

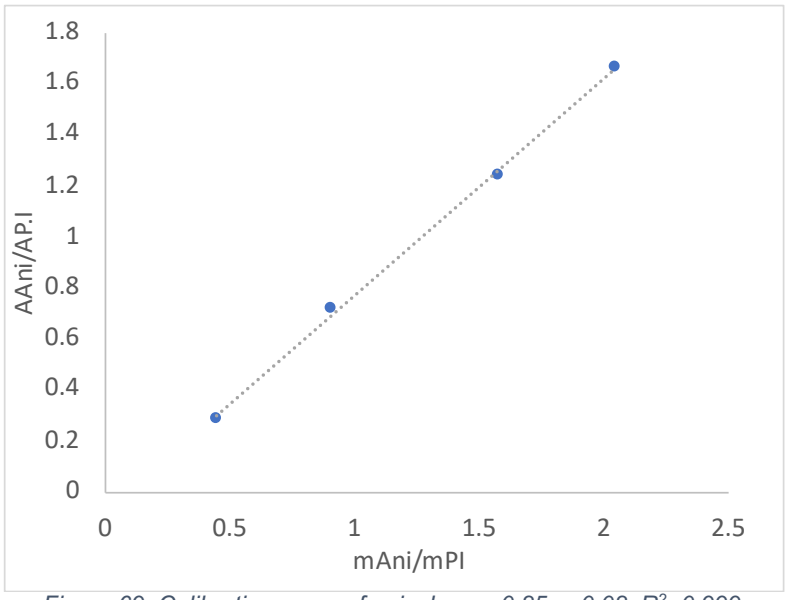

Figure 69: Calibration curve of anisole. y = 0.85x - 0.08; R^2=0.999

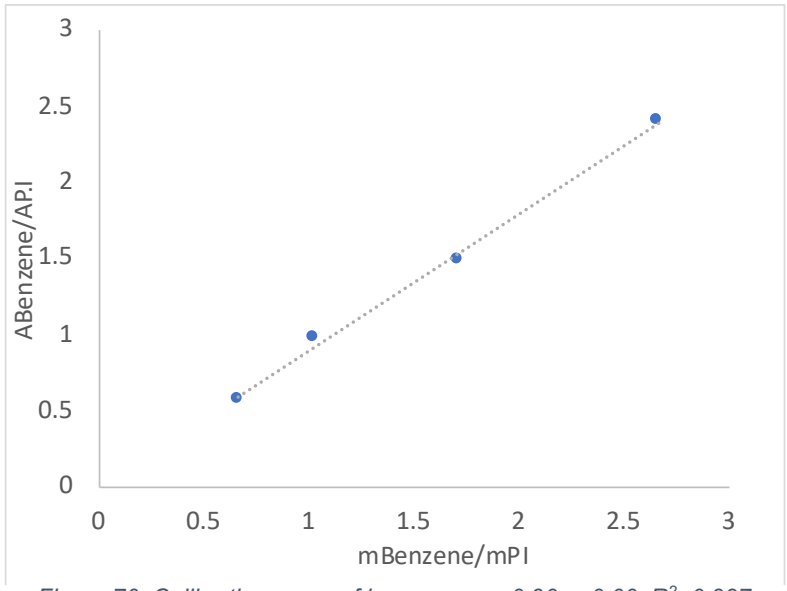

Figure 70: Calibration curve of benzene. y = 0.90x - 0.00; R^2=0.997

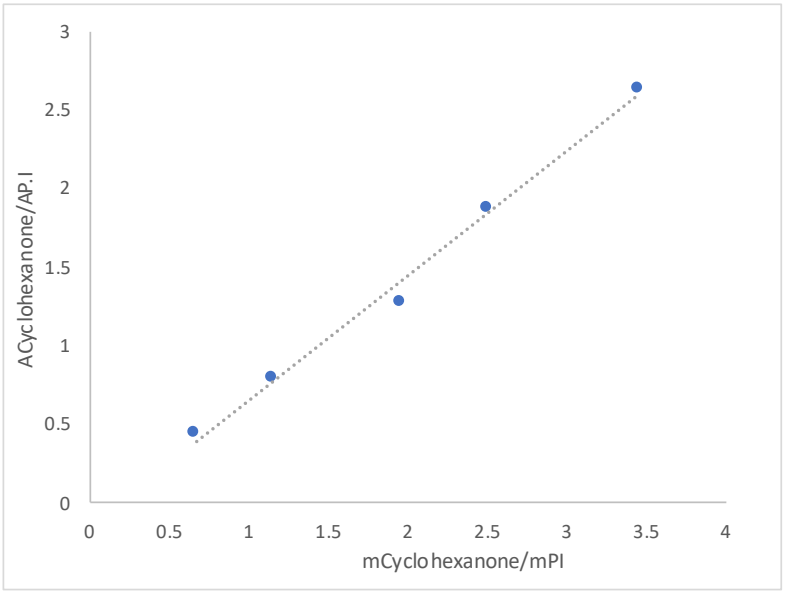

Figure 71: Calibration curve of cyclohexanone. y = 0.79x - 0.14; R^2=0.991

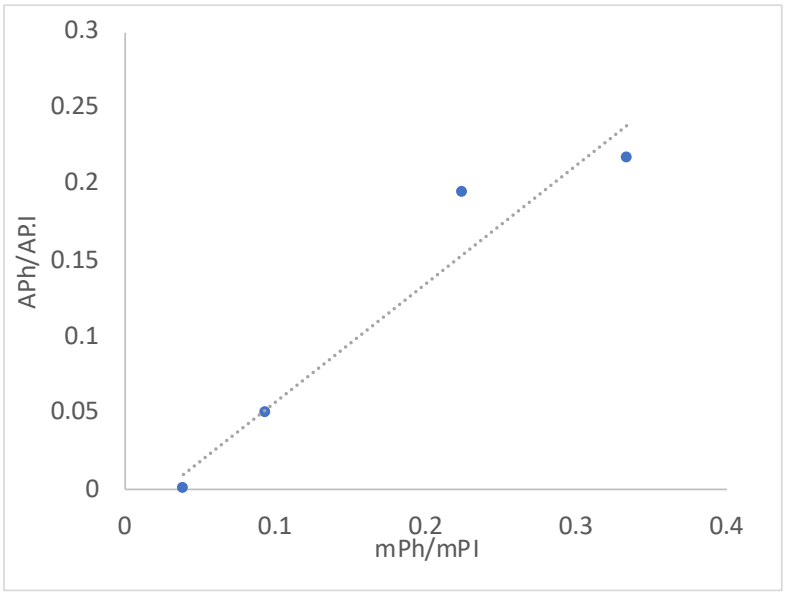

Figure 72: Calibration curve of phenol. y = 0.78x - 0.02; R^2=0.936

Appendix F – X-Ray Diffraction Chromatograms

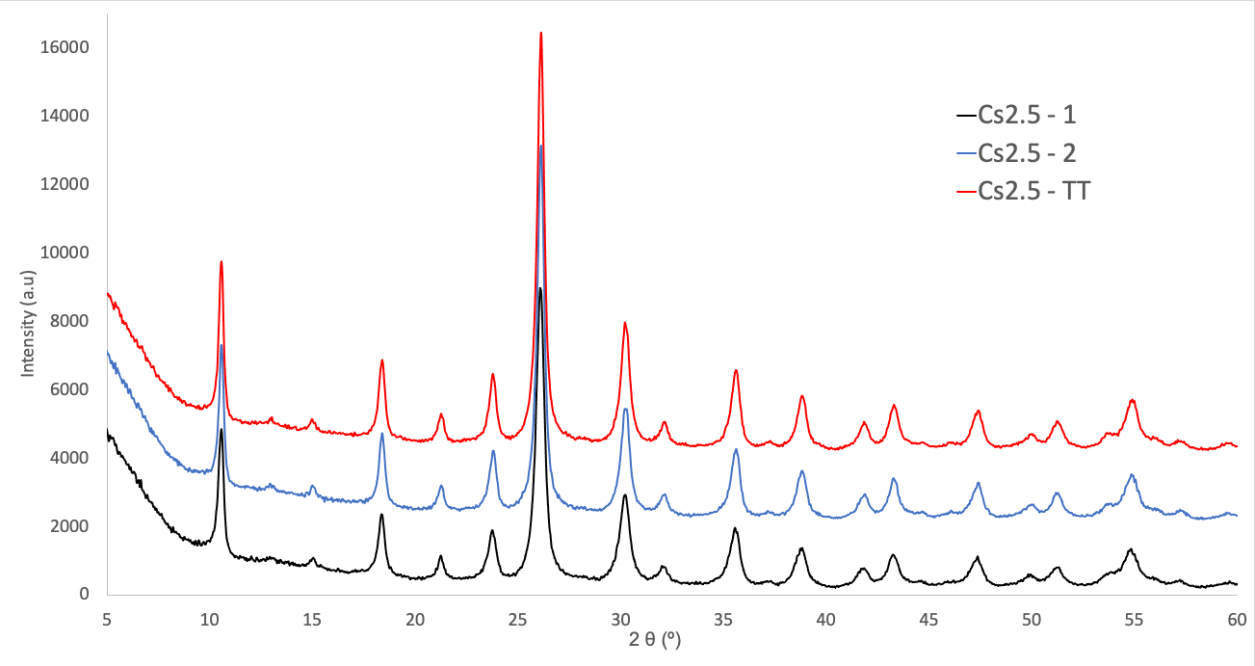

Figure 73: X-Ray Diffractogram of Cesium salts, with and without thermal treatment.